

# Zebrafish lateral line system: The roles of Eya1 in migrating primordium and Notch signaling in hair cell development and regeneration.

Indra Wibowo

---

TESI DOCTORAL UPF / 2011

Thesis Supervisor/Director:

Dr. Hernán López-Schier

Sensory Cell Biology and Organogenesis Group

Cell and Developmental Biology Department

Center for Genomic Regulation



For my family, who offered me genuine pray, love and support  
throughout the course of this doctoral thesis.



## Acknowledgements

First and foremost, I would like to thank my supervisor Dr. Hernán López-Schier. It has been an honor to be one of his first Ph.D. students. Also, for his encouragement, guidance and support from the initial to the final level has enabled me to develop an understanding of the subject.

I thank past and present members of the López-Schier Lab who have created a source of friendships as well as good advice and collaboration. I am especially grateful for the fun group of López-Schier Lab: Filipe “the spicy food and esprit soulmate ever”, Adèle “the Goddess”, Jesus “the Junior”, Mariana “the Sister”, Andrea and Alessandro “the Italians”, Mayra and Rachele “the girls next door”, Sabrina “the Mother of Noelia” and of course Andrea Durán-Sánchez “the Guardian Angel”. I cannot thank you all enough for the opportunities to work with you time-to-time and the adventurous works. Thanks to all of you...I am nothing without you!

I would like to thank to my committee members for fruitful discussions.

I would like to thank Di Croce Lab, especially Dr. Di Croce and Dr. Buschbeck who allow me to include part of the published paper in my thesis.

I would like to thank CRG Advanced Light Microscopy Unit for the assistance that they provide to use the high-tech microscopes.

I would like to thank to Om Nino and Te Anggie family, Mas Fahmi and Mbak Emmy family for their warm welcome and for taking a good care of me. You are my families in Barcelona. Also, untuk mbak Mia yang telah menjadi teman dan tahu perjalananku selama masa “belajarku” di Barcelona. Thanks for everything “yu”!

I would like to thank my parents, sisters, brothers, nieces and nephews. They were always supporting me and encouraging me with their best wishes.

Of course I will not forget to thank many people who have directly or indirectly contributed to this thesis.

Finally, I would like to thank my wife, Mira Mutiyani, for her patient and understanding. I am looking forward for our future times together.

Terima kasih banyak! Muchas gracias! Merci beaucoup! Moltes gràcies! Grazie mille! Danke schön!



## Summary

The interaction and communication among cells are required for adaptability of cell movement and its consequence for tissue formation and remodeling, particularly in embryonic development and cancer metastasis. One example of continuous and periodical/cyclical tissue remodeling is the migration of posterior lateral line primordia. These tissues are known to undergo several coordinated processes from the migration of mesenchymal-like tip cells to the switch from mesenchymal behavior to epithelial one, called mesenchymal-to-epithelial transition (MET), until the formation and the maturation of rosettes and deposition of proneuromasts. These processes can only be performed correctly through the precise coordination of asymmetric expression of Fgf and Wnt/ $\beta$ -catenin signaling. The migrating primordia show the expression of Wnt/ $\beta$ -catenin signaling in the leading zone while Fgf signaling occupies the trailing zone. These differential expression patterns between these two signaling pathways create what so-called morphogenetic territories. However, the question remains how these territories are monitored and maintained during tissue remodeling. In the first part of this thesis, I discuss the importance discoveries on Eya1 functions. Here, I demonstrate that Eya1 is essential to maintain the transition zone that is marked by loss of Wnt/ $\beta$ -catenin signaling and activation of Fgf signaling. I use the previously characterized *eya1/dog-eared* mutants from genetic screening. Loss of Eya1 function leads to the truncation of posterior lateral line. The delay of rosette formation is also pronounced in the *dog* mutants indicating the defect in MET. The two chemokine receptors, CXCR4 and CXCR7, are expressed in the primordium in which the expression of CXCR7 is reduced in the *dog* mutants. Not only defects in the number of neuromasts, but the migration persistence is also affected upon Eya1 loss of function. In this

thesis I show that Wnt/ $\beta$ -catenin activity is expanded in *dog* mutant while Fgf activity is reduced. Transition zone is also a region where the Dkk gene is expressed. Here, I analyze the expression of Dkk and show that Dkk gene expression is reduced which may explain the expansion of Wnt/ $\beta$ -catenin signaling territories in the mutant. Together, these results also support the direct control of Fgf signaling on the Dkk expression. I also take advantage of the availability of zebrafish transgenics in combination with pharmacological approaches to further study Eya1 functions in posterior lateral line primordium. To these extents, I demonstrate that Eya1 is necessary for FGF signaling downstream of the FGFR. Finally, I propose that combinatorial Wnt/ $\beta$ -catenin and Fgf signaling control the spatiotemporal profile of Dkk expression to dynamically confine Wnt/ $\beta$ -catenin to the mesenchyme.

The second part of this thesis is discussing about the bilateral symmetry during tissue development and regeneration. The important question for these processes is how bilateral symmetry is maintained and established after tissue damage. Hair cells in the neuromasts of zebrafish posterior lateral line consist of kinocilia and stereocilia that build up the apical domain of the hair cells. These organelles are arranged so that half of the hair cells are facing the other half to create mirror symmetry of epithelial planar polarity. Like hair cells in the inner ear of mammals, hair cells in neuromasts are also sensitive to the ototoxic drugs. However, while in mammalian inner ear is lacking hair cells regeneration after damage, neuromasts are showing continuous production of hair cells after drug treatments. This phenomenon occurred in neuromasts leads to the recovery of the organs. Thus, it allows them to function properly. In this thesis I demonstrate that neuromasts are found to possess at least five cell populations including supporting cells, mantle cells, polar compartment cells, transient unipotent hair cell progenitors (UHCPs)

and mature hair cells. Polar compartment cells are maintained by low Notch activity. Upon neomycin treatments, the complete loss of hair cells triggers a rapid and precise regeneration process. This process, so-called directional regeneration (regeneration anisotropy), shows the relocation and development of hair cell progenitors from elsewhere in polar compartment. Produced hair cells will be oriented to make planar polarity of the epithelium by participation of planar cell inversions that allows progenitors to invert position after cytokinesis to give rise to two hair cells. The bilateral symmetry in regenerating neuromasts is maintained even though the mature hair cells propagate from the midline toward the periphery of the neuromasts.

## Resumen

La interacción y comunicación entre células son necesarias para la adaptabilidad del movimiento celular y su consecuencia para la formación y remodelación de tejidos, particularmente en el desarrollo embrionario y en la formación de metástasis. Un ejemplo de remodelación de tejidos continua y periódica/cíclica es la migración de los primordios de la línea lateral posterior. Estos tejidos sufren varios procesos coordinados, desde la migración de células de tipo mesenquimal en el borde anterior del primordio y la transición de comportamiento mesenquimal a epitelial (MET), hasta la formación y maduración de *rosetas* y la deposición de proneuromastos. Estos procesos sólo pueden ser ejecutados correctamente mediante una precisa coordinación en la expresión asimétrica de las vías de señalización de Fgf y Wnt/ $\beta$ -Catenina. Durante su migración, el primordio muestra expresión de la vía de señalización Wnt/ $\beta$ -Catenina en el borde anterior mientras que la vía de señalización de Fgf ocupa el borde posterior. Estos patrones de expresión diferenciales entre las dos vías de señalización crean territorios morfogenéticos. Sin embargo, no se conoce como dichos territorios están controlados y mantenidos durante la remodelación del tejido. En la primera parte de la tesis discuto el descubrimiento de la función de Eya1. Demuestro que Eya1 es esencial para mantener la zona de transición de comportamiento mesenquimal a epitelial, caracterizada por la pérdida de la señalización Wnt/ $\beta$ -Catenina y la activación de la señalización Fgf. Utilizo los mutantes *eya1/dog-eared*, previamente caracterizados en

un cribado genético. La pérdida de función de *Eya1* causa un truncamiento de la línea lateral posterior. Los mutantes *dog* también muestran un pronunciado retraso en la formación de rosetas, indicando defectos en la transición mesenquimal a epitelial. Los dos receptores de quimiocinas, CXCR4 y CXCR7, se expresan en el primordio. En los mutantes *dog* la expresión de CXCR7 en el primordio se ve reducida. La persistencia de migración también se ve afectada tras la pérdida de función de *Eya1*. En esta tesis muestro que la actividad de Wnt/ $\beta$ -Catenina está expandida en los mutantes *dog* mientras que la actividad Fgf está reducida. Dkk se expresa en la zona de transición. Analizo la expresión de Dkk y muestro que ésta se ve reducida, lo que podría explicar la expansión de los territorios de señalización Wnt/ $\beta$ -Catenina en el mutante. Juntos, estos resultados también apoyan la idea que Fgf ejerce un control directo sobre la expresión de Dkk. También aprovecho la disponibilidad de transgénicos en combinación con enfoques farmacológicos para avanzar en el estudio de la función de *Eya1* en el primordio de la línea lateral posterior. De esta manera demuestro que *Eya1* es necesario para la señalización Fgf río abajo de FGFR. Por último, propongo que la combinatoria de la señalización Wnt/ $\beta$ -Catenina y Fgf controla el perfil espacio-temporal de la expresión de Dkk para restringir dinámicamente Wnt/ $\beta$ -Catenina a las células mesenquimales.

La segunda parte de esta tesis consiste en la discusión de la simetría bilateral durante el desarrollo y la regeneración de tejidos. La pregunta importante para estos procesos es como la simetría bilateral se mantiene y establece después del daño de un tejido. Las células ciliadas de los neuromastos de la línea lateral posterior del

pez cebra presentan kinocilios y estereocilias en su dominio apical. Estas organelas se disponen de manera que la mitad de las células ciliadas miran a la otra mitad para crear una simetría especular en el epitelio, denominada polaridad planar. Al igual que las células ciliadas del oído, las células ciliadas de los neuromastos son sensibles a los fármacos ototóxicos. A pesar de ello, mientras el oído no presenta regeneración de células ciliadas después de daño, los neuromastos presentan una continua producción de células ciliadas después del tratamiento con fármacos ototóxicos. Este fenómeno permite la recuperación y apropiado funcionamiento de los neuromastos. En esta tesis demuestro que los neuromastos poseen al menos cinco tipos de poblaciones celulares; incluyendo células de soporte, células de manto, células de compartimento polar, progenitores (de células ciliadas) transitorios unipotentes (UHCPs) y células ciliadas maduras. Las células de compartimento polar están mantenidas por niveles bajos de actividad Notch. Después del tratamiento con neomicina, la pérdida completa de células ciliadas dispara un proceso de regeneración rápido y preciso. Este proceso, denominado regeneración direccional (anisotropía en la regeneración), muestra la relocalización y desarrollo de los progenitores de las células ciliadas desde otras partes del compartimento polar. Las células ciliadas producidas son orientadas para crear una polaridad planar en el epitelio mediante inversiones celulares que permiten a los progenitores invertir la posición después de la citoquinesis para dar lugar a dos células ciliadas. La simetría bilateral en los neuromastos se mantiene durante la regeneración a pesar de que las células ciliadas maduras se propagan desde la línea media hasta la periferia del neuromasto.



## Preface

This thesis is submitted to obtain the degree of Doctor at the Pompeu Fabra University. The research described herein was conducted under supervision of Dr. Hernán López-Schier in the Sensory Cell Biology and Organogenesis Group, Department of Cell and Developmental Biology, Center for Genomic Regulation, Barcelona, Spain. This work had been done between October 2006 and April 2011.

The purpose of this thesis is to introduce and demonstrate several biological processes or phenomena using posterior lateral line system of zebrafish as a model. The first part of this work focuses on the highly dynamic tissue remodeling under the control of morphogenetic territories. In particular, *eya1* gene is studied to add a substantial mechanism during migration of lateral line primordium. The second part of this thesis mainly discusses about the existence of tissue compartment whereby Notch signaling involves in governing the regeneration anisotropy. This work is an intellectual collaboration with Filipe Pinto Sousa, a Ph.D. student in Dr. López-Schier laboratory. The last part of this thesis emphasizes on the epigenetic study in order to validate the involvement of macroH2A during development of zebrafish embryos. This work is done in collaboration with Dr. Di Croce laboratory.

This work is to the best of my knowledge original, except where acknowledgements and references are made to previous work. Neither this, nor substantially similar thesis has been or is being submitted for any other degree, diploma, or other qualification at any other university. This thesis contains less than 50,000 words.

This research was supported and funded by the Center for Genomic Regulation, Barcelona, Spain.

Barcelona, 2<sup>nd</sup> of May 2011

Indra Wibowo

## Table of content

ACKNOWLEDGEMENTS.....	III
SUMMARY .....	V
RESUMEN .....	VIII
PREFACE .....	XI
TABLE OF CONTENT.....	XII

## CHAPTER 1 GENERAL INTRODUCTION, AIMS AND OUTLINE OF THESIS..... 1

1.1 LATERAL-LINE SYSTEM IN FISH.....	2
1.1.1 <i>Morphology</i> .....	2
1.1.2 <i>Development of posterior lateral-line system</i> .....	4
1.1.3 <i>Organization of migrating primordium</i> .....	6
1.1.4 <i>Signaling Pathways that Control Lateral-Line Primordial Migration..</i>	8
1.1.5 <i>Hair cell development and regeneration</i> .....	13
1.2 EYA1 FUNCTIONS AS PROTEIN TYROSINE PHOSPHATASE AND TRANSCRIPTION CO-ACTIVATOR.....	16
1.2.1 <i>Conservation of Eya1 protein across animal kingdom</i> .....	18
1.2.2 <i>Eya1 mutant phenotypes</i> .....	21
1.3 AIMS AND OUTLINES OF THE THESIS.....	22
1.3.1 <i>Aims</i> .....	22
1.3.2 <i>Outlines of the Thesis</i> .....	23

## CHAPTER 2 EYA1 IS ESSENTIAL FOR THE HOMEOSTATIS OF FGF AND WNT/ $\beta$ -CATENIN SIGNALING DURING TISSUE REMODELING ..... 27

2.1 ABSTRACT.....	28
2.2 INTRODUCTION .....	28
2.3 MATERIALS AND METHODS .....	32
2.4 RESULTS.....	36
2.4.1 <i>dog/eya1 mutant zebrafish form truncated posterior lateral lines</i> .....	36
2.4.2 <i>Eya1 is necessary for migration persistence</i> .....	39
2.4.3 <i>Loss of Eya1 delays rosette formation and reduces CXCR7b expression</i> .....	41
2.4.4 <i>Eya1 is essential for Dkk1 expression and FGF signaling</i> .....	44
2.5 DISCUSSION .....	49
2.6 SUPPLEMENTARY MATERIALS.....	54

## CHAPTER 3 COMPARTMENTALIZED NOTCH SIGNALING SUSTAINS EPITHELIAL MIRROR SYMMETRY ..... 61

3.1 ABSTRACT.....	62
3.2 INTRODUCTION .....	63
3.2 MATERIALS AND METHODS .....	64
3.3 RESULTS.....	68
3.3.1 <i>Cellular heterogeneity and compartmentalization of neuromasts.....</i>	68
3.3.2 <i>The mitotic division of UHCPs is essential for regeneration .....</i>	71
3.3.3 <i>The orientation of UHCPs divisions is dispensable for bilateral symmetry.....</i>	75
3.3.4 <i>A polar compartment is not a niche nor does it harbor stem cells.....</i>	77
3.3.6 <i>Notch signaling controls the production of hair-cell progenitors.....</i>	79
3.3.7 <i>Compartmentalized Notch signaling controls regeneration anisotropy..</i>	80
3.3.8 <i>Centrifugal movement of hair cells propagates planar polarity horizontally.....</i>	83
3.4 DISCUSSION .....	86
3.4.1 <i>Hair-cell regeneration anisotropy and bilateral symmetry are functionally linked .....</i>	86
3.4.2 <i>Regeneration anisotropy is not due to a localized stem-cell population .</i>	87
3.4.3 <i>Regeneration anisotropy depends on compartmentalized Notch signaling .....</i>	88
3.4.4 <i>The origin of axial references remains unknown.....</i>	88
3.4.5 <i>Centrifugal hair-cell movement propagates planar polarity horizontally</i>	89
3.4.6 <i>Planar cell inversions .....</i>	90
3.5 CONCLUSION .....	91
3.6 SUPPLEMENTARY MATERIALS .....	92

## CHAPTER 4 THE HISTONE VARIANT MACROH2A IS AN EPIGENETIC REGULATOR OF KEY DEVELOPMENTAL GENES ..... 95

4.1 ABSTRACT.....	96
4.2 INTRODUCTION .....	96
4.3 RESULTS.....	98
4.3.1 <i>Genomic analysis of macroH2A target genes.....</i>	98
4.3.2 <i>MacroH2A variants are enriched at developmental genes.....</i>	101
4.3.3 <i>MacroH2A is required for proper zebrafish embryogenesis .....</i>	103
4.4 DISCUSSION .....	106
4.5 SUPPLEMENTARY MATERIALS.....	109

## CHAPTER 5 GENERAL DISCUSSION .....115

5.1 EYA: SEEING IS NOT ALWAYS BELIEVING.....	116
--	-----

5.2 EYA IN DEVELOPMENT AND DISEASE .....	121
5.3 EYA AND OTHER ASPECTS OF BIOLOGICAL PROCESSES .....	122
5.4 INTERPLAY AMONG SIGNALING PATHWAYS DURING POSTERIOR LATERAL LINE MIGRATION .....	124
5.5 MAKING USE OF POLARITY: ROSETTE FORMATION.....	129
5.6 THE LATERAL LINE PRIMORDIUM CONNECTS COLLECTIVE MIGRATION AND DIFFERENTIATION AND/OR CELL FATE SPECIFICATION .....	131
5.7 NOTCH SIGNALING AND HAIR CELL REGENERATION .....	132
5.7 NOTCH-ING TISSUE ON AND OFF .....	135
5.8 VERTEBRATE DEVELOPMENT AND EPIGENETICS: MACROH2AX ON ZEBRAFISH DEVELOPMENT .....	137
5.9 FUTURE DIRECTIONS: .....	138
<b>APPENDIX 1: MATERIALS AND METHODS.....</b>	<b>140</b>
<b>APPENDIX 2: ABBREVIATIONS.....</b>	<b>161</b>
<b>REFERENCES.....</b>	<b>162</b>
<b>CURRICULUM VITAE .....</b>	<b>179</b>

# **Chapter 1**

## **General Introduction**

### **Aims and Outline of Thesis**

## 1.1 Lateral-line System in Fish

### 1.1.1 Morphology

The lateral-line system of fish and amphibians consists of a set of small and discrete sensory organs and the neurons that innervate and connect them to the brain (Figure 1). The lateral line is sensitive to hydrodynamic stimuli caused by moving objects or water. It is now clear that lateral-line systems are involved in several behavioral activities, such as prey detection, predator avoidance, intraspecific communication, schooling behavior, object discrimination, and object entrainment and reothaxis (orientation relative to water current) (Montgomery JC, 1997). There are two branches of lateral-line system in zebrafish, anterior lateral-line (ALL) and posterior lateral-line (PLL) systems (Figure 1). The sensory organs of lateral line, shaped like rosettes, are called neuromast. They are the functional unit of the lateral-line system and are arranged over the animal's body in species-specific manner. Mature neuromasts comprise mechanosensory hair cells and non-sensory supporting cells (mantle and sustentacular cells) (Figure 2). Hair cells of the neuromast, as discovered in inner ear, bear a single bundle composed of tens to hundreds of actins-based stereocilia and a single microtubule-based kinocilium (except in mature mammalian cochlear hair cells). Studies on the hair cell structure and function in the inner ear have discovered many molecules that are involved in the hair cell to function properly (Froehlicher et al., 2009; Nicolson, 2005; Vollrath et al., 2007). These molecules might be applied to hair cell in the neuromasts since they were long assigned an auditory function, mostly because its mechanosensory hair cells are very similar to those of the inner ear (Dijkgraaf, 1963). The eccentric position of kinocilium and stepwise increase in stereocilia heights, with the tallest being the closest to the kinocilium, will define the axis morphology of hair-cell bundles. The hair cells of a lateral-line neuromast are oriented into two

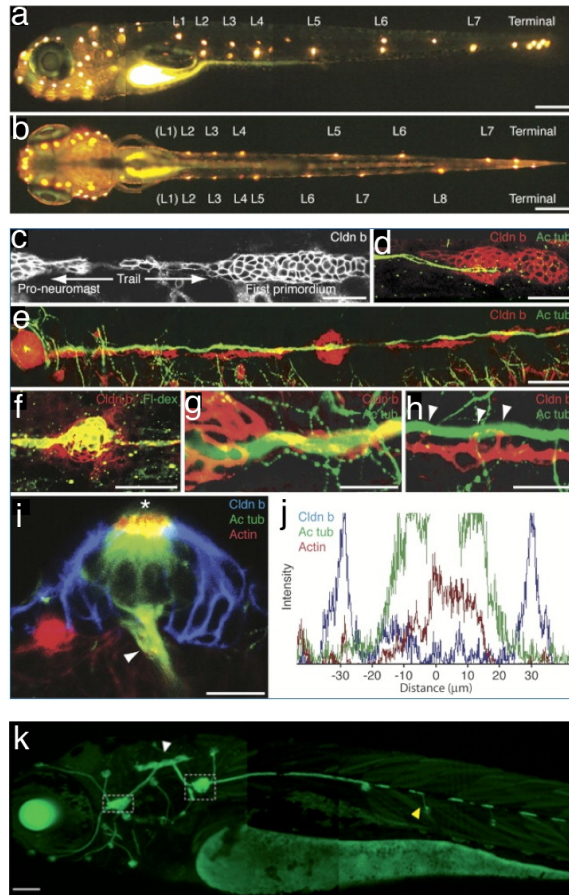


**Figure 1. Zebrafish Lateral Line Systems.** (a,b) The DiASP staining of hair cells in the neuromasts revealed the anterior and posterior lateral line systems. (c-h) Claudin b labeling of primordial cells and mature supporting cells in the posterior lateral-line organ. (c) In a confocal section at 28 hpf, antiserum against claudin b (Cldn b) strongly labels all cells of the first primordium. The trail of cells between the primordium and the most recently deposited pro-neuromast is also marked. (d) The leading neurites, labeled for acetylated tubulin (Ac tub), invade the first primordium at an early stage of migration. (e) In a confocal section of neuromasts at 48 hpf, axons of the octavolateralis nerve extend along the trail of claudin b-positive cells. (f) Labeling of the first primordium with uncaged fluorescein-dextran (Fl-dex) marks neuromasts and trailing cells, which are also positive for claudin b. (g-h) Claudin b-positive cells envelop the extending sensory axons adjacent to a neuromast (g) and along the developing octavolateralis nerve (h). Note several points of apparent contact between the claudin b-positive cells and the axons (arrowheads). (i) Actin-rich hair bundles are evident at hair-cell apices (asterisk) in a lateral view of a 5 dpf neuromast. Anti-claudin b specifically labels mature supporting cells in all neuromasts, whereas acetylated tubulin marks the hair-cell somata and kinocilia (not

evident in this image) as well as neurons delaminating from the basal epithelial surface (arrowhead). **(j)** In an intensity profile of a top view of a neuromast, peripheral supporting cells accumulate high levels of claudin b, which is excluded from the center of the organ where mature hair cells label for acetylated tubulin and rhodamine-phalloidin. The intensity scale is linear but its units are arbitrary. **(k)** HGn39D transgenic zebrafish express GFP in the lateral line afferent neurons. GFP expression pattern in a 4 dpf HGn39D transgenic fish. In these and all subsequent illustrations, the animal's anterior is oriented to the left and its dorsum is situated to the top. Scale bars: 100  $\mu\text{m}$  **(a-b)**, 50  $\mu\text{m}$  in **(c-f)**, 10  $\mu\text{m}$  in **(g-h)**. (Source of Figure 1a-j are from Lopez-Schier *et al.*, 2004; source of Figure 1k is from Faucherre *et al.*, 2009).

opposing directions parallel to the major axis of the neuromast (López-Schier *et al.*, 2004). Each neuromast contains two groups of hair cells of opposite hair-bundle polarity arranged across a plane of mirror symmetry. In the posterior lateral line, most neuromasts contain anterior-posterior polarized hair cells, whereas a particular few neuromasts contain dorso-ventral polarized cells (López-Schier and Hudspeth, 2005). The hair bundles are protected by a cupula, which connects the bundles with the environment (Figure 2b). Neuromasts of lateral-line systems are innervated by afferent neurons (Bricaud *et al.*, 2001; Faucherre *et al.*, 2009; Metcalfe, 1985). A single afferent fibre innervates and makes synapses only to the hair cells with the same orientation of planar polarisation (Faucherre *et al.*, 2009; Nagiel *et al.*, 2009). The neuromast will sense the stimuli by deflecting their cilia or the hair bundles toward the tallest stereocilia (positive deflections) by doing so will open the transduction channel and cause a depolarization, displacement in opposite direction will close the channel and cause a hyperpolarization of the hair cell. Neuromasts therefore provide information about the local water flow.

### 1.1.2 Development of posterior lateral-line system

It has been studied in amphibian that lateral-line development involves a variety of well-orchestrated cellular activities that may include the placode formation, cell proliferation and separation, cell migration and deposition,



hair cell differentiation and axon outgrowth and guidance. Thus, the posterior lateral-line system may prove to be a good model system to study these phenomena because of its simplicity and accessibility and also because of the availability of background information regarding the development of this system.

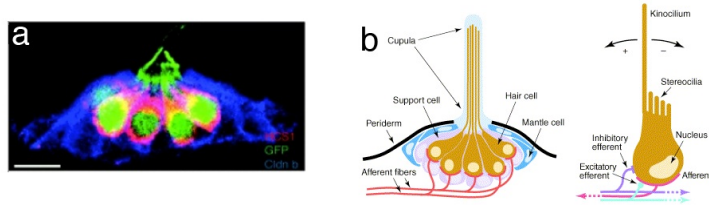


**Figure 2. The Structure of a Neuromast.** (a) In a lateral view of a neuromast from an ET4 transgenic animal labeled for claudin b (blue) and HCS1 (red), GFP-positive hair cells (green) are also marked by HCS1. (b) Scheme of a neuromast, illustrating the different cell types that are involved and their organization. The cupula is secreted by the support cells. The glial cells wrapping the afferent fibers have not been represented. Scheme of a hair cell, illustrating its functional asymmetry, as well as its afferent and efferent innervation. The implication that excitatory efferents act on the afferent fiber rather than directly on the hair cell is plausible but not demonstrated. (Source of Figure 2a is from Lopez-Schier and Hudspeth, 2006; source of Figure 2b is from Ghysen and Dambly-Chaudière, 2004).

As mentioned above, that lateral-line system of the zebrafish consists of two major branches, an ALL located around the head and a PLL located in the trunk and the tail. The PLL are formed by the deposition of neuromasts by migrating primordium (Metcalf et al, 1985). The onset of lateral-line development is marked by the formation of lateral-line placode that is located just posterior of the otic placode. This placode formation occurs around 19 hour-post-fertilization (hpf) Immediately afterwards, lateral-line placode will give rise to sensory ganglia (PLL ganglia) and to migrating primordia that contain a large compartment of around 100 cells (PLL primordial). The latter elongate or migrate between surface ectoderm and basement membrane and deposit a cluster of around 20-30 cells as pre-neuromasts along the head and the body at regular interval of every 5-7 somites. Also, 4-5 interneuromast cells are deposited per somite. At 40-50

hpf, PLL consists of 5-6 neuromasts of the trunk and 2-3 terminal neuromasts at the tail (Figure 3, Gompel et al., 2001, Sapede et al., 2002). While migrating, primordium is followed by neurites from the lateral-line ganglia and innervating neuromast as they are deposited (Faucherre et al., 2009; Metcalfe, 1985; Nagiel et al., 2009).

### **1.1.3 Organization of migrating primordium**

During migration, lateral-line primordium experiences successive changes of cellular organization and these changes in cellular level are repeated periodically throughout the migration. The migrating posterior lateral line primordium shows compartmentalization/segmentation along the axis of migration, with cells in the leading edge shows mesenchymal-like structure with cell protrusions and highly motile (Figure 4). Cells behind the leading undergo morphological changes with columnar shape (epithelial-like structure) and a radial arrangement becoming evident. Cells in this part is subjected to mesenchymal-epithelial transition (MET) that occurs through condensation of mesenchymal-like cells into tightly adhesive groups, generation of apico-basal polarity, adoption of epithelial characteristics and transition to a polarized epithelial tissue. The trailing region of primordium arranges into distinct rosettes of cells, each corresponding to a pro-neuromast that is later deposited, and the leading third remaining unpatterned (Ghysen and Dambly-Chaudiere, 2007; Hava et al., 2009; Lecaudey et al., 2008).

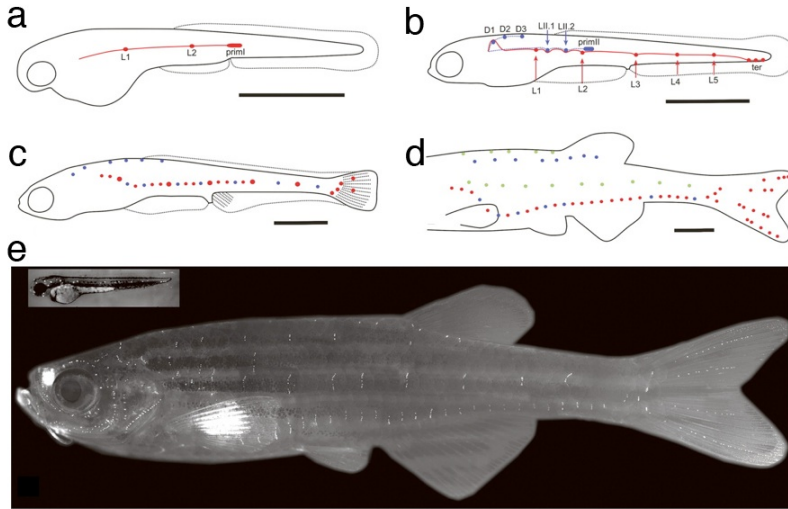


**Figure 3. Development of the posterior lateral-line system in the zebrafish. (a)** At 32 hpf, the migrating primordium is about halfway in its journey to the tip of the tail. It has deposited two neuromasts, L1 and L2, as well as a thin stream on interneuromastic cells (red). **(b)** At 3 d, primI has reached the tip of the tail where it fragments to form two to three terminal neuromasts (red). A second primordium forms ~36 hpf and splits to form primII, which follows the same path as primI along the horizontal myoseptum, and primD, which initiates the dorsal line (blue). **(c)** At 3 wk, intercalary neuromasts are formed by the interneuromastic cells deposited by primI (red). At this time, primD and primII have completed their journey (blue). The dorsal line never extends beyond the dorsal fin. The lateral neuromasts are shifting to more ventral positions. **(d)** At the larval-juvenile transition, the lateral and dorsal lines are complete and are shifted ventrally. Two new lines have formed at the original positions at the embryonic lines: one along the horizontal myoseptum and one along the dorsal midline (light green). **(e)** Young adult fish exposed to a fluorescent vital dye specific for hair cells. All individual neuromasts of the juvenile have given rise to dorso-ventrally aligned clusters of neuromasts (stitches). Stitches continue to expand during the entire life of the fish. (*Inset*) 48-hpf embryo at the same scale as the adult. Scale bars, 1 mm. (Source of this Figure is from Ghysen and Dambly-Chaudière, 2007)

Each rosette exhibits special characteristics with a radial arrangement, apical constriction and elongation of cells becoming bottle-like structure. Apical constriction is denoted by apical positioning of actin-myosin tensile system at the cell junction that increases surface tension into focal points to form rosettes (Hava et al., 2009; Lecaudey et al., 2008). Thus, mature

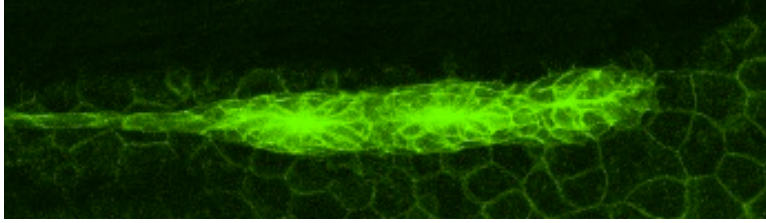


**Figure 4. The structure of posterior lateral line primordium.** *Tg(cldB:lyn-EGFP)* shows the cellular pattern of primordium.

pro-neuromast is identified by the presence of apical membrane condensation and bottlenecked cells. After maturation of rosette to become pro-neuromast, a set of cellular process occurs to separate individual mature pro-neuromast from the rest of the primordium. The dynamic of pro-neuromast deposition is identified by tissue separation where the rosette in the trailing region slows down its speed and the surrounding tissue that connects to the rest of the primordium undergoes cellular changes. The cells between depositing pro-neuromast and the trailing region display elongated shaped due to the pulling forces between depositing pro-neuromast that soon will be stalled and the primordium (Hava et al., 2009). This elongated type of cells will give rise to interneuromast cells.

#### **1.1.4 Signaling Pathways that Control Lateral-Line Primordial Migration**

Not only chemokine signaling that gives polarization in the migrating lateral-line primordium but also two other signaling pathways involve in proper directionality of migration. Two signaling pathways have already been discovered to control migration of primordium by effecting CXCR4 and

CXCR7 expressions and other important cell behaviors. The Wnt/ $\beta$ -catenin signaling pathway is active in the cells of leading region of the primordium where it activates the Fgf signaling in the trailing cells. Fgf pathway activation is initiated by Fgf ligands, Fgf3 and Fgf10, whose expressions are in response to Wnt/ $\beta$ -catenin signaling activity. By diffusion Fgf ligands bind to their receptor, Fgfr1, that is expressed in the trailing cells, thus Fgf pathway is activated. However, Wnt/ $\beta$ -catenin signaling pathway also activates the expression of Fgf signaling inhibitor, Sef1, in the leading cells so that Fgf pathway is inhibited in the trailing region. In the meantime, Fgf signaling pathway drives the expression of Dkk, a diffusible inhibitor of Wnt/ $\beta$ -catenin pathway; thus, Wnt/ $\beta$ -catenin activity is restricted only in the leading region (Figure 5) (Aman and Piotrowski, 2008; Aman and Piotrowski, 2009; Ma and Raible, 2009). These two signaling pathways, therefore, is believed to be one of the key players whose activities show mutual-inhibitory feedback interactions. Other studies also showed that Wnt/ $\beta$ -catenin activation involved in repression of CXCR7b in the leading cells since ectopic expression of Wnt/ $\beta$ -catenin signaling pathways in the trailing region of primordium reduces the expression of *cxc7b*. As a consequence the primordium shows similar phenotypes as observed in *cxc7b* morphants, which is stalling of primordium (Aman and Piotrowski, 2008; Dambly-Chaudiere et al., 2007; Valentin et al., 2007).

It has been studied that migration of lateral-line primordium is driven by a well-known master regulator of migration, which is CXCL12a/CXCR4b (CXCL12a is previously known as SDF1a). CXCL12a is a ligand that is expressed as a stripe thin line along the horizontal myoseptum of the trunk at the both sides (David et al., 2002). In the meantime, the lateral-line primordium expresses the receptor, the CXCR chemokine receptor (CXCR4), at the leading edge. Another chemokine receptor, CXCR7, is found to be expressed in the trailing part of the

primordium. The differential expression of these two chemokines causes polarization in the primordium.

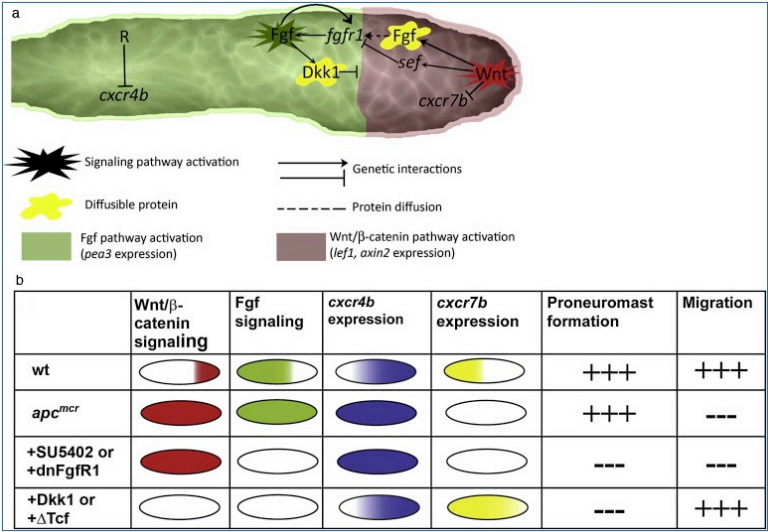


**Figure 5. Schematic Models of Genetic Interactions between Signaling Pathways and Gene Expression Patterns in WT and Manipulated Primordia.** (a) In WT primordia, Wnt/ $\beta$ -catenin pathway activation in the leading zone leads to Fgf pathway activation in the trailing zone. Exclusivity of these domains is maintained by the induction of *dkk1* by Fgf signaling in trailing cells and induction of *sef* by Wnt/ $\beta$ -catenin signaling in leading cells. *cxcr7b* expression in leading cells is inhibited by Wnt/ $\beta$ -catenin signaling, and *cxcr4b* expression is restricted from the trailing zone via the activity of an uncharacterized repressor (R) that is inhibited if Wnt/ $\beta$ -catenin signaling is active throughout the primordium. (b) Summary of gene expression patterns and associated phenotypes in the different experimental manipulations (Adapted from Aman and Piotrowski, 2008 (Source of this figure is from Aman & Piotrowski, 2008)).

Thus, the directionality of primordial migration depends upon the differential interactions between the two chemokines and the ligand. Moreover, it has been suggested that SDF1 ligand determines the path and the receptors control the movement of the lateral-line primordium. Further research revealed that CXCR4 ligand is only needed for the cells at the very

tips of the primordium (Haas and Gilmour, 2006), while CXCR7 seems to be necessary for primordial migration (Dambly-Chaudiere et al., 2007; Valentin et al., 2007).

During the compartmentalization/segmentation of migrating primordium, several cellular morphology changes occur. Rosette formation is one of important events to produce pro-neuromast before deposition. It has been studied that this event is dependent upon FGF signaling pathway (Aman and Piotrowski, 2008; Lecaudey et al., 2008; Nechiporuk and Raible, 2008). Upon inactivation of FGF signaling pathways, primordium shows no rosette formation and as a result migration is stopped, suggesting that rosette formation is absolutely necessary for primordial migration (Lecaudey et al., 2008; Nechiporuk and Raible, 2008). However, study done by Aman and Piotrowski showed that upon inhibition of Wnt/ $\beta$ -catenin and Fgf signaling pathways, rosette formation is prevented but migration of primordium is normal. This result suggests that the stalling of primordial migration in the Fgf-depleted embryos is due to ectopic overexpression of Wnt/ $\beta$ -catenin signaling pathway and loss of *cxc7b* expression (Aman and Piotrowski, 2008). Recent study has shown that Notch signaling pathways is also involved in the morphogenesis of migrating lateral-line primordium (Matsuda and Chitnis, 2010). Notch pathway appears to restrict the expression of *atoh1a* after initiated by Fgf signaling in maturing pro-neuromast. After initiation of *atoh1a* expression by Fgf signaling in the same cells, *atoh1a* drives the expression of *fgf10* ligand and Notch ligand, *deltaD*, while it inhibits *fgfr1* expression. Thus, Fgf pathways will only be active in surrounding cells that will ensure the formation of the rosette. In the mean time, *deltaD* drives the activation of Notch pathway in neighboring cells, as consequence, *atoh1a* expression is inhibited and the cells will become supporting cells. In the absent of Notch, *atoh1a* expression in the surrounding cells is not inhibited, therefore, it drives the expression of *fgf10* ligand but inhibits the expression of *fgfr1* expression. Thus, Fgf signaling

activation is prevented, as a consequence, the formation of rosette is disturbed (Matsuda and Chitnis, 2010).

The pro-neuromast deposition is a regular yet complex process during primordial migration. Several genes are involved for this process to occur accurately. Cadherins are typical surface proteins that play a role in cell-cell adhesion. Several members of cadherin family have been found in zebrafish, *cadherin-1* or *e-cadherin* (*cdh1*), *cadherin-2* or *n-cadherin* (*cdh2*), *cadherin-4* (*cdh4*), and *cadherin-23* (*cdh23*). *Cdh1*, *cdh2* and *cdh4* are expressed in PLL system (Kerstetter et al., 2004; Liu et al., 2003). *Cdh2* knockdown causes a reduced number in neuromasts in LL system and the neuromasts are deposited close to each other (Kerstetter et al., 2004). The exact mechanisms underlying the disrupted processes are not fully understood. Similar to *cdh2* morphants, *cdh4* morphants also displays fewer number of neuromasts compared to wild-type, suggesting a disrupted migration and deposition of the LL primordium after knockdown of cadherins (Wilson et al., 2007). *Cdh23* plays a role in the development and signal transduction of the tip-link of hair bundles (Sollner et al., 2004). It needs yet to be verified whether cadherins are really important for primordial migration or for hair cell development, or for both processes.

Other two genes are also involved in pro-neuromast deposition in LL system. The tumor-associated calcium signal transducer gene (*tacstd*) is a cell surface glycoprotein, homolog to mammalian TACSTD1/2 (Villablanca et al., 2006). This gene is expressed in migrating PLL primordium as well as in pro-neuromasts and neuromasts. The loss-of-function of *tacstd* shows significant reduction of neuromast number or even absence of neuromasts (Villablanca et al., 2006). The other gene is *met* that is expressed in migrating PLL primordium but not in newly deposited pro-neuromast or neuromast (Haines et al., 2004). Met is a receptor tyrosine kinase that is needed for pro-neuromast deposition by PLL primordium. The morpholino injection against



*met* mRNA exhibits not only a reduction of deposited neuromast but also hair-cell and supporting-cell numbers (Haines et al., 2004).

The knowledge of the mechanisms of primordial migration and pro-neuromast deposition could help to decipher the effects of chemicals on this stage of neuromast development.

### **1.1.5 Hair cell development and regeneration**

After pro-neuromast deposition, the process of neuromast maturation starts. First, the progenitor cells that will develop as hair cells must become committed to a hair cell fate and differentiate into hair cells that develop stereocilia and kinocilium also other features that are characteristics of mature hair cells.

Notch signaling has been known to play a role in cell-fate decision in hair cells of the mammalian inner ear (Hawkins et al., 2007). This mechanism is readily applied in hair-cell development in zebrafish neuromast. Efforts to study the process of hair-cell differentiation have been done extensively using *mind bomb* (*mib*) mutants and other mutants and morphants. *mib* mutants display supernumerary hair cells due to failure fulfilling lateral inhibition mediated by Notch signaling (Haddon et al., 1998a; Haddon et al., 1998b; Itoh and Chitnis, 2001; Itoh et al., 2003; Whitfield, 2005). *Mib* encodes a RING E3 ligase required for Notch activation (Itoh and Chitnis, 2001; Whitfield, 2005). The expressions of genes involved in Notch signaling pathways were examined. The *notch3* receptor expression was down-regulated while the two delta ligands, *deltaA* and *deltaB*, expression domains were expanded (Itoh and Chitnis, 2001). The

*atoh1* gene expression was not restricted in the specific cell anymore, thus causing the increased number of hair cells at the cost of supporting cells.

Er $\beta$ 2 is one of estrogen receptors that has been found in supporting cells and hair cells of zebrafish LL (Tingaud-Sequeira et al., 2004). *Er* $\beta$ 2 morphants display a circling swimming behavior, characteristic of mechanosensory mutants, like *tmie*. The lack of hair cells was also observed after knocking down this gene, suggesting a role of *er* $\beta$ 2 in hair cell differentiation. The interaction of *er* $\beta$ 2 and Notch signaling was also studied showing the up-regulation of two Notch receptors, *notch1a* and *notch3* genes (Froehlicher et al., 2009).

Recent study on the identification of gene linked to ET4 transgenic fish has characterized a gene encoding Atp2b1a (Pmca1), whose function it to export Ca<sup>2+</sup> from a cell (Go et al.). The morpholino knockdown of this gene results in the accumulation of hair cell progenitors because of the blocking of Ca<sup>2+</sup> export that leads to defect in cell division. Not only important for cell division, but Ca<sup>2+</sup> intracellular is also important for cell differentiation and physiology of hair cells (Go et al.). Atp2b1a is also elevated upon neomycin treatment. This correlates with the expression of Atoh1a. This study showed that Atoh1a is upstream of Atp2b1a to regulate hair cell progenitor proliferation and differentiation.

The hair cells of zebrafish, in particular, are sensitive to the action of several drugs and heavy metals. For example, aminoglycoside antibiotics, such as gentamycin, neomycin and streptomycin, that are widely used to treat patients with infection problems have been shown to affect the lateral line hair cells (Gobba, 2003). The similar results were obtained from the heavy metal, such as cadmium, metallothionein and copper, treated zebrafish that showed disruption of hair cells (Blechinger et al., 2007; Chen et al., 2007; Gobba, 2003; Hernández et al., 2006; Johnson et al., 2007; Linbo et al.,

2006). The mechanisms of hair cell disruption by these agents are still to be resolved. However, some mechanisms have been proposed of how the hair cell death occurs. At least two mechanisms have been studied, which are the formation of free radicals and apoptotic cell death pathways (Forge and Schacht, 2000). The major interfere of these toxicants are on the cation channels that are embedded in the stereocilia of hair cells, thus accelerates the formation of free radicals and lead to hair cell death through apoptotic pathway (Forge and Schacht, 2000). Chemical screens have been done to identify compounds that induce hair cell loss (ototoxins) and others that protect hair cells (protectants) from known toxins and the potential application of these screens to human medicine (Chiu et al., 2008; Coffin et al., 2010; Ou et al., 2007; Owens et al., 2008).

Hair cell regeneration in the lateral line system has been studied extensively to couple the hair cell progenitor production and location (López-Schier and Hudspeth, 2006). Hair cells regenerate after killing with ototoxic drug, such as copper sulphate (Hernández et al., 2006). The doses and times of copper exposure have been determined to cause reversible and irreversible damage to the zebrafish hair cells (Hernández et al., 2007). High dose of copper causes regeneration of hair cell in posterior lateral line mainly from the proliferation of precursor cells while low dose of copper results in regeneration of hair cells from non-dividing precursor cells (Hernández et al., 2007). This study was performed using transgenic fish that bore GFP in hair cells and hair cell progenitors, SqET4, and in mantle cells, SqET20 (Choo et al., 2006; Parinov et al., 2004). Hernández *et al.* (2007) also analyzed the expression of *atoh1a* and *eya1* genes. These two genes were downregulated upon copper treatment. However, *atoh1a* and *eya1* genes reappeared during recovery times. The *sox2* gene, a neural stem cell marker, was expressed in cells other than hair cells or SqET4-positive cells (Hernández et al., 2007). The Sox2 were partially colocalized with SqET20-positive cells. The authors hypothesized that supporting cells expressing

Sox2 could give rise to new hair cells after damage and support the regeneration in zebrafish neuromasts. This assumption was verified by showing that the expression of Sox2 is maintained after copper treatment. This supports the idea that supporting cells still expressing Sox2 survive the treatment and then serve as hair cell precursors.

A very recent study showed that hair cells can regenerate after neomycin treatment from a transient increase in supporting cell proliferation which is accompanied with an upregulation of *notch3a*, *deltaA* and *atoh1a* (Ma et al., 2008). It could be shown that Notch signaling limits the number of hair cells produced during regeneration by regulating supporting cell proliferation.

A new mutation has been found to affect hair cell regeneration in zebrafish lateral line system. The gene called *phoenix* is involved in the regulation of process that allow supporting cells to enter mitosis after hair cell damage (Behra et al., 2009). The number of hair cells in the mutant prior to neomycin or copper treatment was comparable to wild-type counterpart. But the number of hair cells was greatly reduced upon neomycin or copper treatment. This is also accompanied by reduced cell proliferation activity of supporting cells (Behra et al., 2009).

## **1.2 Eya1 functions as protein tyrosine phosphatase and transcription co-activator**

Eya is a member of Retinal Determination Gene Network (RDGN) that plays important role in the development of *Drosophila* eye (Donner and Maas, 2004; Silver and Rebay, 2005). Apart from Eya, other members of *Drosophila* RDGN are Pax6-like homeodomain proteins, which are Eyeless (Ey) and

Twin of Eyeless (Toy) and Eya's binding partners which are Six1 and Dach. The structure of Eya family has already been study excessively. There are four paralogs of Eya in mammals, Eya1-4 (Abdelhak et al., 1997a; Borsani et al., 1999; Xu et al., 1997b; Zimmerman et al., 1997). *Drosophila* in the other hand has two isoforms of Eya that result from alternative splicing (Bonini et al., 1993; Leiserson et al., 1998). In zebrafish, there are at least three paralogs that are found, Eya1, Eya3 and Eya4 (Kozlowski et al., 2005; Nica et al., 2006; Sahly et al., 1999). The structure of Eya protein family has been known that contains Eya domain (ED), required for the interaction with other co-factors, Six and Dach, and also phosphatase catalytic domain (Chen et al., 1997; Pignoni et al., 1997; Rayapureddi et al., 2003; Tootle et al., 2003; Zimmerman et al., 1997). Eya is required for proper development of *Drosophila* eye. But the function in vertebrate eye is still in debate. Mutations in human *eya1* gene result in brachio-oto-renal (BOR) and brachio-oto (BO) syndromes (Azuma et al., 2000; Xu et al., 1997b). Although the ocular defects and congenital cataracts have accompanied to these syndromes, eye defects are largely absent. The same pathological symptoms have been observed in mice (Azuma et al., 2000; Xu et al., 1999).

The conservation of catalytic and transcription domains is shown in Figure 6. The Eya1 protein in animal kingdom is highly conserved with four adjacent motifs are found. These motifs were spread over ~250 amino acids and formed  $\alpha/\beta$  folds of HAD family protein to form an active site (Hisano et al., 1996). Motif I showed the consensus sequence DXDX(T/V) with the first aspartate function as the nucleophile (Collet et al., 1998; Lahiri et al., 2002). Motif II is defined by a serine or threonine residue and motif III by a lysine residue (Lahiri et al., 2002). Motif IV's consensus sequence is characterized by GDX<sub>(3-4)</sub>D sequence (Thaller et al., 1998). Despite the fact that Eya1 is transcription factor, it does not have DNA-binding domain (Ohto et al., 1999). To operate as other transcription factors, Eya1 requires co-factors that will help Eya1 to regulate gene expression through either *cis*-

or *trans* interactions (Mutsuddi et al., 2005; Silver et al., 2003). At least two known co-factors have been discovered, Six gene family (Ohto et al., 1999) and Dach gene family (Chen et al., 1997; Li et al., 2002; Zimmerman et al., 2000). The Six- and Dach-binding regions of Eya1 are located in the Eya Domain (ED) at the C-terminal together with HAD motifs (Figure 7). However, recent finding showed that transcriptional activities of Eya works independently from phosphatase activities (Xiong et al., 2009).

## 1.2.1 Conservation of Eya1 protein across animal kingdom.

Dm	GRARGRRHQPSPTRSTASDTGNSEAVKPPERVFVW	<b>DLDET</b> LIIFHTLLSGSYAN--RYT	520
Ag	GRARGRRHAHPSPTRSSTSEPGIS--EKAPERIFVW	<b>DLDET</b> IIIFHSLLTGSYAG--RYN	253
Hs	-RGRGRRNNNPSPPPDS-----	LERVFIW <b>DLDET</b> IIVFHSLLTGSYAN--RYG	344
Pt	-RGRGRRNNNPSPPPDS-----	LERVFIW <b>DLDET</b> IIVFHSLLTGSYAN--RYG	349
Bt	-RGRGRRNNNPSPPPDS-----	LERVFIW <b>DLDET</b> IIVFHSLLTGSYAN--RYG	344
Rn	-RGRGRRNNNPSPPPDS-----	LERVFIW <b>DLDET</b> IIVFHSLLTGSYAN--RYG	344
Cf	-RGRGRRNNNPSPPPDS-----	LERVFIW <b>DLDET</b> IIVFHSLLTGSYAN--RYG	342
Gg	-RGRGRRNNNPSPPPDS-----	LERVFIW <b>DLDET</b> IIIFHSLLTGSYAN--RYG	353
Dr	-RGRGRRNNNPSPPPDS-----	LERVFIW <b>DLDET</b> IIVFHSLLTGSYAN--RFG	366
At	--MNNDTSKKLGLTLVSDDG-----	PVNVYVW <b>DMDET</b> LILLRSLNLTGTAESFNLS	48
Os	--MDGVVAASADATRDEIK-----	IMNVYIW <b>DMDET</b> LILLKSLDGSYAGAFDGL	48
Dm	KDHSSLMTIAFRMEEMVFNMADTHFFNEIEECDQVHIDDVSSDDNGQDL	SAYNFATDGF	580
Ag	KNRDHQVQLGYRMEELIFNMADAYFFFNDEECDQIHIDDVASDDNGQDL	NNYNFAADGF	313
Hs	R-----	ECQVHIDDVSSDDNGQDLSTYNFGTDGF	374
Pt	RDPPTSVSLGLRMEEMIFNLADTHLFFNDEECDQVHIDDVSSDDNGQDL	STYNFGTDGF	409
Bt	RDPPTSVSLGLRMEEMIFNLADTHLFFNDEECDQVHIDDVSSDDNGQDL	STYNFGTDGF	404
Rn	R-----	ECQVHIDDVSSDDNGQDLSTYNFGTDGF	374
Cf	RDPPTSVSLGLRMEEMIFNLADTHLFFNDEECDQVHIDDVSSDDNGQDL	STYNFGTDGF	402
Gg	RDPPTSVSLGLRMEEMIFNLADTHLFFNDEECDQVHIDDVSSDDNGQDL	STYNFGTDGF	413
Dr	RDPPTSVSLGLRMEEMIFNLADTHFFNDEECDQVHIDDVSSDDNGQDL	STYNFSTDGF	426
At	KDVKRGEIGRMWEKHILKICDDFFFEQVEECNEPFLDSLQYDDGKDL	SRYEYFKQDDF	108
Os	<u>KDHDKSVDIGRKENLLELCDEHFFYEEIENYNEPFLSAVKEYDDGKDL</u>	<u>TTTYDFEADCF</u>	108
Dm	HTNTPPGAPPNLCPLTGVRCGVDWMRKLAFRYRKIKDIYNSYRGNVGTL	LGPQKREAWLQ	640
Ag	HTATPQGAPPNVCLPNGVRCGVDWMRKLAFRYRKIKDTYNTYRNNVG	LLGPQKRDHWLQ	373
Hs	PAAATS---ANLCLATGVRCGVDWMRKLAFRYRRVKEIYNTYKNNVG	LLGPQKREAWLQ	431
Pt	PAAATS---ANLCLATGVRCGVDWMRKLAFRYRRVKEIYNTYKNNVG	LLGPQKREAWLQ	466
Bt	PAAATS---ANLCLATGVRCGVDWMRKLAFRYRRVKEIYNTYKNNVG	LLGPQKREAWLQ	461
Rn	PAAATS---ANLCLATGVRCGVDWMRKLAFRYRRVKEIYNTYKNNVG	LLGPQKREAWLQ	431
Cf	PAAATS---ANLCLATGVRCGVDWMRKLAFRYRRVKEIYNTYKNNVG	LLGPQKREAWLQ	459
Gg	PAAATS---ANLCLATGVRCGVDWMRKLAFRYRRVKEIYNTYKNNVG	LLGPQKREAWLQ	470
Dr	HAAATS---ANLCLATGVRCGVDWMRKLAFRYRRVKEIYTTYKNNVG	LLGPQKREAWLQ	483
At	STPTDDLN-----	KRKLAYRHRAVAERY---EKGLCPFIDSEMSGLDE	149
Os	<u>SSPYDDLN-----</u>	<u>KRKLAYRHRAIGEKY---TKGLEKILDHMHKIVWND</u>	149
Dm	IRSEIEVATDNWATLALKCL	SMISQ-----RENCVN <b>VLVT</b> STOLAPALAKVL	687
Ag	VRSDIEHETDSWHSLTLKCLNMIAQ-----	RENCVN <b>VLVT</b> TTQLVPALAKIL	420
Hs	LRAEIEALTDSWLTLALKALSLIHS-----	RTNCVN <b>VLVT</b> TTQLIPALAKVL	478
Pt	LRAEIEALTDSWLTLALKALSLIHS-----	RTNCVN <b>VLVT</b> TTQLIPALAKVL	513

```

Bt  LRAEIEALTDSWLTALAKALSLIHS-----RTNCVNIILVTTTQLIPALAKVL 508
Rn  LRAEIEALTDSWLTALAKALSLIHS-----RANCVNIILVTTTQLIPALAKVL 478
Cf  LRAEIEALTDSWLTALAKALSLIHS-----RTNCVNIILVTTTQLIPALAKVL 506
Gg  LRAEIEALTDSWLTALAKALSLIHS-----RTNCVNIILVTTTQLIPALAKVL 517
Dr  LRAEIEALTDSWLTALAKALSLIHS-----RSNCVNIILVTTTQLIPALAKVL 530
At  LYNVTDEYTDRLWSSARAFLEQCSCEVESSDGTSAIEQSSQDIHILVTSGALIPSLVKCL 209
Os  LYSATDKYTDGWLSSAHKLLEEAMG---KSTAESTAKHSS--INCIVTSGSLIPSLAKCL 204
-----

Dm  LFGLGGIFNIENIYSAHKIGHETCYERIVTRFGR-KSTYVVIGDGNEEETAAKAMNFPFW 746
Ag  LYGLGVFPVENIYSAHKIGKEQCFERIVTRFGR-KSTYVVVGDGQDEENAAKNLNFPFW 479
Hs  LYGLGIVFPIENIYSATKIGKESCFERIIQRFGR-KVVYVVIGDGVVEEEQGAKKHAMPFW 537
Pt  LYGLGIVFPIENIYSATKIGKESCFERIIQRFGR-KVVYVVIGDGVVEEEQGAKKHAMPFW 572
Bt  LYGLGIVFPIENIYSATKIGKESCFERIIQRFGR-KVVYVVIGDGVVEEEQGAKKHAMPFW 567
Rn  LYGLGIVFPIENIYSATKIGKESCFERIIQRFGR-KVVYVVIGDGVVEEEQGAKKHAMPFW 537
Cf  LYGLGIVFPIENIYSATKIGKESCFERIIQRFGR-KVVYVVIGDGVVEEEQGAKKHAMPFW 565
Gg  LYGLGVVFPPIENIYSATKIGKESCFERIIQRFGR-KVVYVVIGDGVVEEEQGAKKHAMPFW 576
Dr  LYGLGVVFPPIENIYSATKIGKESCFERIIQRFGR-KVVYVVIGDGVVEEEQGSKKHNPFW 589
At  LFRLDTFLLRHENVYSSIDVGKLQCFKWKIKERYDGNVRFCAIGDGWEECAAAQALQWPFV 269
Os  LYRLDDVVAFENVYSSWEVGLQCFKWKIKERYDGNVRFCAIGDGHEECTAAQIMKWPFV 264
-----

Dm  RISAHSDIRALYTALDMGFL----- 766
Ag  RISSHSDIRSLHTALEMGFL----- 499
Hs  RISSHSDLMALHHALELEYL----- 557
Pt  RISSHSDLMALHHALELEYL----- 592
Bt  RVSSHSDLMALHHALELEYL----- 587
Rn  RVSSHSDLMALHHALELEYL----- 557
Cf  RISSHSDLMALHHALELEYL----- 585
Gg  RISSHSDLMALHHALELEYL----- 596
Dr  RISSHSDLMALHHALELEYL----- 609
At  KIDLQPDSSHRFPGLTPKTVSYFFAAVYGNADSSKE 307
Os  KIEFHPDAPHRFPGLNLTPIHRIMDVTYDSSNDG--- 299

```

**Figure 6. Partial alignment of Eya1 protein across kingdom.** Haloacid dehalogenase (HAD) motifs are highlighted. Interaction domain with Six family is shown by solid line and with Dach family is shown by dashed line. Mutations found in human are indicated by bold abbreviations, adapted from Mutsuddi *et al.* (2005). Hs: *Homo sapiens* (NP\_742056.1); Pt: *Pan troglodytes* (XP\_001164379.1); Cf: *Canis familiaris* (XP\_849806.1); Bt: *Bos taurus* (DAA22681); Rn: *Rattus norvegicus* (XP\_578437.2); Gg: *Gallus gallus* (XP\_418290.2); Dr: *Danio rerio* (NP\_571268.1); Dm: *Drosophila melanogaster* (NP\_723188.1); Ag: *Anopheles gambiae* str. PEST (XP\_314837.2); At: *Arabidopsis thaliana* (NP\_565803.1); Os: *Oryza sativa* (NP\_001056580.1). Alignments were generated using ClustalW.

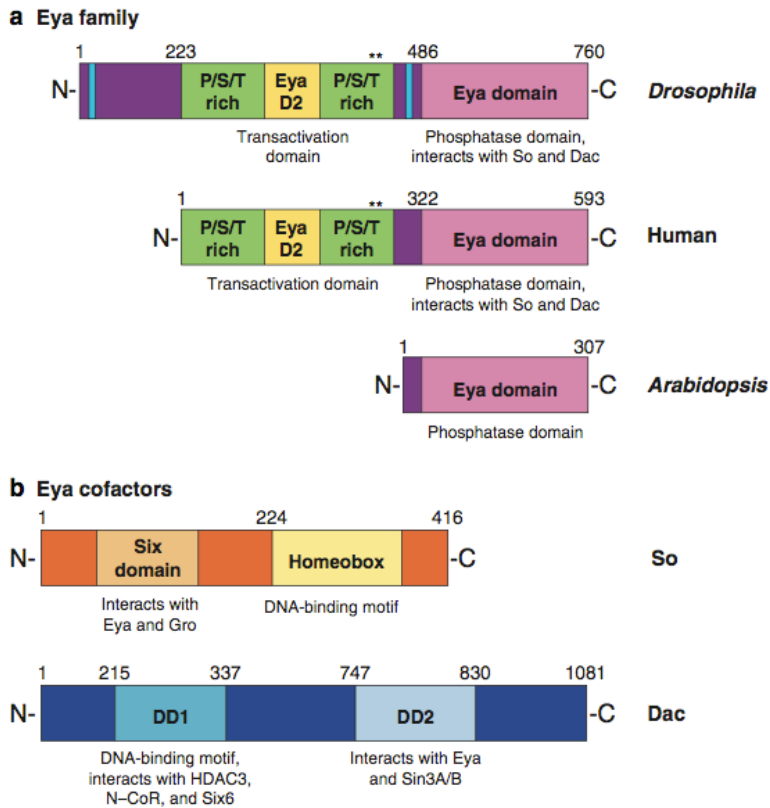


**Figure 7. Domain structures of Eyes absent (Eya) and its retinal determination gene network binding partners. (a)** Drosophila Eya (DmEya), Human Eya1, and Arabidopsis Eya (AtEya). Numbers represent the amino Acid number; C, C terminus; EyaD2, Eya domain 2; N, N terminus; P/S/T, proline/serine/threonine. Double asterisks (\*\*) represent conserved mitogen-activated protein kinase phosphorylation sites; blue Bars indicate predicted nuclear localization sequences at amino acids 1–23 and 457–465 in DmEya. For DmEya, the P/S/T-rich regions stretch from amino acid 223 to 438. The Eya domain of AtEya starts at Amino acid 21. **(b)** Drosophila members of the Six (So) and Dachshund (Dac) families are represented. Abbreviations: N-CoR, nuclear receptor corepressor; DD1, Dachshund domain 1; DD2, Dachshund domain2; Gro, Groucho; HDAC3, histone deacetylase 3; Sin3A, Sin 3 homolog A. Adapted from Silver & Rebay (Source of this figure is from Silver & Rebay, 2005).



## 1.2.2 Eya1 mutant phenotypes

Zebrafish *eya1* cDNA has been cloned and the protein showed 84.7% identity with the human Eya1 (Sahly et al., 1999). Several mutant alleles in *eya1* gene have been identified in *dog-eared* zebrafish mutants, *dog<sup>tm90</sup>*, *dog<sup>tp85b</sup>* and *dog<sup>lc257e</sup>* (Kozlowski et al., 2005) and *aal<sup>l22744</sup>* (Herzog et al., 2004; Nica et al., 2006). The mutations effecting *eya1* allele were represented in Figure 8.

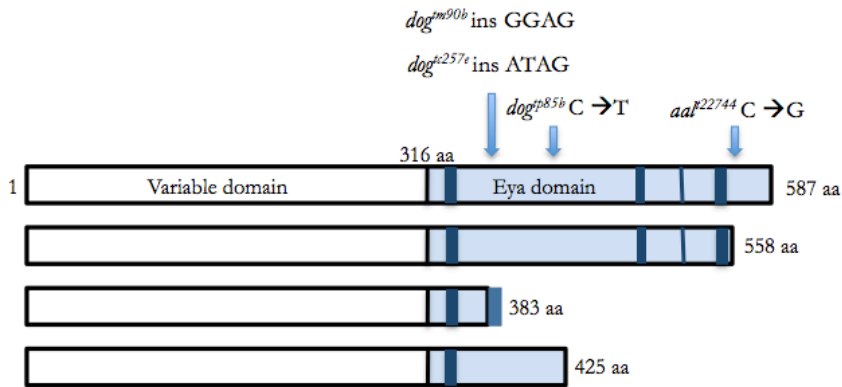


Figure 8. The representation of *dog-eared* locus encodes *eya1*. Box diagrams depict the wild-type, first panel, *dog<sup>tm90</sup>* and *dog<sup>lc257e</sup>*, second panel, *dog<sup>tp85b</sup>*, third, and *aal<sup>l22744</sup>*, last panel. Dark blue boxes depict the four motifs in Eya domain (this figure is modified from Kozlowski *et al.*, 2005 and Nica *et al.*, 2006).

*dog<sup>tm90</sup>* and *dog<sup>lc257e</sup>* give the same number of base insertion but two different types of bases. These insertions introduce a stop codon due to a frame-shift on the splice donor sequence and give rise to truncated proteins that are missing a big part of ED (Fig. 8, (Kozlowski et al., 2005). While *aal<sup>l22744</sup>* allele introduces a stop codon and cuts the last 29 amino acids of ED but leaves the motifs characteristic of HAD keep intact (Fig. 8, (Nica et al., 2006). All

the mutants identified in these screenings showed similar phenotypes to each other. This suggests that the 29 aa are indispensable to Eya1 function. Moreover, these amino acid residues are highly conserved cross animal kingdom with 90% conservation (Fig. 7). In this thesis, I used two *dog* alleles, *dog<sup>tm90</sup>* and *aal<sup>l22744</sup>*, during the study. The most used mutant allele was *dog<sup>tm90</sup>* since this allele gave the most severe truncation on the Eya1 protein.

## 1.3 Aims and Outlines of the Thesis

### 1.3.1 Aims

The first aim of this thesis is to study the basic mechanisms underlying homeostasis of morphogenetic territories. Specifically I wanted to explore the function of Eya1 during tissue remodeling with the zebrafish lateral line primordium as a model system. The second aim of this thesis is to investigate the establishment of bilateral symmetry in developing tissue and tissue repair. This will specifically be addressed using mechanosensory hair cell during development and regeneration in the neuromasts of zebrafish lateral line system. The last aim of this thesis is to demonstrate the contribution of epigenetics during vertebrate development. This is aimed at validating *in vivo* the function of macroH2A in developing zebrafish embryos. I use forward- and reverse-genetic analysis in combination with pharmacological approaches to demonstrate the biological processes in questions. The state-of-the-art in imaging technologies is employed to gain insight into the cellular basis in fixed and live tissues.

### 1.3.2 Outlines of the Thesis

**Chapter 1** of this thesis introduces the system that is used and the important biological knowledge that is receiving increased attention.

In **Chapter 2**, I report the participation of Eya1 in the combinatorial activity of Fgf and Wnt/ $\beta$ -catenin signaling. I demonstrate the importance of Eya1 during the development of posterior lateral lines in zebrafish. This study is based on the observations done in the mutations of Eya1 (*eya1/dog-eared*) that produce defects in the ear and lateral line. Hair cells in these organs initially develop, but are not maintained and the organs of the lateral line eventually degenerate after few days of development. In order to analyze the activity of Eya1 in lateral line development, we will employ several approaches, such as reverse- and forward-genetic approaches. I use several zebrafish mutant alleles of Eya1 that abrogate all function of the protein. Here, I show that Eya1 is necessary for the production of a complete number of neuromasts in the posterior lateral line since the mutation in this protein results in truncation of posterior lateral line. I then demonstrate that instead of neuromast survival, the persistent migration of posterior lateral line is affected if Eya1 is lost. In this study, I also demonstrate the rosette formation delay which may indicate the defects of mesenchymal-to-epithelial transition. In correlation to the chemokine signaling, I analyze the two well-known chemokine receptors, CXCR4 and CXCR7, and one chemokine ligand, SDF1a/CXCL12, that involve in the proper directionality of primordial migration. Results indicate that Eya1 regulates the expression of CXCR7 since there is a reduction of CXCR7 expression due to Eya1 loss-of-function. I also demonstrate in Chapter 2 that Eya1 is essential to regulate the expression of Dkk and Fgf signaling. Finally, I discuss the influence of Eya1 on the homeostasis of Fgf and Fgf and Wnt/ $\beta$ -catenin signaling during migration of lateral line primordium.

Study discussed in **Chapter 3** is a collaboration work with another Ph.D. student, Filipe Pinto-Teixeira, in our research laboratory. In this study, we used a combination of genetic and pharmacological studies and high-resolution time-lapse videomicroscopy to better understand the biological questions that we ask. In Chapter 3 we analyze and discuss the compartmentalization in the neuromast and the signaling mechanisms that trigger cellular response after damage or during development. We also report that there is a polar compartment in the neuromast and that Notch signaling is activated outside this compartment to control the production of hair cells. Since there is still a discussion on which biological processes involved in the production of hair cells in the neuromast, we also examine the mitotic proliferation during hair cell regeneration in combination with pharmacological approach to block specific cell cycle phase. Here, we explain that mitosis is essential for hair cell regeneration since the BrdU and blocking of cell cycle result in complement observations. We also demonstrate that there is planar cell inversions involved in the bilateral symmetry during neuromast recovery after damage. We also explain that polar compartment is characterized by low Notch activity and indicate that this compartment is neither a niche nor a place harboring stem cells since cells that give rise to the hair cell progenitors appear from elsewhere rather than polar compartment itself. During hair cell regeneration in neuromast, we observe that the directional regeneration is controlled by Notch signaling that in turn controls the production of hair cells. Finally, in Chapter 3, we discuss the importance of centrifugal movement of hair cell progenitors to propagate and maintain bilateral symmetry in the neuromasts.

In brief, I will discuss a research done by a collaboration with a research group at our centre, Luciano di Croce's Group, to study the epigenetics in development. This study is mentioned in **Chapter 4** that consists of several observations regarding zebrafish development. Based on the microarray analysis in human male pluripotent cells that shows the macroH2A variants

occupy at many genes encoding key regulators of development and cell fate decisions, we then make observations on the zebrafish macroH2A by using gain- and loss-of-function analysis. This *in vivo* analysis on zebrafish demonstrates that macroH2A is essential for normal embryogenesis. I indicate in Chapter 4 that several genes involved in brain segment development are regulated by loss of macroH2A function by injecting morpholino oligos. Injection experiment on zebrafish embryos using human macroH2A mRNA together with morpholino rescue the morphant phenotypes, indicating the functional conservation across species.

Finally, in the **Chapter 5** of this thesis, I summarize the overall results and discuss the importance of our findings on both migration of lateral line primordium and hair cell regeneration as well as perspectives for future directions.

"It is not birth, marriage, or death, but gastrulation which is truly the most important time in your life."

- *Lewis Wolpert* -

# Chapter 2

## **Eya1 is essential for the homeostasis of FGF and Wnt/ $\beta$ -catenin signaling during tissue remodeling**

**Indra Wibowo, Andrea Durán-Sánchez and**

**Hernán López-Schier**

*Laboratory of Sensory Cell Biology & Organogenesis, Centre de Regulació*

*Genòmica, Doctor Aiguader 88, (08003) Barcelona, Spain*

*Submitted manuscript*

## 2.1 Abstract

Long-range intercellular communications are indispensable for organogenesis. Tissue remodeling during growth, repair or disease presents an enormous challenge to the stability of signaling territories. For example, during the invasive migration of the zebrafish lateral-line primordium, the iterative conversion of mesenchymal cells into epithelial rosettes depends on their rapid and concurrent loss of Wnt/ $\beta$ -catenin and activation of FGF signaling within a small transition zone. Here we provide direct evidence that *Eya1*, mutated in the branchio-oto-renal syndrome in humans, is essential to maintain the transition zone. We propose that combinatorial Wnt/ $\beta$ -catenin and FGF signaling control the spatiotemporal profile of *Dkk1* expression to dynamically confine Wnt/ $\beta$ -catenin to the mesenchyme. These results underscore a robust genetic network that governs the homeostasis of morphogenetic territories in a constantly remodeling tissue.

## 2.2 Introduction

Morphogenesis and pattern formation are fundamental for the compartmentalization and division of work by different cellular groups in multicellular organisms. Secreted proteins with morphogenetic capacity spread across tissues several cell diameters away from their source (Vincent and Dubois, 2002). Organogenesis frequently involves a balance between the propagation of secreted morphogens that co-opt cells to acquire specific fates, and the spatial restriction of their influence to permit cellular diversity to arise (Dessaud et al., 2007; Jaeger and Martinez-Arias, 2009). Cellular proliferation, intercalation and migration pose enormous challenges to the



control of the spatial activity of secreted morphogens (Dahmann et al., 2011). The mechanisms that regulate morphogenetic territories in remodeling tissues are almost entirely unknown (Wartlick et al., 2009). The Wg/Int-1 (Wnt) and Fibroblast Growth Factor (FGF) families of secreted signaling proteins are essential for a variety of fundamental biological processes that include embryonic development, organ regeneration and stem-cell physiology (Aulehla et al., 2008) (Dodé et al., 2003; Goessling et al., 2009). These morphogens have also been implicated in numerous pathological conditions affecting epithelial dynamics, such as cancer, inflammation and wound healing (Grigoryan et al., 2008; Nguyen et al., 2009; van Amerongen and Nusse, 2009). One example of a remodeling tissue whose development depends on the concerted activity of the Wnt/ $\beta$ -catenin and FGF pathways is the lateral-line system of the zebrafish (Aman and Piotrowski, 2008; Lecaudey et al., 2008; Nechiporuk and Raible, 2008). The posterior lateral line develops during embryogenesis from a group of just over 100 cells that migrate collectively as a primordium invading the animal's trunk and tail (Figure 1a-b) (Ghysen and Dambly-Chaudière, 2007; Lecaudey and Gilmour, 2006). The primordium is compartmentalized along its long axis, which runs parallel to the migratory pathway. A mitotically active leading area contains around 30 cells that display a mesenchymal behavior, whereas trailing cells form epithelial rosettes that are deposited periodically as discrete groups, the neuromasts, during migration (Figure 1c). The directionality and persistence of primordium migration is mediated by the complementary expression pattern of the CXCR4b and CXCR7b chemokine receptors. Leading primordial cells express CXCR4b, whereas CXCR7b is expressed by trailing cells (Figure 1c). In a transition zone the expression of both chemokine receptors overlaps. CXCR4b controls directional migration upon binding the Sdf1a/CXCL12 chemokine expressed along the embryo's trunk and tail (David et al., 2002; Haas and Gilmour, 2006). CXCR7b also binds Sdf1a/CXCL12 but the prevalent view suggests that it acts as a decoy

receptor that create a chemokine gradient along the migratory path to allow persistent forward migration (Boldajipour et al., 2008; Dambly-Chaudiere et al., 2007; Knaut and Schier, 2008; Valentin et al., 2007). Most of the cells that express CXCR7b are lost when the rosettes are deposited. Thus, the primordium must periodically regenerate the CXCR7b expressing cells to maintain migratory persistence. The current model to explain lateral-line formation involves intercellular signals that act on non-overlapping parts of the moving primordium. The primordial leading region activates  $\beta$ -catenin (Figure 1c). The activating signal is likely to be a Wnt protein because its activity range is controlled by the extracellular Wnt inhibitor Dkk1 (Aman and Piotrowski, 2008). Mesenchymal-to-epithelial transitions (MET) and rosetogenesis are under the control of FGF signaling acting within the primordial trailing region.

The leading and trailing regions represent morphogenetic “territories”, as opposed to “compartments”, because they are not defined by lineage but are dynamically maintained by continuous signaling (Theisen et al., 1996). Thus, the lateral-line primordium faces the challenge of maintaining the spatial domains of Wnt/ $\beta$ -catenin and FGF signaling while undergoing periodic losses of the trailing epithelium and expansions of the leading mesenchyme. Therefore, this system is ideal to study the mechanistic bases underlying the homeostasis of morphogenetic territories. Seminal work has demonstrated that tightly regulated interactions between Wnt/ $\beta$ -catenin and FGF signaling are at the core of this process (Figure 1d) (Aman and Piotrowski, 2008; Ma and Raible, 2009). However, the complexity of their interactions has made it difficult to clarify how the dimensions of the morphogenetic territories are monitored and maintained. Here we combine forward- and reverse-genetic analyses with pharmacology, gene expression profiling and high-resolution quantitative live imaging to find an essential component of the gene- regulatory logic underlying the homeostasis of FGF and Wnt/ $\beta$ -catenin signaling during primordium migration.

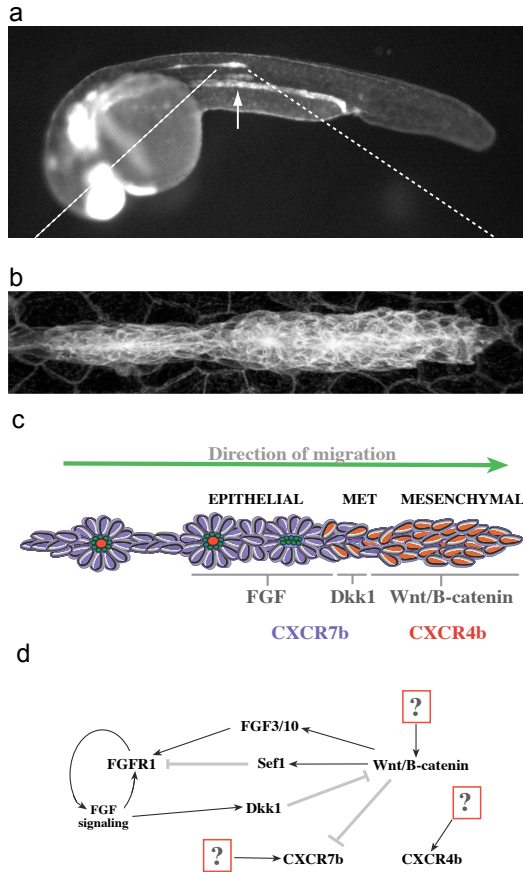


**Figure 1. Posterior lateral line primordium and genetic network involved in primordial remodeling.** (a) Confocal image of a *Tg[CldB:lynEGFP]* embryo at 32 hpf showing strong EGFP expression in the posterior lateral-line primordium (white arrowhead). (b) Magnification of the posterior lateral-line primordium of a confocal image of a *Tg[CldB:lynEGFP]* embryo at 32 hpf. (c) Scheme of the posterior lateral-line primordium depicting a leading zone composed by cells with mesenchymal characteristics (red), followed by a zone of mesenchymal-to-epithelial transition (MET) (red+purple), and ending with epithelial rosettes in the trailing zone (purple). In the leading zone Wnt/ $\beta$ -catenin signaling is activated, its inhibitor Dkk1 is expressed at the MET. Epithelial cells activate FGF signaling. Two chemokine receptors are expressed in complementary fashion. CXCR4b (red) in the leading zone whereas CXCR7b (lilac) is expressed in the trailing zone. Their expression overlaps in the transition zone. (d) Schematic representation of current genetic network that maintains primordium compartmentalization and migratory persistence. The arrows indicate activation and the T-bars inhibition. The question marks indicate that sources of activation or inhibition are unknown.

## 2.3 Materials and Methods

### Zebrafish animals and strains

Fish used were maintained under standardized conditions and experiments were performed in accordance with protocols approved by the PRBB Ethical Committee of Animal Experimentation. Eggs were collected from natural spawning and maintained at 28.5°C, embryos were staged by hour post-fertilization (hpf). Two *dog/eya1* mutant alleles were used in this study, *aalt22744* and *dogtm90* (Kozłowski et al., 2005; Nica et al., 2006). Embryos were genotyped according to Kozłowski *et al.* (Kozłowski et al., 2005). Both alleles showed identical phenotypes in all results obtained. In this study we mainly used the *dogtm90* allele. The Apc allele was *mcr* (Haramis et al., 2006). Transgenic lines used were SqET10, SqET20, SqET4 (Parinov et al., 2004), Tg[Cldnb:lynEGFP] (Haas and Gilmour, 2006), Tg[hs70:ca-FGFR1] (Lee et al., 2005), Tg[hs70:EGFP-Dkk1] (Stoick-Cooper et al., 2007), Tg[erm:Gal4;UAS:Kaede] (Esain et al.). For live imaging, *dogtm90* carriers were crossed to transgenic fish and homozygous mutants were identified by the ear defects. Heat-shock treatments were performed by immersing 2-ml Eppendorf tubes containing the embryos in E3 medium in a water bath at 39°C during 20 min.

### Drug treatments

To inhibit Wnt signaling, 10 mM stock solutions of IWR-1 drugs (Millipore) diluted in DMSO were used. Twenty-four zebrafish embryos were dechorionated and allowed to develop in E3 medium supplemented with 75-100 µM IWR-1-endo or IWR-1-exo or in 0.1% DMSO as a control.

## DNA constructs

To make dominant negative Eya1, *Danio* Eya1 cDNA was amplified using forward primer:

(Eya1\_KOZAK\_NotI\_Fw):

CGGCGGCCGCTGCCACCATGGAAATGCAGGATCTAGC and

reverse primer:

(Eya1\_her6WRPWstop\_XhoI\_Rv):

CCTGGAGCTACCAAGGCCGCCACACCAAGGCCGCCACAAATACT  
CCAGGTCCAG.

The 5' end of the amplicon was cloned between NotI and XhoI restriction sites in pCS2+ vector for synthetic cRNA production.

## mRNA and morpholino antisense oligonucleotides

cRNAs were synthesized using T7/SP6/T3 RNA polymerase according to manufacturer's instructions (mMessage mMachine, Ambion). Dominant-negative or full-length Eya1 cRNAs were injected into 1-2-cell stage embryos. Morpholinos that were used in this study were: Eya1 mo (5'-AAACAAAGATGATAGACCTACTTCC-3') (Kozłowski et al., 2005), Six1b (5'-CGAAAGAAGGCAACATTGACATGAC-3'), a gift from V. Korzh (Bessarab et al., 2004) and p53 (5'-GCGCCATTGCTTTGCAAGAATTG-3') (Langheinrich et al., 2002).

## DIASP staining

For vital labeling hair cell, E3 medium containing a 500  $\mu$ M DiASP solution were used to immerse the fish larvae for 5 min at room temperature in the

dark. Larvae were immediately washed with E3 medium to get rid of excessive dye and then anesthetized by using 0.02% tricaine (Ethyl 3-aminobenzoate methanesulfonate salt, A5040, Sigma).

### **BrdU treatment**

10 mM 5-Bromo-2'-deoxyuridine (BrdU, B5002, Sigma) stock solution in DMSO was diluted to 10  $\mu$ M in E3 medium and used to soak embryos. BrdU was incorporated into newly synthesized DNA in the S-phase; therefore, it functioned as a marker for cell proliferation. Embryos at 24 hpf were dechorionated and allowed to develop in this solution until desired stages. Embryos were fixed in 4% Paraformaldehyde (PFA) overnight at 4°C and then used for immunohistochemistry.

### **TUNEL assays**

Apoptosis in the migrating primordium was identified using terminal transferase-mediated dUTP nick end-labeling (TUNEL) assay according to manufacture's instruction with minor modifications (In situ Cell Death Detection Kit, TMR Red, Roche). Embryos at 30-42 hpf were dechorionated and fixed in 4% PFA overnight at 4°C, then stored in 100% methanol at -20°C for at least 1 day. They were rehydrated, permeabilized in 10  $\mu$ g/ml Proteinase K in 0.1% PBSTw and post-fixed in 4% PFA then washed several times in 0.1% PBSTw. Embryos were then incubated in fresh TUNEL buffer for 1 h followed by incubation in the TUNEL reaction mix for 3 hrs at 37°C in dark. As negative control, embryos were incubated in TUNEL buffer only. As positive control, embryos were first incubated in polymerase chain reaction buffer containing 3 U/ml DNase I recombinant (Roche) for 1 h at 37°C before incubation in TUNEL reaction mix. After the reaction,

embryos were washed several times in 0.1% PBSTw at room temperature and stored in 0.1% PBSTw containing Vectashiled mounting medium with DAPI (VectorLabs).

## **Whole-mount immunohistochemistry and in situ hybridization**

For immunohistochemistry and ISH, staged embryos were dechorionated and fixed in 4% PFA for overnight at 4°C and washed several times with 0.1% Tween-20-containing Phosphate Buffer Saline (0.1% PBSTw). For immunohistochemistry, larvae were immediately blocked in 10% Bovine Serum Albumin (BSA) for at least 2 hours. Incubation with primary antibody was done overnight at 4°C. Primary antibodies and monoclonal antibodies were used at the following dilutions: mouse monoclonal antibody anti-BrdU, 1:100 (Upstate), rabbit anti-N-cadherin, 1/500. Texas red-labeled donkey anti-mouse and -rabbit and Cy5-labeled donkey anti-mouse and -rabbit immunoglobulin secondary antibodies (Jackson ImmunoResearch) were used at 1/150. For BrdU labeling detection, before blocking and applying primary antibody anti-mouse, additional steps were needed to permeabilize the nuclear membrane and to denature DNA strands. Larvae were incubated with 10 µg/ml Proteinase K in 0.1% PBSTw for 20 min at room temperature. Immediately afterwards, larvae were post-fixed in 4% PFA for 15 min and washed several times in 0.1% PBSTw. To denature DNA, samples were incubated in fresh 2 N HCl for 1 h and washed several times in 0.1% PBSTw. Samples were blocked in BrdU blocking solution for at least 2 hrs at RT and then incubated in BrdU blocking solution containing the antibodies at 4°C.

For chromogenic ISH, antisense digoxigenin- and fluorescein-labeled riboprobes were synthesized according to manufacture's instructions (Roche) by using T7/SP6/T3 RNA Polymerases. Probes used were: *cxcr7b*, *cxcr4b*, *fgfr1a*, *fgf3*, *pea3*, *sef1*, *erm1*, *lef1*, *axin2*, *dkk*, *sfrp1a*, *eya1* and *six1b*. Whole-

mount two-color fluorescence *in situ* hybridization was performed using anti-DIG and -fluorescein POD antibodies (Roche) and Tyramide Signal Amplification (TSA, PerkinElmer) to detect the riboprobes: *cxcr7b*, *cxcr4b*, *sdf1a/cxcl12a*, *lef1* and *pea3*. Larvae were mounted in 0.1% PBSTw with Vectashield with DAPI (1/100, Vector Labs.)

## **Imaging and time-lapse videomicroscopy**

For whole-mount ISH, embryos were deyolked, flat mounted and photographed on a Olympus BX61 microscope using 20X or 40X dry objectives with transmission light. Whole embryo images were acquired on a Leica MZ10 stereomicroscope. Fluorescent images were acquired using either a Leica SP5 or SPE microscope using 20X dry objective or 40X oil immersion objective. Images were processed using Imaris and/or ImageJ software packages, and assembled with Adobe Photoshop CS2, Adobe Illustrator CS2, and Macromedia FreeHand MX. For time-lapse imaging, staged and dechorionated embryos were anesthetized with tricaine and mounted in 0.8-1% low-melting-point agarose on a glass-bottom culture dish (MatTek). Z-stack series were acquired every 5-10 min using either using 20X dry objective of Leica SPE or SP5 confocal microscope. All movies were processed by using Imaris or ImageJ softwares.

## **2.4 Results**

### **2.4.1 *dog/eya1* mutant zebrafish form truncated posterior lateral lines**



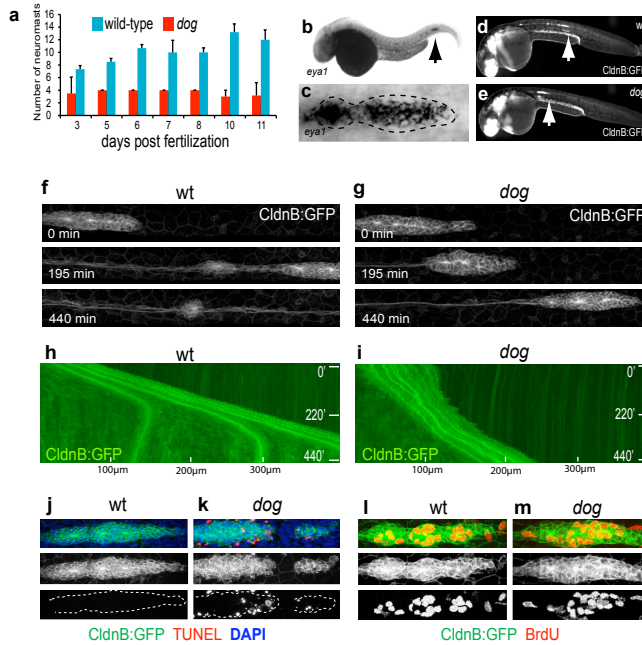


**Figure 2. Lateral-line phenotypes of *dog/eya1* mutants.** (a) Quantification of the number of neuromasts in *dog* (blue bars) and wild type (red bars). From 3 to 11 dpf shows that while the number of neuromasts doubles in wild types, it remains constant in *dog* (N = 3-7 larva/stage/condition). The data are represented as mean  $\pm$  standard deviation (s.d.). The quantifications were performed using the SqET20 transgenic line. (b,c) Chromogenic whole-mount in situ hybridization (WM-ISH) using an antisense probe to *Eya1*. It shows *Eya1* expression in the lateral-line primordium (black arrowhead), interneuromast cells and neuromasts in the whole fish (b) and in the primordium and depositing proneuromast (dotted outline) (c). (d-g) Confocal image of a *Tg[CldB:lynEGFP]* embryo (d) and a *dog;Tg[CldB:lynEGFP]* (e) at 36 hpf showing the delayed migration of the primordium in the mutants (white arrowheads). (f,g) Still images from a time-lapse videomicroscopy analysis of wild type (f) and *dog* mutant (g). The primordium of mutant embryo migrates less than that of the wild type. At 195 minutes of migration, the wild-type primordium has deposited one pro-neuromast, whereas the *dog* primordium failed to do so even after 440 minutes. (h,i) Kymography of wild type (h) and *dog* primordia in the *Tg[CldB:lynEGFP]* transgenic background (i). The wild-type primordium shows regular speed and periodical deposition of two pro-neuromasts (h), whereas the *dog* mutant primordium shows irregular speed and no depositions (i). (j,k) Cell viability analysis of wild type and *dog* primordia by the TUNEL assay (red) on *Tg[CldB:lynEGFP]* embryos (green). Increase of apoptosis is observed in the *dog* mutant primordium (dotted outline on the lowered panels). (l,m) Cell proliferation analysis of wild type and *dog* primordia. BrdU incorporation (red) on *Tg[CldB:lynEGFP]* embryos (green) shows no obvious differences in S-phase completion between wild types and *dog* mutants.

Because alterations of Wnt/ $\beta$ -catenin activity during the migration of the posterior lateral-line primordium lead to defects in neuromast deposition, we hypothesized that mutations affecting the number of neuromasts would identify additional factors involved in the control of Wnt/ $\beta$ -catenin signaling (Aman and Piotrowski, 2008). Following this rationale, we conducted a small-scale forward-genetic rack screen and identified that *dog/eya1* mutants had defective lateral lines. Eya1 is a homolog of the *eyes absent* gene of *Drosophila*. It encodes a protein tyrosine phosphatase with transcriptional activity when in association with the DNA-binding protein So/Six1 (Li et al., 2003; Rayapureddi et al., 2003; Tootle et al., 2003). Mutations in Eya1 and Six1 are associated with the branchio-oto-renal (BOR) syndrome in humans, defined by branchial arches and ear defects, hearing loss and kidney and lung malfunction (OMIM 113650), with a prevalence of 1:40,000 in the general population (Kochhar et al., 2007; Xu et al., 1999). In the zebrafish, recessive mutations in Eya1 cause developmental defects in the adenohypophysis, the inner ear and the lateral line (Fig. 2a, d-e and Supplementary Fig. 1a-d) (Kozlowski et al., 2005; Nica et al., 2006). We found that *dog/eya1* mutant fish developed an average of only 4 neuromasts (Fig. 2a). We observed identical phenotypes in two independently generated *dog/eya1* mutant alleles and in animals injected with a translation-blocking morpholino targeted to Eya1, confirming the specificity of the mutant phenotype (data not shown). To further assess the extent to which lateral-line truncations are specific to the loss of Eya1, we injected fertilized eggs with synthetic mRNA coding for a functional Eya1. RNA injections in wild type eggs did not cause any defect, but they fully rescued the lateral-line defects of *dog/eya1* mutant (Supplementary Fig. 1e-h). Finally, the expression of a transcriptional dominant-negative form of Eya1 (Eya1WRPW) in wild type eggs produced larvae displaying the landmark phenotypes associated with *dog/eya1*, including smaller ears, fewer hair cells, and truncated lateral lines (Supplementary Fig. 1i-l). Because lateral-line truncations can arise from defects in primordium

migration or neuromast survival, we analyzed mature neuromasts by combining mutant *dog/eya1* alleles with the SqET4 and SqET10 transgenic zebrafish lines that express the green-fluorescent protein (GFP) in, respectively, the hair cells and supporting cells of the lateral line (Supplementary Fig. 1m,n,p) (Parinov et al., 2004). These transgenic lines showed that homozygous *dog/eya1* mutant neuromasts contained both cell types without obvious defects in epithelial architecture (Supplementary Fig. 1o-q). Mutant neuromasts bore fewer hair cells than wild type controls, however, which is likely due to accelerated hair-cell degeneration rather than defects in hair-cell fate acquisition because neomycin-mediated ablation of existing hair cells in *dog/eya1;SqET4* led to a regeneration success similar to that of control fish (Supplementary Fig. 1r). Together, these results demonstrate that Eya1 is necessary for the production of the full complement of neuromasts along the posterior lateral line.

## 2.4.2 Eya1 is necessary for migration persistence

The observation that neuromast survival was not affected by the loss of Eya1 suggests that the lateral-line defects arise during its development. We examined this possibility by first ascertaining that Eya1 is expressed by the migrating primordium (Fig. 2b,c) (Sahly et al., 1999). Next, we analyzed the behavior of primordial cells *in vivo* using the transgenic line *Tg[Cldnb:lyn-EGFP]*, which expresses a membrane-targeted form of GFP in the lateral-line placodes and primordia (Fig. 1a-b) (Haas and Gilmour, 2006). This line offers the possibility to analyze cellular behavior at high spatial and temporal resolution from the onset of migration. We combined the *dog/eya1* mutations with *Tg[Cldnb:lyn-EGFP]* and compared them with wild type siblings by live confocal videomicroscopy. Although the initial stages of primordium formation were not affected, mutant primordia migrated over shorter distances than controls (Fig. 2d,e). To quantify migration we created

kymographs from time-lapse imaging acquired over 440 minutes starting at 32 hours-post-fertilization (hpf) (Fig. 2f,g). This experiment showed that the wild-type pirmordium moves at a constant velocity of around 150  $\mu\text{m}/\text{hour}$ , whereas mutant primordia underwent cycles of migration and stalling (Fig. 2h,i and Supplementary movie 1). This result indicates that loss of *Eya1* does not block primordium migration, but creates pronounced defects in its persistence. *Eya1* cannot bind DNA, but activates gene expression when recruited to target regulatory sequences by its DNA-binding partner *Six1*. There are two known *Six1* genes in the zebrafish, of which only *Six1b* is expressed in the lateral line (Supplementary Fig. 2a,b) (Bessarab et al., 2004). To assess whether *Six1b* plays any role in lateral-line development, we injected a previously-validated translation-blocking *Six1b* morpholino into fertilized *Tg[Cldnb:lyn-EGFP]* eggs (Bessarab et al., 2004). *Six1b* morphant pirmordia were smaller and rounder than those of uninjected controls (Supplementary Fig. 2c-d). Comparative time-lapse studies clearly showed that loss of *Six1b* blocked the production of neuromasts, and dramatically reduced the size and the migratory persistence of the primordium, as evidenced by the zigzag of its frontline in the kymographs (Supplementary Fig. 2e-i). Loss of *Six1b* also led to pronounced cyclical cellular apoptosis in the leading area of the primordium (Supplementary Fig. 2g and Supplementary movie 2). Interestingly, we found a perfect correlation between the cycles of apoptosis and primordium stalling, suggesting that loss of viability of leading cells produces transient migratory arrest in the *Six1b* morphants. These results further support the conclusion that *Eya1* is essential for migratory persistence. Because loss of *Six1b* and *Eya1* has been associated with decreased cellular viability in several organ primordia, we assessed apoptosis in wild type and *dog/eya1* mutants by the TUNEL assay. This showed that whereas most primordial cells in wild type animals remained viable during migration (Fig. 2j), *dog/eya1* mutants experienced increased apoptosis throughout the primordium (Fig. 2k). The injection of a

morpholino to p53 in *dog/eya1* almost completely abolished apoptosis, but did not rescue the lateral-line defects (Supplementary Fig. 3). We also performed BrdU incorporation experiments in wild type *Tg[Cldnb:lyn-EGFP]* and *dog/eya1;Tg[Cldnb:lyn-EGFP]*, which showed that primordial cells actively divided in both samples (Fig. 2l,m), suggesting that the migratory defects in *dog/eya1* are not a consequence of problems in cellular proliferation. These results demonstrate that Eya1 is essential for the persistent migration of the lateral-line primordium, and that apoptosis is not a major causative of this mutant phenotype.

### **2.4.3 Loss of Eya1 delays rosette formation and reduces CXCR7b expression**

Previous reports were inconclusive as to whether rosetogenesis and proneurogenic cell-fate acquisition in the primordium are necessary for its persistent migration (Aman and Piotrowski, 2008; Lecaudey et al., 2008; Matsuda and Chitnis, 2010; Nechiporuk and Raible, 2008). Our observations that loss of Eya1 affects migration but does not block hair-cell production in neuromasts suggest that the analysis of *dog/eya1* mutants may shed light on this controversy. Thus, we examined the expression of two complementary proneurogenic markers, DeltaA and Notch3, in wild type and *dog/eya1* mutant primordia by whole-mount two-color fluorescent *in situ* hybridization. We found proneurogenic *foci* in the mutant primordia, although their number and spatial distribution were slightly abnormal (Fig. 3a,b). Next, we examined primordia in *Tg[Cldnb:lyn-EGFP]* transgenic embryos that were stained with an antibody to N-Cadherin to highlight the prominent adherens junctions at the center of the rosettes (Fig. 3c,d). This experiment showed purse-like junctions along the long axis of mutant primordia, rather than the discrete focal constrictions of the wild type,

suggesting delayed rosetto-genesis in *dog/eya1* mutants. Therefore, the primordium migration defects in *dog/eya1* appear not to be caused by proneurogenic failure, although delayed rosetto-genesis may contribute to the mutant phenotype. To gain further insights into the molecular bases of the *dog/eya1* mutant phenotype, we decided to analyze the pathway that governs the collective migration of primordial cells: the CXCR4b and CXCR7b chemokine receptors and the Sdf1a/CXCL12 chemokine. We hypothesized that loss of Eya1 does not affect the chemokine because migration occurred along the normal path in *dog/eya1*. Indeed, the expression of Sdf1a/CXCL12 was normal in the mutants (Fig. 3e,f). However, we observed that while CXCR4b remained strongly expressed in the leading primordial zone in *dog/eya1*, the expression domain of CXCR7b was strongly reduced (Fig. 3g,h). A detailed analysis of *dog;Tg[Cldnb:lyn-EGFP]* specimens by confocal videomicroscopy and kymography showed frequent splitting of the primordium during migration (Fig. 3i,j and Supplementary movie 3), a phenotype that has so far only been associated to the loss of CXCR7b 22. These results indicate that Eya1 function is intrinsic to the primordium and necessary for normal CXCR7b expression. We conclude that loss of Eya1 causes intermittent migration and primordium splitting primarily due to defective CXCR7b expression.

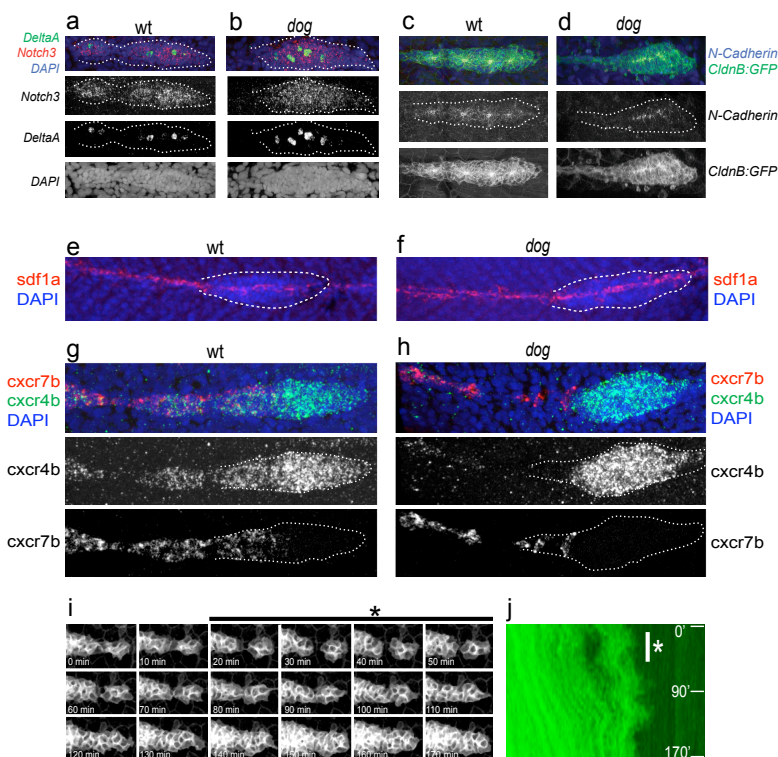


**Figure 3. Loss of CXCR7b expression and primordium splitting in *dog* mutant.** (a,b) TC-FISH of *Notch3* (red) and *DeltaA* (green) and DAPI (blue) shows that proneurogenesis occurs in the mutant primordium, although the number and spatial distribution of the expression foci of *DeltaA* are affected. (c,d) Antibody labelling of N-cadherin (red) on *Tg[CldnB:lynEGFP]* embryos (green) shows that adherens junction and the apical constriction of rosettes are disrupted in *dog* mutants. (e-h) Two-color fluorescent whole-mount in situ hybridization (TC-FISH) analysis of *Sdf1a*/*CXCL12* (red), *CXCR4b* (green) and *CXCR7b* (red) gene-expression profiles in wild type (e,g) and *dog* mutants (f,h), counterstained with DAPI (blue) to reveal the nuclei for better identification of the primordium (white dotted outline). It shows that *Sdf1a*/*CXCL12* (red) gene similarly expressed along the horizontal myoseptum in the wild type and *dog* mutants. The *CXCR4b* gene is strongly expressed in the leading region of primordium in both in wild type and *dog* mutants. The expression of *CXCR7b*, however, is strong in the trailing region of the wild-type primordium (overlapping with *CXCR4b*), but almost completely lost in *dog* mutants, as it is restricted to the very end of the trailing region and never overlaps with *CXCR4b*. A white dotted outline identifies the primordium in each panel. (i) Still images of 170 minutes time lapse videomicroscopy and (j) kymography of a *dog* mutant showing a transient splitting of the leading zone of the primordium. The three time frames of time lapses (i) correspond to the dark hole in the kymograph (j) (asterisks on the black overline in i and white vertical line in j).

#### 2.4.4 Eya1 is essential for Dkk1 expression and FGF signaling

Little is understood about the dynamic maintenance of primordium regionalization during migration. Our previous results suggest that Eya1 controls the expression of only a subset of the genes relevant to lateral-line patterning. We further explored this possibility by profiling gene expression by chromogenic whole-mount *in situ* hybridization. We focused on the FGF and Wnt/ $\beta$ -catenin signaling pathways because their activity domains are always spatially segregated in the primordium. Lef1, Sef1 and Fgf3 are targets of Wnt/ $\beta$ -catenin signaling that are normally expressed by the leading mesenchymal cells (Fig. 4a-c) (Ma and Raible, 2009). In *dog/eya1* mutants, however, the expression domain of Lef1 and Sef1 extended throughout the primordium and Fgf3 appeared upregulated (Fig. 4d-f), suggesting an expansion of  $\beta$ -catenin activity. We next assessed the expression of Pea3, a *bona fide* target of FGF signaling, and also of Fgfr1a, whose expression is maintained by a positive feedback loop of FGF signaling (Aman and Piotrowski, 2008). Both genes are normally highly expressed by the trailing cells (Fig. 4g,h). Remarkably, their expression was almost completely abolished in *dog/eya1* mutants (Fig. 4i,j). These results indicate that in the absence of Eya1, the primordium experiences a concomitant expansion of Wnt/ $\beta$ -catenin activity and a reduction of FGF signaling. This combination of phenotypes has already been reported for zebrafish embryos treated with the FGFR inhibitor SU5402, supporting our conclusion that loss of Eya1 specifically impairs FGF signaling (Aman and Piotrowski, 2008). The observed expansion of Wnt/ $\beta$ -catenin activity in SU5402-treated embryos results from the decreased expression of the Wnt-signaling inhibitor Dkk1, which is normally expressed as one or two *foci* in the primordium's transition zone (Fig. 4k). Thus, we assessed the expression of Dkk1 in *dog/eya1* to find



that it was almost completely lost (Fig. 4l), which may explain the expansion of the Wnt/ $\beta$ -catenin signaling territory in the mutants.

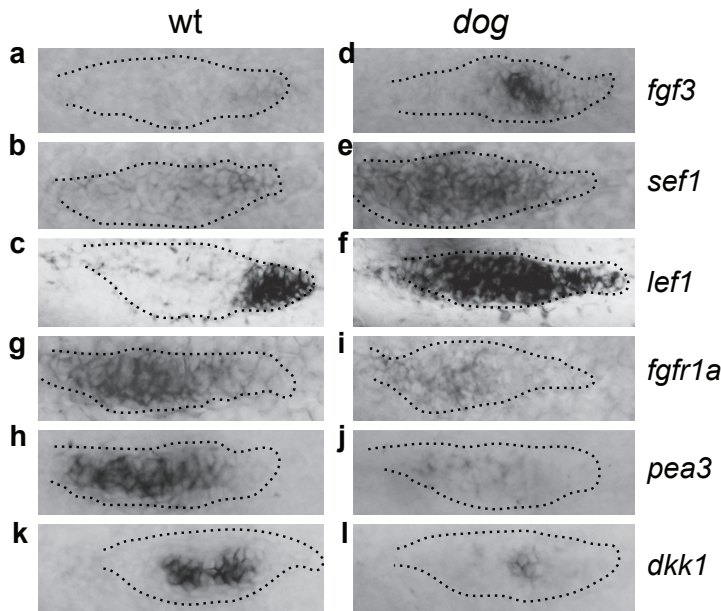


**Figure 4. Eya1 loss of function de-regulates gene expression.** All panels on the left correspond to wild type, and those on the right to *dog* mutants. (a-f) *fgf3*, *sef* and *lef1* genes are normally expressed in cells of leading zone, while *fgf3* expression is up-regulated (a), and *sef1* (b) and *lef1* (c) expanded throughout the primordium in *dog* mutants. (g,i) *fgfr1a* and *pea3* (h,i) are normally expressed in the trailing epithelial cells, whereas their expression is almost completely lost in *dog* mutants. (k,l) *Dkk1* expression domain is normally found in the transition zone, while in *dog* mutant the *dkk1* is strongly down regulated. A black dotted outline identifies the primordium in each panel.

Whole-mount two-color *in situ* hybridizations showed that the expression domains of *Lef1* and *CXCR7b* do not overlap in wild type or *dog/eya1* mutants (Fig. 5a,b). This observation supports previous conclusions indicating that Wnt/ $\beta$ -catenin represses *CXCR7b* expression. Under this scenario, the expansion of Wnt/ $\beta$ -catenin in *dog/eya1* mutants would explain the restriction of *CXCR7b* expression to a very few trailing primordial cells, leading to intermittent migration. An alternative hypothesis is that *Eya1*

controls CXCR7b expression independently of Wnt/ $\beta$ -catenin. To discriminate between these possibilities, we decided to abrogate Wnt/ $\beta$ -catenin signaling in animals lacking *Eya1*. We first assayed a previously used approach based on the misexpression of *Dkk1* by heat shock using the *Tg[hsp:Dkk1-EGFP]* transgenic line. However, *Dkk1* overexpression exhausted the primordium, producing a non-migrating thin trail of epithelium resembling interneuromast cells (Supplementary Fig. 4). Therefore, this approach was not useful. Thus, to better control the extent and timing of Wnt/ $\beta$ -catenin inhibition, we turned to a pharmacological approach. We used the small molecules IWR-1-endo that stabilizes the  $\beta$ -catenin destruction complex, and its inactive diastereomer IWR-1-exo as a control (Chen et al., 2009). IWR-1-endo suppressed *Lef1* expression in the wild type and also in *apc* and *dog/eya1* mutant primordia (Fig. 5f-h,l-n,r-t), indicating that this drug can potently inhibit  $\beta$ -catenin activity even when the destruction machinery is attenuated by the loss of *Apc*. IWR-1-exo had no discernible effect on gene expression and was used as control (Fig. 5c-e,i-k,o-q). IWR-1-endo treatments in wild type fish also strongly reduced *Dkk1* expression (Fig. 5r), but had no effect on CXCR7b's (Fig. 5l). However, IWR-1-endo-mediated Wnt inhibition did not rescue the expression of CXCR7b in *apc* or *dog/eya1* mutants (Fig. 5m,n). Inhibition of Wnt/ $\beta$ -catenin produces a compound effect because it also decreases FGF signaling (Aman and Piotrowski, 2008), which may be necessary for CXCR7b expression. Thus, we next tested whether we could rescue CXCR7b expression in *dog/eya1* mutants by artificially activating FGF signaling. To this end, we injected a translation-blocking morpholino against *Eya1* in eggs from the *Tg[hsp:CA-FGFR1]* transgenic line that expresses a constitutively active form of the FGFR under a heat-shock promoter. Induction of CA-FGFR by heat shock expanded the expression domain of the live sensor of FGF signaling *Tg[erm:Gal4;UAS:Kaede]* 37 (Fig. 6a,b) and also that of *Pea3* (Fig. 6c,d), indicating that FGF signaling was upregulated. However, constitutive

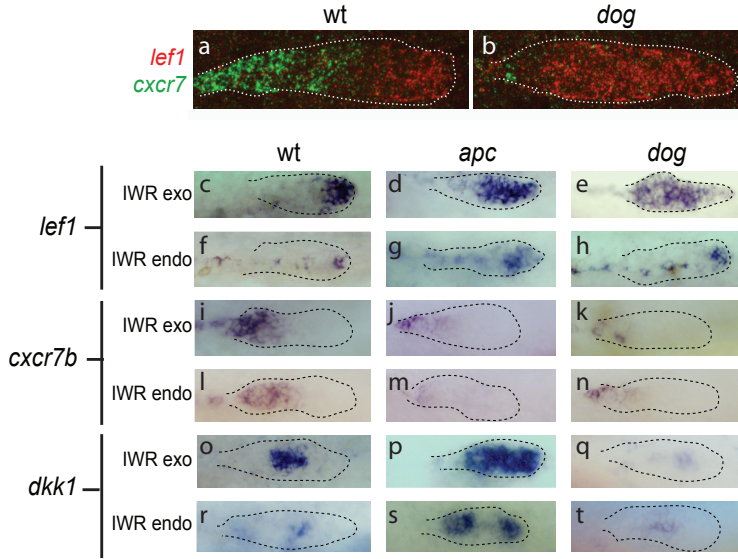


**Figure 5. Loss of Eya1 down-regulates CXCR7b expression independently of Wnt/ $\beta$ -catenin.** (a,b) TC-FISH of *lef1* (red) and CXCR7b (green) shows non-overlapping domains of expression in wild type and *dog* mutants. (c-h) Chromogenic whole-mount *in situ* hybridization (WM-ISH) show that IWR-endo inhibits Wnt/ $\beta$ -catenin signaling as assessed by *lef1* expression in wild type (c), *apc* (d) and *dog* (e) mutant zebrafish lateral-line primordia, whereas the inactive IWR-exo causes no effects (f-h). (i-n) Neither IWR-endo, nor IWR-exo revert the loss of CXCR7b in *apc* (j,m) or *dog* (k,n) mutants. (o-t) IWR-endo reduces the expression of Dkk1 wild type (o,r) and diminishes Dkk1 expansion in *apc* (p,s) mutants, but does not rescue Dkk1 expression in *dog* (q,t) mutants. IWR-exo causes no effect on gene expression profiles. A black dotted outline identifies the primordium in each panel.

FGF signaling did not expand the Dkk1 or CXCR7b expression domains in control transgenics or in Eya1 morphants (Fig. 6e-n). Collectively, these results demonstrate that Eya1 is necessary for FGF signaling downstream of the FGFR, and that the spatial expansion of the Wnt/ $\beta$ -catenin activity in *dog/eya1* mutants results from reduced Dkk1 expression. We also conclude that FGF signaling is necessary but not sufficient for Dkk1 expression, and that the decrease in CXCR7b expression in *dog/eya1* mutants is a direct consequence of the loss of Eya1 and not a result from a repressive activity of the expanded Wnt/ $\beta$ -catenin signaling territory.

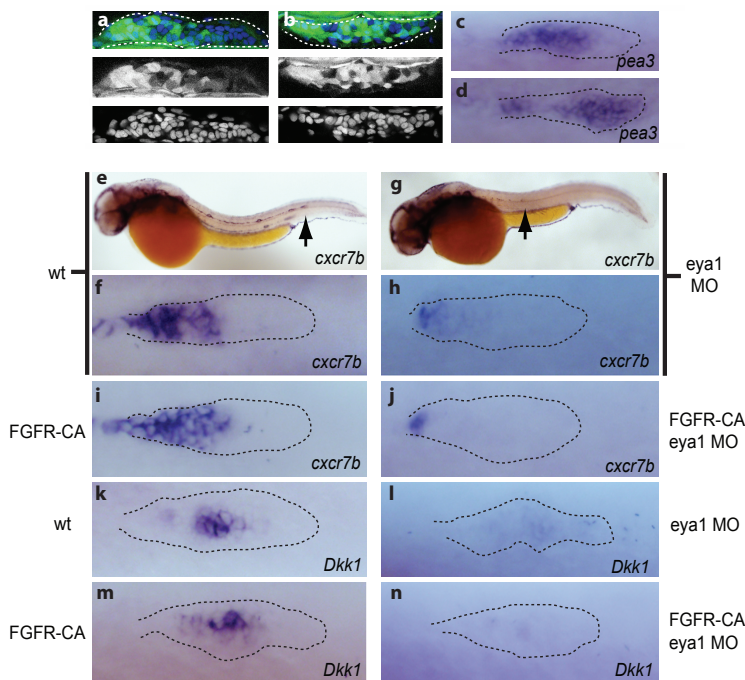


**Figure 6. Eya1 is necessary for FGF signaling downstream of FGFR. (a,b)** Fluorescent images of the posterior lateral-line primordium in the *Tg[hsp70:ca-fgfr1;erm:gal4;uas:kaede]* transgenic line (green) counterstained with DAPI (blue) without (a) and with (b) heat-shock. Note the conspicuous absence of Kaede in the front of the primordium in the control (a) and its expansion throughout the primordium upon heat shock (b). (c,d) Chromogenic whole-mount *in situ* hybridization (WM-ISH) to *pea3* in the posterior lateral-line primordium in wild type controls (c) and *Tg[hsp70:ca-fgfr1]* transgenics (d). Note the expression of *pea3* in the trailing area of the primordium in the control and its expansion throughout the primordium upon heat shock in the transgenics. These results show that the *Tg[hsp70:ca-fgfr1]* transgenic line activates FGF signaling broadly upon heat shock. (a-d) WM-ISH to CXCR7b in the posterior lateral-line primordium in wild type controls (e,i) *Tg[hsp70:ca-fgfr1]* transgenics (i) Eya1 morphants (g,h) and *Tg[hsp70:ca-fgfr1]* transgenics + Eya1 morphants (j). They show that overactivation of FGF signaling does not affect the migration of the lateral-line primordium (e), does not expand the expression domain of CXCR7b (f,i), and does not rescue the down-regulation of CXCR7b expression upon loss of Eya1 (g,h,j). WM-ISH to *Dkk1* in the posterior lateral-line primordium in wild type controls (k) *Tg[hsp70:ca-fgfr1]* transgenics (m) Eya1 morphants (l) and *Tg[hsp70:ca-fgfr1]* transgenics + Eya1 morphants (n). They show that overactivation of FGF signaling neither expands the expression domain of *Dkk1* (m), nor it rescues its expression upon loss of Eya1 (l,n). A black dotted outline identifies the primordium in each panel.

## 2.5 DISCUSSION

Our results show that Eya1 is essential for the persistent invasive migration of lateral-line primordial cells. Several lines of evidence indicate that Eya1 activity is intrinsic to the primordium. First, loss of Eya1 did not affect the directionality of migration, a phenotype associated to the absence of chemotactic cues, which was confirmed by the normal expression of Sdf1a/CXCL12 along the horizontal myoseptum in the mutants. Live imaging clearly showed that *dog/eya1* mutant primordia fail to maintain migratory persistence. In addition, we observed frequent fragmentations of the primordium that coincided with migratory failure. These phenotypes have previously been observed in only one other instance, when the function of the chemokine receptor CXCR7b was abrogated. Therefore, we reasoned that the *dog/eya1* mutant phenotype might derive from defective CXCR7b function. We confirmed this prediction by assessing the expression of the chemokine receptors and showing that whereas the expression of CXCR4b was not dramatically affected, most trailing primordial cells failed to express CXCR7b in the absence of Eya1 function. According to published reports, loss of CXCR7b expression could be a consequence of decreased FGF signaling, or expanded CXCR4b or Wnt/ $\beta$ -catenin signaling (Aman and Piotrowski, 2008; Dambly-Chaudiere et al., 2007). We tested these possibilities by increasing and decreasing Wnt/ $\beta$ -catenin signaling in wild type embryos and in those without Eya1 function using a combination of genetic and pharmacological approaches. In contrast to previously published conclusions, our results show that the loss of CXCR7b expression in *dog/eya1* mutant zebrafish is not a consequence of expanded CXCR4b or Wnt/ $\beta$ -catenin signaling.

A coincident loss of CXCR7b and FGF signaling, together with an expansion of  $\beta$ -catenin activity has been observed when FGF signaling is abrogated pharmacologically by SU5402-treatments or by the expression of a

dominant-negative form of a FGFR1 (Aman and Piotrowski, 2008). Our gene-expression profiling demonstrates that primordial FGF signaling is strongly inhibited in *dog/eya1*. Therefore, our discovery that Eya1 is an essential mediator of FGF signaling in the lateral-line primordium provides a simple explanation for the migration defects that have previously been observed in animals lacking FGF signaling (Aman and Piotrowski, 2008; Lecaudey et al., 2008; Nechiporuk and Raible, 2008). It remains to be determined if FGF signaling plays any direct role in CXCR7b expression. Previous work suggested that FGF signaling represses CXCR7b in the zebrafish fin blastema, which is clearly the opposite situation of that of the lateral line (Bouzafeffour et al., 2009). Our results from the expression of a constitutively active form of FGFR (Fig. 6) suggest that Eya1 and FGF signaling are necessary but not sufficient to induce CXCR7b expression.

Loss of Eya1 delayed rosetogenesis, which may indicate defects in the mesenchymal-to-epithelial transition. It is now useful to compare mesenchymal-to-epithelial transitions in mammals with the zebrafish lateral-line system. The transition between the two cell states is a prominent process in embryonic development and during the generation and spread of several human cancers –in some of which FGF and Wnt/ $\beta$ -catenin have clearly contrasting roles (Ceol et al., 2007; Chamorro et al., 2005; Micalizzi et al., 2010; Pai et al., 2008; Thiery et al., 2009). FGF and Wnt/ $\beta$ -catenin signaling pathways have been shown to have antagonistic effects on epithelial and mesenchymal transitions in other contexts (Thiery et al., 2009). Thus, the roles of Wnt/ $\beta$ -catenin and FGF in these cell-state transitions are often context-dependent and not well understood. Is Eya1 involved in tumorigenesis or cancer metastasis? An exhaustive search of the literature only revealed an indirect link between Eya1's overactivation and Wilm's tumor development (Drake et al., 2009). However, our results suggest that Eya1 activity may not be involved in primary tumorigenesis, but may instead enhance the capacity of tumor cells to metastasize. Supporting this

prediction, Eya1's transcriptional partner Six1 is a key promoter of metastasis from rhabdomyosarcomas and breast cancer (Coletta et al.; Yu et al., 2004). It may be interesting to know if BOR patients are more resistant to metastasis. The protein tyrosine-phosphatase activity of Eya1 may render itself amenable to pharmacological inhibition. Thus, if the role that we have uncovered for Eya1 in invasive cell migration is conserved in humans, Eya1 may represent a promising target for anti-metastatic therapy.

During migration, the lateral-line primordium replaces the cells that are lost with every neuromast deposition by an iterative conversion of mesenchymal progenitors to epithelial rosettes. The mesenchymal-to-epithelial transition zone, formed by around 20 cells, represents the boundary between the regions of Wnt/ $\beta$ -catenin and FGF signaling activity. In keeping with the convention, we call these regions "morphogenetic territories" as opposed to "compartments", because the later represents cellular fields that are defined by lineage, whereas the former are dynamically maintained by continuous signaling (Theisen et al., 1996). Notably, the rapid movement of mesenchymal cells across the transition zone does not shift significantly the spatial activity domains of Wnt/ $\beta$ -catenin and FGF signaling. How does the lateral-line primordium maintain signaling territories and persistent migration while undergoing periodic losses of trailing FGF(+)/CXCR7b(+) cells, and expansions and movements of leading Wnt/ $\beta$ -catenin(+)/CXCR4b(+) cells? Previous work has shown that a tightly regulated expression of Dkk1 in the transition zone establishes the rear boundary of  $\beta$ -catenin activity. Also, that Wnt/ $\beta$ -catenin signaling promotes FGF activity within the epithelial area, which is achieved through a  $\beta$ -catenin-dependent expression of the FGFR ligands Fgf3 and Fgf10. In turn, FGF signaling promotes the expression of the FGFR by a positive feedback loop, and represses Wnt/ $\beta$ -catenin signaling by activating Dkk1 expression (Fig. 1D) (Aman and Piotrowski, 2008; Ma and Raible, 2009). Although this model is consistent with the expression profile of most genes,

it cannot explain that of Dkk1 because the strongest FGF output is located within the entire epithelial zone, which does not express Dkk1 (Fig. 7a). Therefore, although Dkk1 represents the node of the gene-regulatory network that governs the robust homeostasis of FGF and Wnt/ $\beta$ -catenin signaling during primordium migration, how its expression is dynamically controlled has remained unknown. Because Dkk1 expression appears tightly linked to the mesenchymal-to-epithelial transition, a combinatorial activity of Wnt/ $\beta$ -catenin and FGF activity would suffice to govern Dkk1 expression in space and time. This hypothesis predicts that expanding FGF and Wnt/ $\beta$ -catenin signaling should also expand Dkk1, which has been observed in *apc* mutant fish. However, ectopic activation of FGF signaling is not sufficient to expand Dkk1 expression. Our analysis of *dog/eya1* mutant zebrafish offers a novel perspective to this problem (Fig. 7c). We propose that both FGF and Wnt/ $\beta$ -catenin signaling underlie the dynamic maintenance of Dkk1 at the transition zone. Our model involves two activators in combination: concentration-dependent FGF and time-dependent Wnt/ $\beta$ -catenin signals. Under this scenario, both the strength of FGF signaling output and the temporal component (time of exposure) of Wnt/ $\beta$ -catenin signaling will have to coincidentally reach a threshold to initiate and maintain Dkk1 expression (Fig. 7d).

In concluding, these results refine our understanding of the complex regulatory interactions between FGF and Wnt/ $\beta$ -catenin signaling. They provide strong *in vivo* support for the conclusion that secreted effectors (FGF ligands) and secreted inhibitors (Dkk1) acting as feed-forward elements, combined with a positive feed-back loop (FGF signaling autoactivation), can provide the necessary robustness to the genetic networks that dynamically control the spatial influence of morphogens in remodeling tissues. Further dissection of the simple network in the lateral-line primordium will surely yield deeper insights on the basic mechanisms underlying rapid and orderly cell-fate transitions in a wide variety of



biological processes.

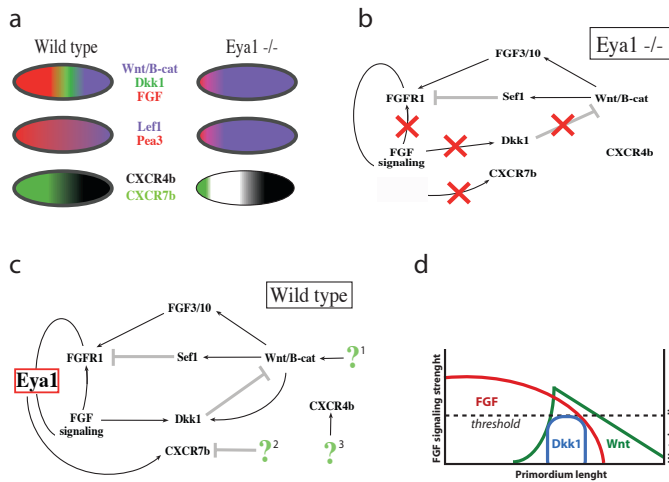
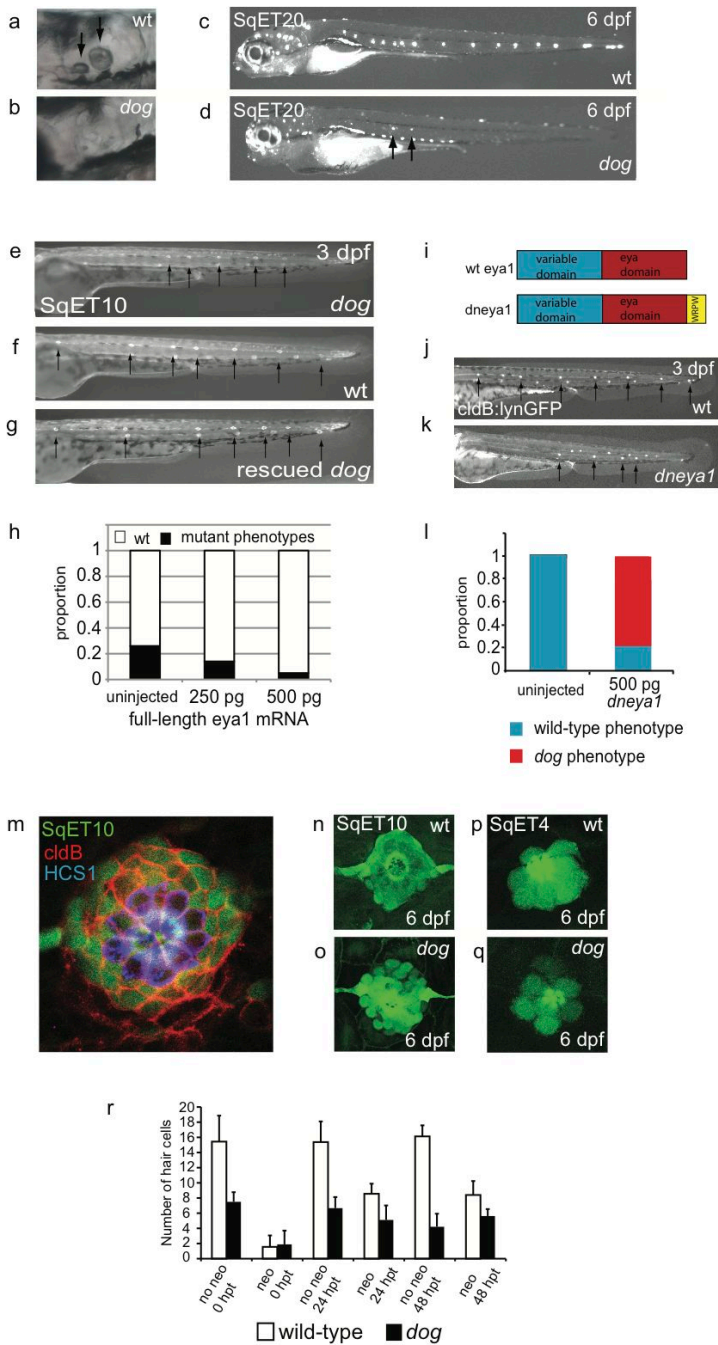
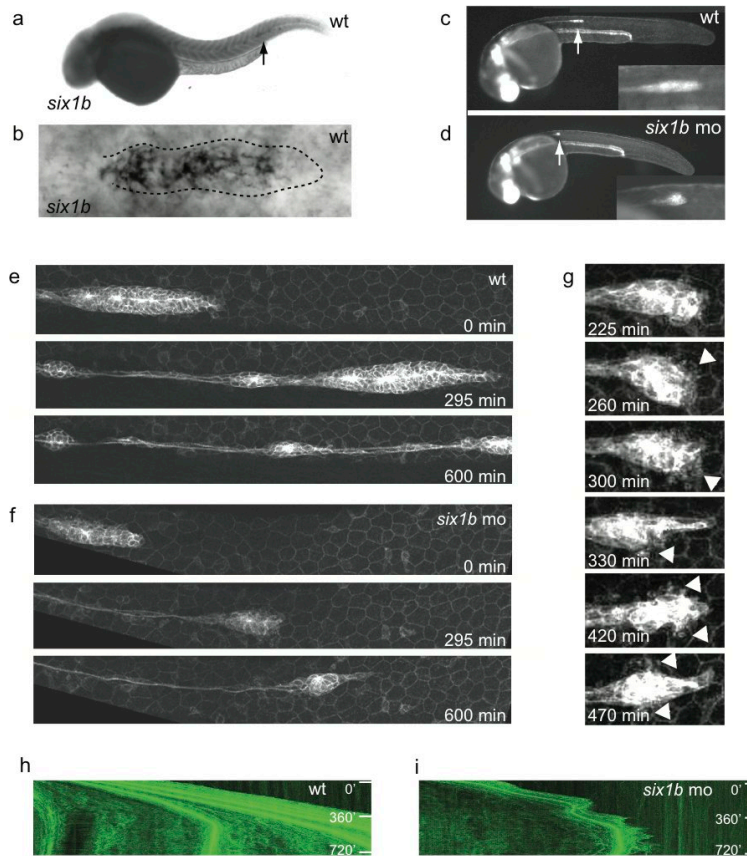


**Figure 7. Summary of the results and new model of the genetic network organizing the posterior lateral-line primordium.** (a) Diagram of the primordium (ovals). Signaling territories and gene-expression patterns are color coded in wild type (left) and Eya1 loss-of-function. (b) A model of the genetic network and its de-regulation upon loss of Eya1. Red crosses indicate the interactions that are mostly affected by loss of Eya1. (c) The model of the genetic network organizing the posterior lateral-line primordium places Eya1 downstream of the activation of FGFR. The three green question marks indicate that the activating or inhibiting signals are currently unknown. The scheme indicates that two feed-forward loops (Wnt/ $\beta$ -catenin to FGF via the activation of FGF3/10; and FGF to Wnt/ $\beta$ -catenin, via the activation of Dkk1) and one positive feedback loop (FGF signaling autoactivation) dynamically maintain the spatial domains of activity of Wnt/ $\beta$ -catenin and FGF signaling during primordium migration. (d) The new model proposes that only the cells that coincidentally reach a threshold of FGF signaling strength and of time of exposure to Wnt/ $\beta$ -catenin signaling will be able to initiate and maintain Dkk1 expression.

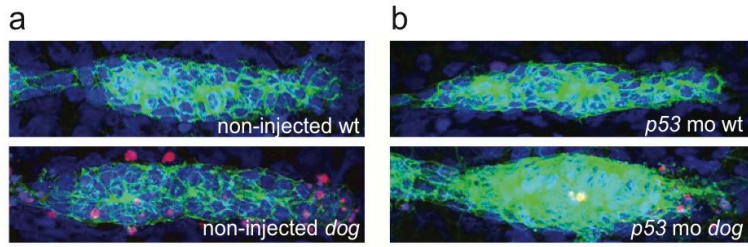
# 2.6 Supplementary Materials



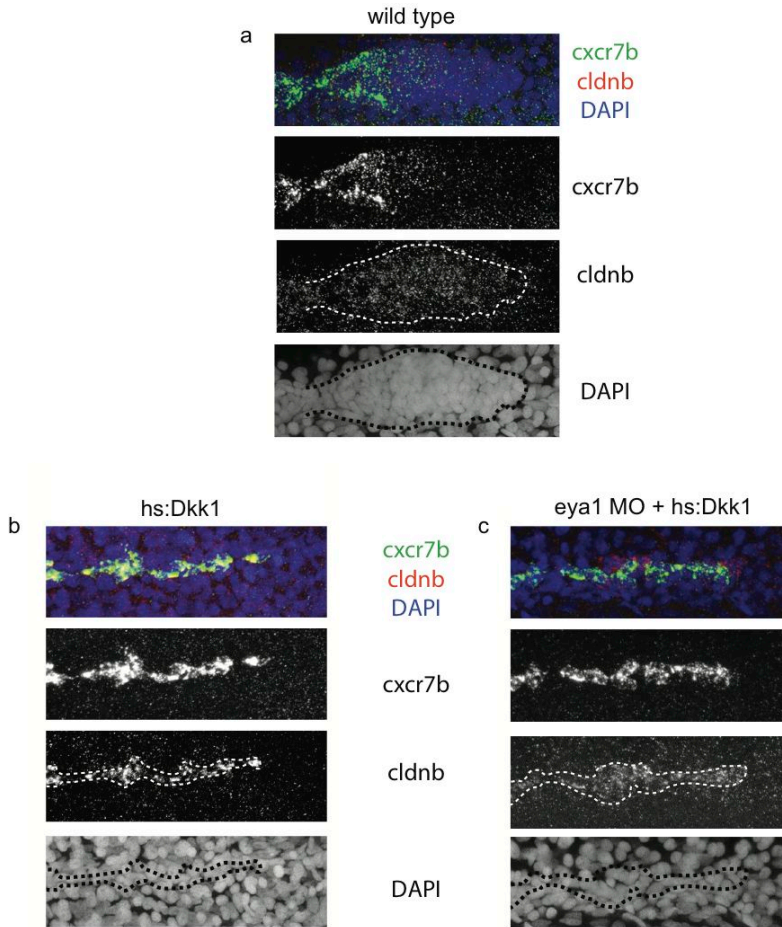
**Supplementary Figure 1.** Phenotypic characterization of the *dog/eya1* mutation. **(a,b)** Bright-field images of the ear of wild type **(a)** and *dog/eya1* mutant **(b)** fish at 6 dpf. Wild type ears have two otoliths (arrows), whereas *dog/eya1* mutant ears have very small otoliths and defective otic vesicles. **(c,d)** The posterior lateral-line system of wild type and *dog/eya1* mutant in SqET20 transgenic background. At 6 dpf, wild type larvae display around 11 neuromasts **(c)**, whereas in *dog/eya1* mutants the number of neuromasts is much lower **(d)** (two of the three neuromasts of this sample are indicated by arrows). **(e-h)** *dog/eya1* mutant phenotype is rescued by the injection of mRNA coding for full-length Eya1. **(h)** Graphic showing the proportion of wild type and *dog/eya1* mutant phenotypes with and without injections of mRNA coding for full-length Eya1. The embryos were obtained from crossing *dogtm90*<sup>+/−</sup> carrier parents, obtaining 13 *dog/eya1* mutant embryos (N=50 embryos). **(i-l)** The injection of mRNA coding for dn-Eya1 phenocopies *dog/eya1* mutant phenotypes. The dn-Eya1 construct contains a WRPW tetrapeptide at the C terminus of Eya1 **(i)**. Larvae at 3 dpf expressing dn-Eya1 bear fewer neuromasts **(j)** compared to non-injected control larvae **(k)**. **(l)** Quantification dn-Eya1 mRNA injections. Injection of 500 pg dn-Eya1 fully phenocopies the *dog/eya1* mutant phenotype (81/100, N=100). **(m)** A neuromast of a SqET10 transgenic larva (green) and immunostained with an antibody to Claudin b (red) and HSC1 (blue). SqET10 expresses EGFP in sustentacular supporting cells, Claudin b antibody shows all supporting cells and HSC1 to marks the hair cells. **(n,o)** wild type and *dog/eya1* mutants in SqET10 background. These images show the presence of supporting cells (green) without changes in the architecture of the neuromast. **(p,q)** wild type and *dog/eya1* mutants in SqET4 background. These images show the presence of hair cells in the mutant neuromast. **(r)** Quantification of hair-cell numbers in *dog* (black bars) and wild type (white bars), with and without neomycin treatments to promote hair-cell regeneration. Quantifications were performed using SqET4 transgenic line at 6 dpf. It shows that even though *dog/eya1* bears fewer hair cells than wild types, they can regenerate them efficiently (N=10-45 neuromasts. The data are represented as mean  $\pm$  standard deviation (s.d.).



**Supplementary Figure 2.** *Six1b* is involved in posterior lateral-line primordium morphogenesis. **(a,b)** Chromogenic whole-mount *in situ* hybridization shows that *six1b* is expressed in the primordium and the deposited neuromasts **(a)**. **(b)** Higher magnification of primordium showing the expression domain of *six1b*. **(c,d)** The migration of posterior lateral-line primordium in Tg[CldnB:lynEGFP] control embryos **(c)** and Tg[CldnB:lynEGFP] *Six1b* morphants **(d)** at 30 hpf. *Six1b* morphant embryos show migratory delay and rounder primordia (white arrows). **(e,f)** Still images of 600-minute time-lapse videomicroscopy of Tg[CldnB:lynEGFP] control embryos **(e)** and Tg[CldnB:lynEGFP] *Six1b* morphants **(f)**. The wild type primordium migrated constantly and deposited two neuromasts during the 600 minutes. The *Six1b* morphant embryo, however, showed a much smaller primordium and aberrant migration. **(g)** Higher spatial- and temporal-resolution images of the time-lapse videomicroscopy of Tg[CldnB:lynEGFP] *Six1b* morphants showing the cyclical loss of cell viability. Extruded cellular debris were often observed in the morphant primordia (white arrowheads). **(h,i)** Kymographs quantifying the migration of Tg[CldnB:lynEGFP] and Tg[CldnB:lynEGFP] *Six1b* morphants over 720 minutes of time-lapse videomicroscopy. Control primordia show persistent migration as indicated by straight front line described by the tip cells **(h)**. The migration of *Six1b* morphant primordia was intermittent, as shown by the zigzag pattern of the front line **(i)**.



**Supplementary Figure 3.** Injection of a translation-blocking morpholino to p53 rescues the apoptosis associated to *dog/eya1* in the lateral line. **(a-b)** TUNEL assay performed in non-injected and p53-injected Tg[CldnB:lynEGFP] controls and *dog*:Tg[CldnB:lynEGFP]. Non-injected wild type and p53-injected primordia rarely show apoptosis. Non-injected *dog/eya1* mutants show many TUNEL-positive cells. However, the injection of the p53 morpholino rescues the apoptosis in the mutants.



**Supplementary Figure 4.** Broad overexpression of Dkk1 exhausts the primordium. **(a)** Two-color whole-mount fluorescent *in situ* hybridization combined with DAPI staining (blue) showing the expression profile of CXCR7b (green) and Claudin b (red) in the primordium of control fish. **(b)** Tg[hs:Dkk1-GFP] expression after heat shock results in a thin line of epithelial cells resembling interneuromast cells, which express CXCR7b (green) and Claudin b (red). **(c)** Tg[hs:Dkk1-GFP] expression in *Eya1* morphants shows a similar depletion of the primordium.

**Supplementary Movie 1.** Time-lapse movie showing the migration of wild type and *dog/eya1* mutant primordia starting at 32 hpf. The wild-type primordium is highly organized and persists in its migration, depositing 2 neuromasts during 440 minutes. The *dog/eya1* mutant primordium showed delayed and intermittent migration with no neuromast deposition. Images were taken every 5 minutes using Leica SP5 confocal microscopy.

**Supplementary Movie 2.** Time-lapse movie showing a *dog/eya1* mutant primordium showing the transitory splitting of a group of leading cells. The dislodged group moved in circles and later re-joined the rest of the primordium. Images were taken every 5 min using Leica SP5 confocal microscopy. Length of the movie is 180 minutes.

**Supplementary Movie 3.** Time-lapse movie showing the migration of wild type and *Six1b* morphant primordia starting at 32 hpf. The wild-type primordium showed the typical persistent migration and the deposition of 2 neuromasts. The *Ssix1b* morphant primordium showed intermitten migration and cyclical cell death and debris extrusion, causing the primordium to become smaller and rounder. There is no neuromast deposition. Images were taken every 5 min using Leica SP5 confocal microscopy. Length of the movies is 720 minutes.

“If you knew what you are doing it wouldn’t be called research

- *Albert Einstein* -



# Chapter 3

## Compartmentalized Notch signaling sustains epithelial mirror symmetry

**Indra Wibowo<sup>1\*</sup>, Filipe Pinto-Teixeira<sup>1\*</sup>, Chie Satou<sup>2</sup>, Shin-ichi  
Higashijima<sup>2</sup> and Hernán López-Schier<sup>1</sup>**

*<sup>1</sup>Laboratory of Sensory Cell Biology & Organogenesis, Centre de Regulació Genòmica-  
CRG, c/Dr Aiguader 88, Barcelona 08003, Spain*

*<sup>2</sup>National Institutes of Natural Sciences, Okazaki Institute for Integrative Bioscience,  
Higashiyama 5-1, Myodaiji, Okazaki, Aichi 444-8787, Japan*

*\*Both the authors contributed equally to the work*

*Development 2011 (138), 1143-1152*

### 3.1 Abstract

Bilateral symmetric tissues must interpret axial references to maintain their global architecture during growth or repair. The regeneration of hair cells in the zebrafish lateral line, for example, forms a vertical midline that bisects the neuromast epithelium into perfect mirror-symmetric plane-polarized halves. Each half contains hair cells of identical planar orientation but opposite to that of the confronting half. The establishment of bilateral symmetry in this organ is poorly understood. Here, we show that hair-cell regeneration is strongly directional along an axis perpendicular to that of epithelial planar polarity. We demonstrate compartmentalized Notch signaling in neuromasts, and show that directional regeneration depends on the development of hair-cell progenitors in polar compartments that have low Notch activity. High-resolution live cell tracking reveals a novel process of planar cell inversions whereby sibling hair cells invert positions immediately after progenitor cytokinesis, demonstrating that oriented progenitor divisions are dispensable for bilateral symmetry. Notwithstanding the invariably directional regeneration, the planar polarization of the epithelium eventually propagates symmetrically because mature hair cells move away from the midline towards the periphery of the neuromast. We conclude that a strongly anisotropic regeneration process that relies on the dynamic stabilization of progenitor identity in permissive polar compartments sustains bilateral symmetry in the lateral line.

## 3.2 Introduction

The three-dimensional organization of tissues is essential for the efficient function of organs. It must also be maintained during the entire life of the individual and be recovered during organ repair because its loss can generate devastating pathologies (Wodarz and Nathke, 2007; Zallen, 2007). The pervasive planar cell polarity has emerged as an architectural property of tissues that allows investigations of the link between form and function (Axelrod, 2009; Strutt, 2002). One group of organs that relies on planar cell polarity for coherent sensory function is the acusticolateralis system that comprises the inner ear and lateral line, the shared plane-polarized elements of which are the mechanosensory hair cells (Lewis and Davies, 2002; Rida and Chen, 2009). The planar polarization of the hair cells allows animals to detect and interpret the direction of propagation of a sound (Hudspeth, 1985). Hair cells are substantially similar in their development and physiology across species. However, although their loss in mammals is irreversible leading to permanent deafness, other vertebrates are endowed with a hair-cell regenerative capacity during their entire lives (Collado et al., 2008; Corwin and Cotanche, 1988; López-Schier et al., 2004; Ryals and Rubel, 1988). During organ repair, cell fate and tissue architecture are often acquired concurrently to allow functional recovery before full anatomical repair, which may be essential for organs on which animals depend for survival. In the sensory organs of the zebrafish lateral line, called neuromasts, the complete loss of hair cells triggers a rapid and precise regeneration process (Brignull et al., 2009; López-Schier and Hudspeth, 2005; Williams and Holder, 2000), during which cell fate and epithelial planar polarity are recovered progressively along three phases (Fig. 1a). Phase I commences when hair cells begin to regenerate. During this phase, the central part of the neuromast epithelium (the macula) becomes increasingly oval because it elongates along a single axis (Fig. 1c,d) (López-Schier and

Hudspeth, 2006). Phase II begins when the neuromast macula expands symmetrically to regain its circular shape. During this phase epithelial planar polarity propagates laterally (Fig. 1a,e). Phases I and II last circa 30 hours each. A Phase III of homeostasis begins after around 60 hours from the onset of regeneration. During Phase I, the neuromast becomes bilaterally symmetric because a vertical midline separates the epithelium in two halves. Each half contains hair cells of identical orientation but opposite to that of the confronting half (Fig. 1d). This occurs because three processes integrate with remarkable spatiotemporal precision. First, hair cells regenerate in pairs and their soma localize adjacent to each other along the direction of epithelial planar polarity. Second, each hair cell of the pair orients opposite to its sibling within the plane of the macula. Third, all the hair cells at each side of the midline orient identically. It is not known how these processes integrate to generate bilateral symmetry. In the present study we use high-resolution live imaging in transgenic zebrafish, genetic and pharmacological perturbations of regeneration, and fluorescent sensors to address this question.

## 3.2 Materials and Methods

### Zebrafish strains and husbandry

Zebrafish used were maintained under standardized conditions and experiments were performed in accordance with protocols approved by the PRBB Ethical Committee of Animal Experimentation. To show different cell populations in the zebrafish neuromasts, SqET4 and SqET20 were used. For time-lapse imaging SqET4 fish were crossed to *Tg[CldB:lynGFP]* (Haas and Gilmour, 2006) to generate double transgenic larvae. The *Tg[atoh1a:tdTomato]* line was constructed from zC247L22 BAC and dTomato

cDNA, and was used to analyze the expression profile of Atoh1a during regeneration. The *Tp1[bglob:hmb1-mCherry]* line (Parsons et al., 2009) was used to report the Notch activity. *Tg[hsp70:gal4;UAS:Nicd-myc]* line, a gift from P. Chapouton (Helmholtz, Zentrum, München, Germany), was used to express a constitutively active form of Notch by heat shock during regeneration.

### **Neomycin treatments**

Selected larvae for fixation and live imaging were treated in E3 medium containing 250  $\mu$ M neomycin for 1 hour at room temperature. After treatments, larvae were washed several times using small diameter strainer to wash off residual neomycin. Larvae were allowed to recover from neomycin treatment for couple of hours before live imaging and treatments with other drugs to avoid high mortality.

### **DAPT and BrdU incubation**

A 10 mM 5-bromo-2'-deoxyuridine (Sigma, St Louis, MO, USA) stock solution in DMSO was diluted to 10  $\mu$ M in E3 medium and used to soak SqET4 larvae. Larvae were allowed to swim in this solution for 8, 24 or 48 hours, and fixed in 4% paraformaldehyde (PFA) overnight at 4°C, and then processed for immunostaining. N-[N-(3,5-Difluorophenacetyl)-L-alanyl]-S-phenylglycine t-butyl ester (DAPT, Sigma) in DMSO were used at the final concentration of 50-100  $\mu$ M in E3 medium to inhibit the  $\gamma$ -secretase. Larvae were allowed to swim in this solution for desired time points at 28°C. As a control, larvae were treated with 1% DMSO.

### **Immunohistochemistry, vital labeling and fluorescent in situ hybridization**

For immunohistochemistry and fluorescent in situ hybridization, larvae were fixed in 4% PFA overnight at 4°C and washed several times with 0.1% Tween-20-containing phosphate-buffered saline (0.1% PBSTw). For immunohistochemistry, larvae were immediately blocked in 10% bovine serum albumin (BSA) for at least 2 hours. For fluorescent in situ hybridization, samples were washed in gradual 25-100% PBSTw:methanol and stored at -20°C for at least 1 day. Primary antibodies and monoclonal antibodies were used at the following dilutions: mouse monoclonal antibody anti-BrdU, 1:100 (Upstate/Millipore, Billerica, MA, USA); mouse monoclonal anti-cMyc, 1:150 (NewMarkers, Fremont, CA, USA); rabbit anti-claudinB, 1:500; mouse anti-HCS1, 1:100; and rabbit anti-parvalbumin 3, 1/2000. Texas Red-labeled donkey anti-mouse and -rabbit and Cy5-labeled donkey anti-mouse and -rabbit immunoglobulin secondary antibodies (Jackson ImmunoResearch, West Grove, PA, USA) were used at 1/150. Antisense digoxigenin- and fluorescein-labeled riboprobes were synthesized according to manufacturer's instructions (Roche) by using T7/SP6/T3 RNA Polymerases. Anti-DIG and -fluorescein POD antibodies (Roche) and Tyramide Signal Amplification (TSA, PerkinElmer, Waltham, MA, USA) were used to detect antisense riboprobes. Probes used were notch3a, deltaA and atoh1a. For vital labeling of hair cells, larvae were immersed in 5 µg/ml of DiASP (Invitrogen, Carlsbad, CA, USA) in E3 medium for 2 minutes at room temperature and then washed several times to remove the excess of dye. For phalloidin staining, samples were fixed in 4% PFA overnight at 4°C then washed several times in 0.1% PBSTw and incubated in phalloidin-Alexa 568 or Alexa 488 (Invitrogen) diluted 1:20 in 0.1% PBSTw overnight at 4°C. Samples were washed several times in 0.1% PBSTw before being mounted.

### **Imaging and time-lapse imaging**

Fluorescent images were obtained using either a Leica SP5 or SPE or Andor Spinning disk using a 40× oil immersion objective. All images were

processed using ImageJ software package. For time-lapse video-microscopy, larvae were anesthetized in 0.02% tricaine (ethyl 3-aminobenzoate methanesulfonate salt, A5040, Sigma) and mounted in 1% low melting point agarose (Agarose, low melting point, A9414, Sigma) in E3 medium. Samples were imaged using either Leica SPE Leica SP5 or Andor spinning disk using a 40× oil immersion objective. Embryos were maintained at 21-25°C and z-stacks were collected at 2- to 10-minute intervals. Fixed samples were mounted in 0.1% PBSTw with Vectashield with DAPI (1/100, Vector Laboratories, Burlingame, CA, USA) (Faucherre et al., 2009).

### **Cell cycle inhibitors**

Compounds for cell cycle inhibitors were used as described before (Murphey et al., 2006). Larvae were treated for the desired period with aphidicolin at 100  $\mu$ M, genistein at 25  $\mu$ M, nocodazole at 150  $\mu$ M or colchicine at 1 mM in E3 medium supplemented with 1% DMSO.

### **Statistical analyses**

Quantifications of BrdU-labeled cells and hair cells in whole-mounts were carried out from 10 larval-stage samples and seven neuromasts per sample. Hair cells were counted both based on GFP marker of SqET4 and apical part each hair cell as an indicator of mature hair cell. Anti-BrdU antibody was used to detect cells or hair cells incorporated BrdU. Proliferation of hair cells that appeared with or without regeneration/neomycin was calculated according to this formula: BrdU-labeled hair-cell nuclei/total number of hair cell nuclei. Total number of cells in neuromasts was calculated from DAPI staining of the nuclei. All data of BrdU incorporation are represented as percentage of the standard deviation. For experiments with the presence of DAPT, averages for controls and treated larvae were compared within each group. The same statistical analysis was used to compare between groups of controls and cell-cycle inhibitor-treated larvae. To compare the distribution

of hair cell polarities in the macula of regenerating and mature neuromasts, we performed, for each condition, a one-way ANOVA that tests the null hypothesis that samples in two or more groups are drawn from the same population. For each polarity we assumed the null hypothesis that polarity distribution is homogeneous in the neuromast, comparing distributions between the ventral and dorsal halves of a neuromast and between the rostral and caudal halves.

### **3.3 Results**

#### **3.3.1 Cellular heterogeneity and compartmentalization of neuromasts**

Previous work has revealed that the mature neuromast is formed by the mechanosensory hair cells and by two types of supporting cells: peripheral mantle cells and central sustentacular cells (Chezar, 1930; Ghysen and Dambly-Chaudiere, 2007). Lateralis hair cells regenerate in pairs and sequentially on the dorsal or ventral aspect of parallel neuromasts (Fig. 1b) (López-Schier and Hudspeth, 2006). The spatiotemporal precision of the regenerative process suggested further heterogeneity in the neuromast. We decided to interrogate cellular identity in mature organs at 7 days post fertilization (7 dpf) by characterizing transgenic lines that express the green-fluorescent protein (GFP) in the lateral line (López-Schier and Hudspeth, 2006; Parinov et al., 2004). The SqET20 line expresses the GFP in supporting cells (Hernández et al., 2007). The staining of SqET20 animals with an antibody to the pan-supporting cell marker Claudin B revealed that GFP expression was heterogeneous, showing areas with low levels of green fluorescence located at both poles of a line perpendicular to the axis of planar cell polarity of the neuromast (Fig. 1f). Strikingly, this line shifts



through 90° in perpendicular neuromasts to remain perpendicular to the direction of epithelial planar polarity (Fig. 1h). The GFP<sup>low</sup> areas in SqET20 also coincide with those expressing high levels of alkaline phosphatase (Fig. 1g) (Ghysen and Dambly-Chaudiere, 2007; Villablanca et al., 2006). These SqET20<sup>GFP-low</sup>/AP<sup>+</sup> areas demonstrate previously unknown compartments located at the poles of the midline of bilateral symmetry. We call them ‘polar compartments’. We have previously shown that the SqET4 transgenic line expresses high levels of GFP in postmitotic hair cells, as revealed by their incorporation of the fluorescent dye DiASP, which permeates through the mechanotransduction channels (López-Schier and Hudspeth, 2006). Every DiASP(+) cell was also GFP(+), excluding the possibility that SqET4 reveals only a subset of the hair cells in the neuromast. In addition to hair cells, live imaging of SqET4 animals also identified individual cells expressing lower levels of GFP (Fig. 1b,c) (López-Schier and Hudspeth, 2006). Live imaging showed that SqET4<sup>GFP-low</sup> cells invariably undergo a single mitosis to produce a pair of hair cells (Fig. 1b) (López-Schier and Hudspeth, 2006). SqET4<sup>GFP-low</sup> cells never generated cell types other than hair cells, suggesting that they are ‘unipotent hair-cell progenitors’ (UHCPs). From these results, we conclude that the neuromast is compartmentalized and that it contains at least five distinct cell populations: mantle cells, sustentacular cells, polar-compartment cells, transient UHCPs and the hair cells.

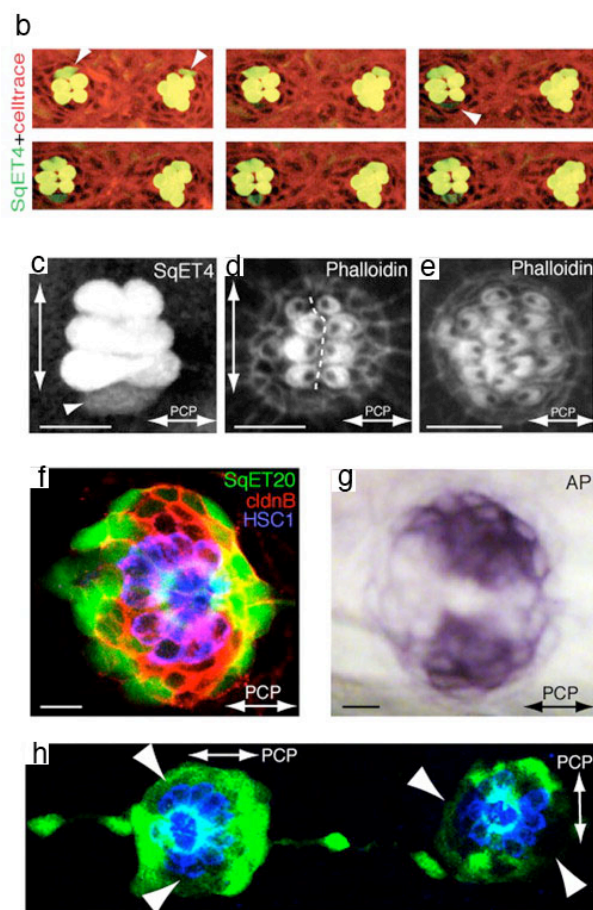
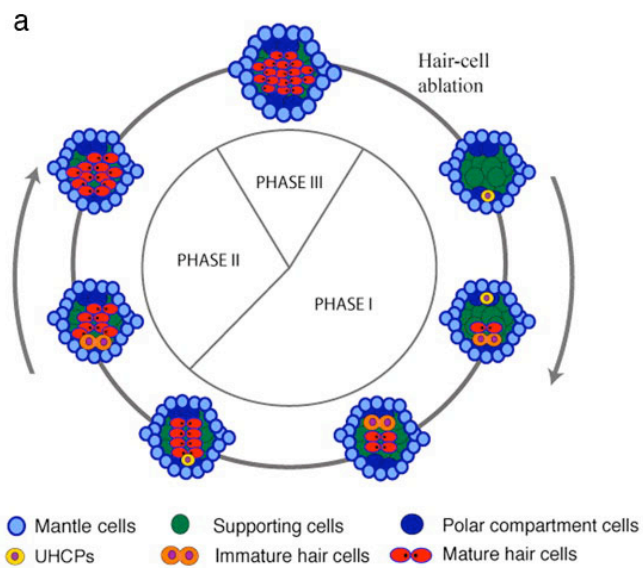


**Figure 1. Epithelial planar polarization of neuromasts. (a)** Schematic description of the three phases of regeneration and homeostasis and the planar polarization of the neuromast epithelium (macula). Cell types are color-coded: most peripheral mantle cells (light blue), central supporting (sustentacular) cells (green), polar compartment resident cells (dark blue), UHCPs (yellow), immature hair cells (orange) and mature hair cells (red). The axis of planar polarity is evidenced by the position of the kinocilium within the mature hair cells (black dot). **(b)** Time-lapse of two adjacent parallel SqET4 neuromasts showing hair cells and their progenitors (green) and stained with Celltrace to reveal cellular boundaries (red). White arrowheads on the first panel indicate a pair of newly developed hair cells on the dorsum of both neuromasts. The white arrowhead on the third panel indicates a new ventral UHCP, which divides into two hair cells on the last panel. Hair cells develop in pairs, sequentially, and on the dorsal or ventral aspect of the neuromasts. **(c)** A regenerating SqET4 neuromast revealing six GFP-positive hair cells. A UHCP develops at the lower edge of the neuromast (arrowhead). The orthogonal axes of planar polarization (horizontal) and direction of regeneration (vertical) are indicated by double-headed arrows. **(d)** Actin staining of a regenerating neuromast, showing the orientation of four pairs of hair bundles and revealing the vertical line of bilateral symmetry (dotted white line). **(e)** Actin staining of neuromast in Phase III of regeneration showing the lateral expansion of the macula. A double-headed arrow indicates the axis of planar polarity. **(f)** A SqET20 neuromast expressing GFP (green) and stained with antibodies to Claudin-b (red), which marks all the supporting cells, and to HCS1 (blue), which highlights the hair cells. GFP<sup>low</sup> compartments are located at the poles of the vertical axis of bilateral symmetry. **(g)** The GFP<sup>low</sup> compartments coincide with the endogenous expression of alkaline phosphatase. In all figures, anterior is leftwards and dorsal is upwards. **(h)** A SqET20 larva expressing GFP (green) and stained with the antibody HCS1 (blue). The neuromast to the left of the image is L1 (a parallel neuromast), whereas the one on the right is L2 (a perpendicular neuromast). This image shows that the GFP<sup>low</sup> compartments rotate through 90° in parallel versus perpendicular neuromasts. Arrowheads indicate polar compartments. Scale bars: 10 µm.

### 3.3.2 The mitotic division of UHCPs is essential for regeneration

It has been previously reported that mitotically active supporting cells are the main contributors to hair-cell regeneration in the zebrafish lateral line (Ma et al., 2008). However, other data suggested a role of supporting-cell transdifferentiation for the regeneration of hair cells (Hernández et al., 2007). Therefore, the relative contribution of supporting-cell proliferation versus transdifferentiation remains unknown. We decided to use the SqET4 line to

resolve this issue. We started by treating 5 dpf SqET4 animals with 250  $\mu$ M of neomycin for 1 hour. We have previously demonstrated that this regime eliminates the hair cells of the lateral line (López-Schier and Hudspeth, 2006). Neuromasts achieve near complete regeneration 48 hours after hair-cell ablation. After neomycin treatment, regenerating animals were left to recover in water containing the DNA synthesis marker bromo-deoxy-uridine (BrdU) (Fig. 2a). We found that 59% of the hair cells were BrdU(+) at 48 hours post treatment (hpt) (Fig. 2b,c), suggesting that proliferation and transdifferentiation could contribute to hair-cell regeneration. However, neomycin cannot kill young non-mechanoreceptive hair cells because this aminoglycoside antibiotic permeates through the mechanotransduction channels. Thus, the presence of immature neomycin-resistant hair cells in the neuromast could explain why just over half of the hair cells were BrdU(+) at 48 hpt. Another explanation for this result is that hair-cell precursors remain arrested in a stage of the cell cycle beyond the S phase, and would progress to mitosis upon hair-cell loss without incorporating BrdU. To discriminate between these possibilities, we exposed fish to BrdU for 8 hours at 4 dpf before neomycin treatment at 5 dpf, in order to incorporate the BrdU in UHCPs and non-mechanoreceptive hair cells that may be present in the neuromast (Fig. 2d). These animals were also left to recover for 48 hours, again in the presence of BrdU. Under this condition, almost 100% of the hair cells were BrdU(+) at 48 hpt (Fig. 2e,f). This result strongly suggests that cell division is the main or the obligatory process underlying hair-cell regeneration. To further test the extent to which mitotic activity is essential for hair-cell regeneration, we ablated hair cells in SqET4 animals with neomycin, and let them to recover in the presence of several inhibitors of the cell cycle (Fig. 2g,i). Treatments with nocodazole, aphidicolin, genistein and colchicine revealed that genistein and colchicine were the most effective suppressors of regeneration (Fig. 2h). However, control animals showed that genistein and colchicine were toxic to hair cells (Fig. 2g). Aphidicolin and

nocodazole, by contrast, did not affect the viability of hair cells over a 48-hour period (Fig. 2g,i). Therefore, the nearly complete lack of hair-cell regenerates in genistein- and colchicine-treated animals may represent a compound effect of these drugs on UHCPs mitoses and hair-cell viability. This assertion is further supported by the progressive reduction of the number of hair cells at 48 hpt compared with 24 hpt in animals not treated with neomycin (Fig. 2g). Aphidicolin and nocodazole strongly suppressed hair-cell regeneration but did not completely prevent the production of GFP(+) cells. In control animals not treated with neomycin, the number of GFP(+) cells in neuromasts did not vary between 0, 24 and 48 hpt under aphidicolin and nocodazole treatment (Fig. 2g). Thus, the few GFP(+) cells present in inhibitor-treated neuromasts are likely to be hair cells that were immature at the time of neomycin treatment. Alternatively, under cell-cycle inhibition, the UHCPs that may have been already present by the time of neomycin treatment could transdifferentiate into hair cells without undergoing mitosis. To address this possibility, we directly visualized regeneration using SqET4 fish, and compared hair-cell production between control animals and those under nocodazole. Live imaging revealed that over a period of 10 hours, control animals developed 6 hair cells (Fig. 2i), whereas nocodazole-treated animals developed two hair cells and sometimes a single UHCP that could never divide or produce hair cells (Fig. 2j; see Movie 1 in the supplementary material), with the consequent arrest of regeneration. The pair of hair cells that frequently developed in nocodazole-treated fish could have been immature at the time of neomycin treatments, which may also explain why we did not achieved 100% of BrdU(+) hair cells after regeneration. We interpret these results as an indication that supporting-cell transdifferentiation does not contribute to hair-cell regeneration in the lateral line.

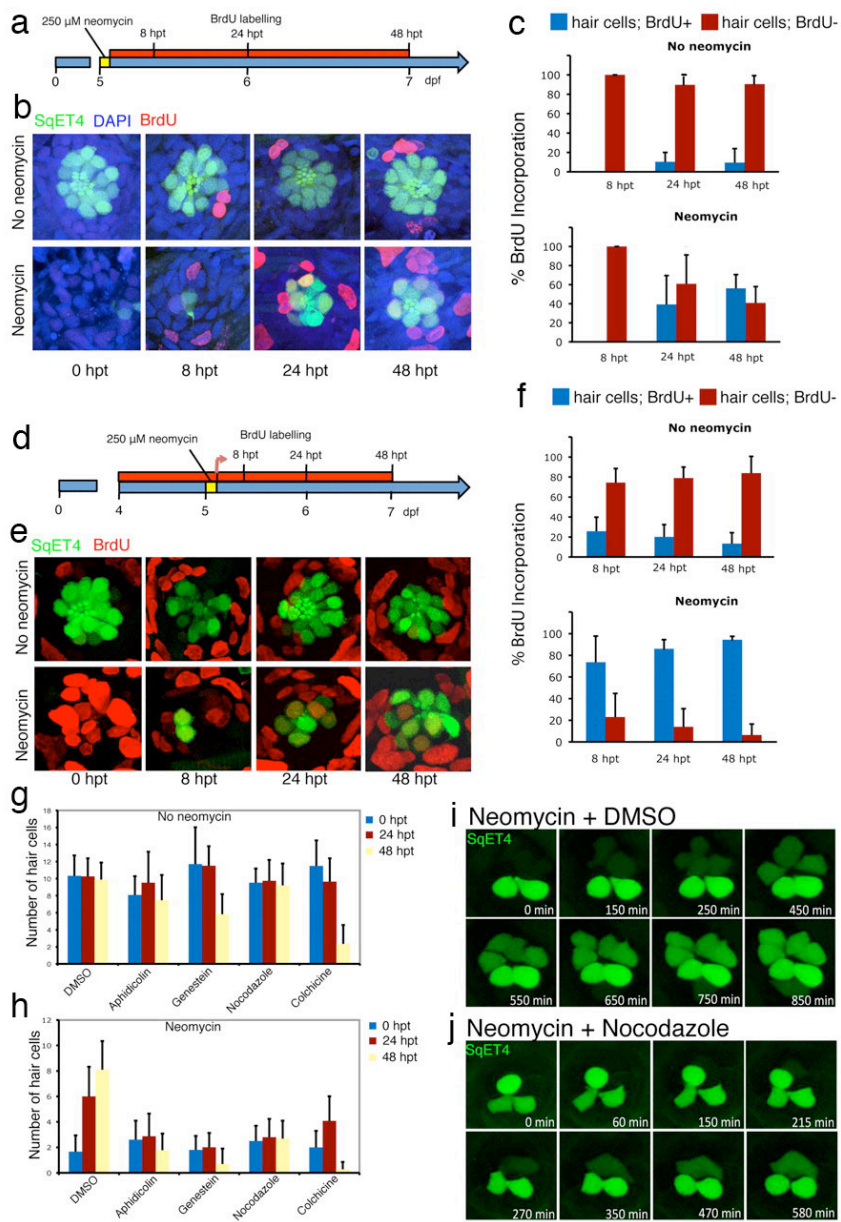


**Figure 2. Mitotic activity is essential for hair-cell regeneration neuromasts. (a)** Scheme representing the experiments in which hair cells were ablated with neomycin in SqET4 transgenic zebrafish larvae at 5 dpf, and subsequently incubated continuously in BrdU for 8, 24 and 48 hours after neomycin treatment (8,24 and 48 hpt). **(b)** Confocal images of neuromasts showing hair cells in green and BrdU in red. All cell nuclei were labeled with DAPI (blue). **(c)** The mean number of GFP(+) hair cells that were BrdU(+) versus BrdU(-) in control and treated larvae at 8, 24 and 48 hpt ( $n=70$  neuromasts for each timepoint). In control samples not treated with neomycin, few hair cells were labeled with BrdU at 48 hpt, whereas 59% of regenerated hair cells were BrdU(+) in neomycin-treated fish at 48 hpt. Error bars indicate s.e.m. **(d)** The experiments in which SqET4 transgenic zebrafish at 4 dpf were incubated continuously in BrdU, treated with neomycin to ablate hair cells at 5 dpf and subsequently incubated continuously in BrdU for 8, 24 and 48 hpt (results are shown in **e,f**). **(e)** Confocal images of neuromasts showing hair cells in green and BrdU in red. **(f)** In control samples not treated with neomycin, 74% of regenerated hair cells at 8 hpt are BrdU positive ( $n=70$ ), compared with only 26% BrdU-positive hair cells in untreated larvae ( $n=70$ ). By 48 hpt, 94% of regenerated hair cells are BrdU(+), compared with only 13% in untreated specimens. This finding indicates that virtually all regenerated hair cells develop from progenitors that have undergone cell division following neomycin-induced hair-cell ablation and that progenitors enter the cell cycle less than 8 hours after hair-cell death. Results are mean $\pm$ s.e.m. **(g,h)** SqET4 transgenic larvae were incubated in several inhibitors of the cell cycle for 24 and 48 hours following neomycin treatment. The quantification shows that the number of hair cells remains relatively constant following treatments with the cell-cycle blockers aphidicolin, genistein and nocodazole in control samples (not treated with neomycin). All cell-cycle inhibitors blocked hair-cell regeneration in samples treated with neomycin. Results are mean $\pm$ s.e.m. **(i,j)** These results were confirmed by time-lapse videomicroscopy in regenerating SqET4 control **(i)** and nocodazole-treated **(j)** larvae. Controls regenerated normally, whereas nocodazole blocked regeneration and the division of a UHCP that appears at the top of the neuromast in **j**.

### 3.3.3 The orientation of UHCPs divisions is dispensable for bilateral symmetry

Regeneration in neuromasts is always progressive. Live imaging of SqET4 fish showed that UHCPs develop within or in close proximity of the dorsal and ventral polar compartments (Fig. 1b). Consequently, hair-cell regeneration is strongly directional along an axis perpendicular to that of the eventual planar polarity of the epithelium. Hair-cell siblings develop opposite planar orientation and remain adjacent to each other during Phase I. Thus,

regeneration anisotropy defines the midline of bilateral planar-polarity symmetry (Fig. 1c,d). These observations led us to ask how regeneration anisotropy is controlled. Oriented cell divisions can direct growth anisotropy in epithelia (Baena-López et al., 2005; Lecuit and Le Goff, 2007). Therefore, the orientation of UHCP divisions could underlie hair-cell regeneration anisotropy and the formation of the midline of bilateral symmetry. We tested this possibility by direct visualization of 23 independent UHCPs in SqET4 animals, which showed that 14 UHCPs divided obliquely (Fig. 3a,b; see Movie 2 in the supplementary material), suggesting that the orientation of UHCP division is not directly translated into bilateral symmetry. We further validated this conclusion by directly revealing the dynamics of UHCPs using the double transgenic line *Tg[Cldnb:mGFP; SqET4]*, which express a membrane-targeted GFP in all supporting cells and a cytoplasmic GFP in UHCPs and hair cells, allowing the evaluation of cellular behavior in vivo (Haas and Gilmour, 2006). Unexpectedly, we found that ~60% of UHCP divisions produced hair-cell pairs that rotated within the plane of the epithelium after progenitor cytokinesis ( $n=36$ ). This is clearly demonstrated in the example shown in Fig. 3c, and Movie 3 in the supplementary material, where, 276 minutes into the time series, the immature hair-cell siblings begin to rotate within the plane of the epithelium, transiently and locally breaking the midline of mirror symmetry. This is most evident 306 minutes into the time series. A complete inversion of the hair cells precisely realigns them along the axis of planar polarity of the neuromast to reform mirror symmetry, which is evident 730 minutes into the time series. Therefore, oriented UHCP divisions are not essential for directional regeneration or bilateral symmetry.



### 3.3.4 A polar compartment is not a niche nor does it harbor stem cells

To further assess the relationship between regeneration anisotropy and bilateral symmetry, we deemed it essential to determine the mechanism that mediates the localized acquisition of the UHCP fate. We focused on the polar compartments, hypothesizing that their constituent cells either directly differentiate into UHCPs or that they represent a stem-cell niche from where UHCPs originate. An alternative possibility is that a localized stem cell population does not exist in the neuromast. An extension of this proposition is that the polar compartment is not a niche. We tested these hypotheses by continuous imaging of regenerating neuromasts at single-cell resolution for periods ranging between 32 and 48 hours using *Tg[Cldnb:mGFP; SqET4]* double transgenic fish. We evaluated cellular behavior before and after UHCP development, and directly tracked cellular movement, proliferation and fate acquisition in vivo. Prospective UHCPs were identified retrospectively by playing the time series backwards, and each labeled with a colored dot. Cells were followed forward over time in all 10 successful long-term recordings, which consistently showed that although most neuromast cells do not change their relative position, some individual supporting cells relocated to the areas defined by the polar compartments, where they subsequently became UHCPs (Fig. 3d; see Movie 4 in the supplementary material). This result shows that prospective UHCPs originate elsewhere in the neuromast. It also indicates that the polar compartments are not stem-cell niches. On the contrary, these compartments represent an environment that opposes a niche to permit the differentiation of UHCPs.

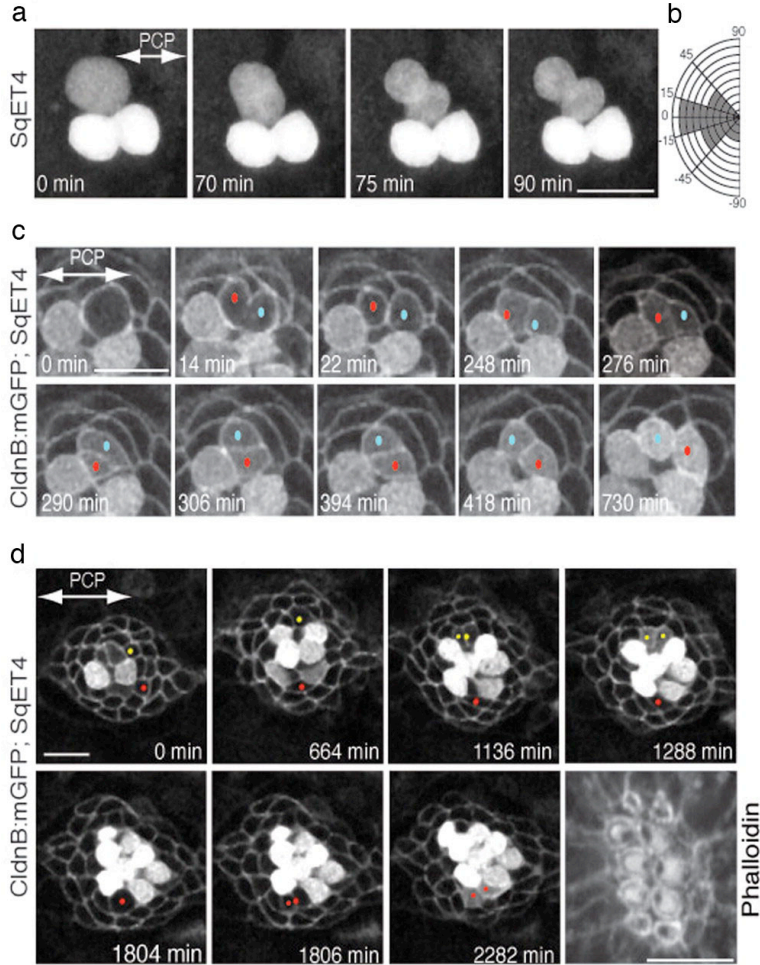


**Figure 3. Orientation of UHCP divisions and planar cell inversion. (a)** A 90-minute series of confocal images of a regenerating SqET4 neuromast revealing two GFP-positive hair cells aligned along the axis of planar polarity (double-headed arrow). An UHCP develops at the upper edge of the neuromast. Over the next hour, this UHCP commences mitosis and divides obliquely into a pair of hair cells. **(b)** Quantification of the angle of division of UHCPs in 23 neuromasts, which indicates that the majority of UHCP divide obliquely respect to the axis of planar polarity of the epithelium. **(c)** A 12-hour series of confocal images of a regenerating neuromast of a double-transgenic *Tg[Cldnb:mGFP;SqET4]* larva revealing two GFP-positive hair cells at the lower aspect of the image, and a UHCP at the top. At 14 minutes into the time-series, this UHCP divides into two hair cells, each identified with a dot (red and blue). At 264 minutes after cytokinesis (276'), the sibling hair cells begin to rotate around their contact point within the plane of the epithelium, which locally breaks the line of mirror symmetry (this is most evident at 306 minutes into the time series). A complete inversion of the hair-cell pair eventually reforms the line of mirror symmetry and precisely realigns the cells along the axis of planar polarity of the neuromast (double-headed arrow in the first panel). **(d)** A 44-hour series of confocal

images of a regenerating neuromast of a double-transgenic Tg[Cldnb:mGFP;SqET4] larva reveals plasma-membrane GFP-positive supporting cells and cytoplasmic GFP-positive hair cells and UHCPs. Two prospective UHCPs were identified retrospectively by playing the time series backwards, and each labeled with either a red or yellow dot. Their position was followed over time, showing that prospective UHCPs moved into the dorsal (yellow) and ventral (red) polar compartments, where they became UHCPs (weak cytoplasmic GFP). Each UHCP eventually divided into a pair of hair cells. The last panel of the image is an actin staining, showing the resulting planar polarization of the epithelium. The axis of planar polarity of the neuromast is indicated by a double-headed arrow in the first panel. Scale bars: 10  $\mu$ m.

### 3.3.6 Notch signaling controls the production of hair-cell progenitors

Notch signaling is universally required for hair-cell development in vertebrates (Eddison et al., 2000; Haddon et al., 1998a; Lanford et al., 1999; Ma et al., 2008). To understand the mechanism that underlies UHCP-fate acquisition, we used as tools two complementary approaches that combined live imaging with genetic and pharmacological alterations of Notch signaling. First, we expressed a constitutively active form of Notch ( $N^{ICD}$ ) by heat-shock during regeneration using triple transgenics *Tg[hs70p:Gal4; UAS:N<sup>ICD</sup>-Myc; SqET4]*, which blocked the production of UHCPs and hair cells (Fig. 4a). In a converse experiment, we abrogated Notch activity by treating SqET4 fish with the  $\gamma$ -secretase inhibitor DAPT, which generated ectopic and supernumerary UHCPs and hair cells (Fig. 4a,b) (Ma et al., 2008). These results suggest that a majority of supporting cells can become UHCPs upon loss of Notch signaling. To test this possibility directly, we continuously imaged regenerating *Tg[Cldnb:mGFP; SqET4]* fish under DAPT treatment and found that UHCPs developed ectopically and in excess (Fig. 4b,c; see Movie 5 in the supplementary material). Importantly, loss of Notch broke directional regeneration and led to planar polarity defects (Fig. 4b).

### 3.3.7 Compartmentalized Notch signaling controls regeneration anisotropy

Our previous results clearly show that Notch signaling controls the differentiation of UHCPs, but do not explain why UHCPs are produced within the polar compartments. The spatiotemporal development of UHCPs shadows the expression pattern of the hair-cell determination factors *DeltaA* and *Atoh1a* (Ma et al., 2008), suggesting that these genes are first expressed by the UHCPs. To test this possibility directly, we imaged hair-cell regeneration in a double-transgenic line expressing a red-fluorescent protein under the transcriptional control of the *Atoh1a* promoter, combined with the UHCPs marker *SqET4*. Live imaging of *Tg[Atoh1a:TdTomato; SqET4]* fish showed that *Atoh1a* is expressed at low levels in some supporting cells that we regard as prospective progenitors (see below), and is strongly upregulated by the UHCPs at the dorsal or ventral part of parallel neuromasts, where the polar compartments are located (Fig. 4d; see Movie 6 in the supplementary material). Cells expressing high levels of *Atoh1a:TdTomato* were also GFP(+) and divided to produce a pair of hair cells, indicating that *Atoh1<sup>strong</sup>* cells are UHCPs. *Atoh1* is a well-characterized negative transcriptional target of Notch (Itoh and Chitnis, 2001), suggesting that either Notch activity is low in the polar compartments, or that prospective progenitors become refractory to Notch signaling. Our previous live imaging analyses of regenerating *Tg[SqET4; Cldnb:mGFP]* fish under DAPT treatment indicated that the majority of supporting cells can become UHCPs upon loss of Notch signaling.

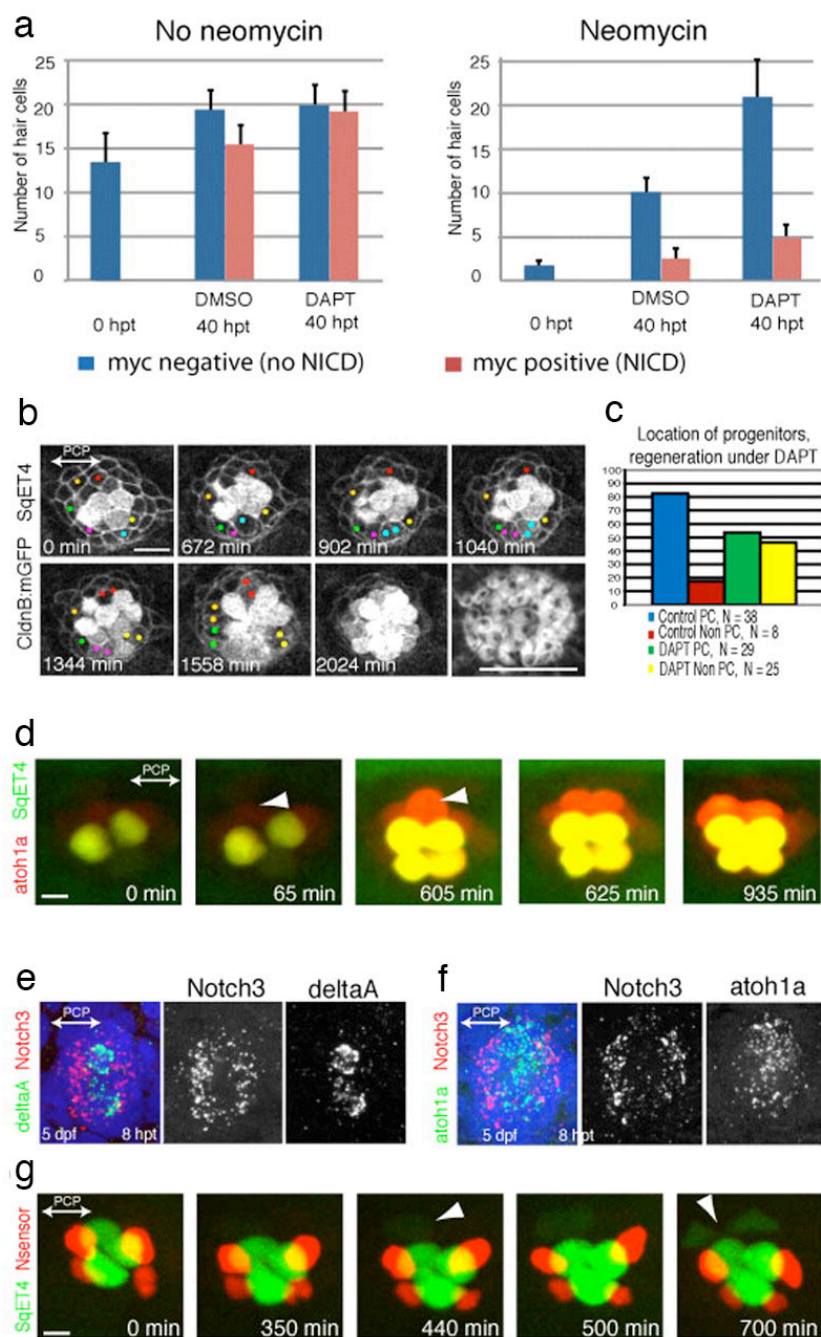


**Figure 4. UHCP develop in polar compartments.** (a) Quantification of the average number of hair cells in samples that were treated with neomycin (right) or that were not treated (left), and later exposed to DMSO or DAPT, and that expressed (red) or did not express (blue) a constitutively active form of Notch. It shows that DAPT induces the overproduction of hair cells, and this effect is suppressed by Notch activity. Results are mean $\pm$ s.e.m. (b) A 34-hour time series of a regenerating *Tg[Cldnb:mGFP; SqET4]* neuromast treated with DAPT. UHCPs were identified retrospectively by playing the time series backwards, and labeled with colored dots. UHCPs develop in excess, producing pairs of hair cells ectopically. Actin staining shows the resulting defective planar polarization (last panel). (c) A graph showing the position of UHCPs relative to the polar compartments in control and DAPT-treated neuromasts during regeneration. More than 80% of UHCPs develop within the polar compartments in controls, compared with just over 50% in DAPT-treated samples ( $n=25$ ). Results are mean $\pm$ s.e.m. (d) Time series of a *Tg[Atoh1a:TdTomato; SqET4]* double-transgenic neuromast revealing GFP-positive UHCPs and hair cells (green), and Atoh1a-expressing cells (red). It shows the temporal gene-expression hierarchy. Arrowheads indicate UHCPs. (e,f) Fluorescent whole-mount in situ hybridizations of regenerating neuromasts, revealing Notch3 (red) and DeltaA (green) (e), and Notch3 (red) and Atoh1a (green) (f). Cell nuclei are in blue. Notch3 is never expressed by the DeltaA(+) or Atoh1a(+) cells, and was absent from the polar compartments. (g) A 700-minute live imaging of a double-transgenic SqET4 (green) neuromast expressing a red-fluorescent Notch sensor (red). Notch signaling occurs outside the polar compartments. Arrowheads indicate UHCPs.

These results, together with the evidence that loss of Notch signaling expands Atoh1a expression (Itoh and Chitnis, 2001; Ma et al., 2008), indicate that supporting cells are not intrinsically refractory to Notch. Thus, some supporting cells are able to express the UHCP fate within the permissive environment of the polar compartments where Notch activity may be low or absent. Notch3 is the main receptor expressed in neuromasts and is dynamically regulated during hair-cell regeneration (Ma et al., 2008). To reveal the spatial expression pattern of Notch3, we used whole-mount fluorescent two-color in situ hybridization in combination with the UHCP markers Atoh1a and DeltaA. We found that Notch3 is strongly enriched in neuromast areas complementary to those expressing DeltaA and Atoh1a (Fig. 4e,f). Importantly, Notch3 was absent from the areas representing the polar compartments. To assess Notch signaling status directly in neuromasts, we used a validated red-fluorescent Notch sensor in combination with SqET4 (Parsons et al., 2009). Live imaging of neuromasts expressing this

combination of markers showed that Notch activation occurs outside the polar compartments (Fig. 4g). Collectively, these results indicate that Notch activity governs hair-cell regeneration anisotropy by preventing supporting cells from becoming progenitors outside the polar compartments.

### **3.3.8 Centrifugal movement of hair cells propagates planar polarity horizontally**

During phase II of regeneration, the neuromast macula loses its oval shape to become rounder because the hair-cell population expands in a direction perpendicular to that of regeneration. Consequently, planar polarity propagates laterally across the epithelium (López-Schier and Hudspeth, 2006) (Fig. 1a,e). This may occur because hair cells move away from the midline, or because UHCPs begin to appear ectopically in the neuromast during this phase. To discriminate between these possibilities, we divided the neuromast by a Cartesian grid and gave positional values to the hair bundle of each hair cell to calculate the spatial distribution of each polarity (Fig. 5a-d). This analysis showed that nearly 100% of the hair cells of each orientation were placed in separate compartments at either side of the vertical midline during phase I (Fig. 5a,b). A strongly biased distribution of polarities is maintained at either side of a vertical midline bisecting fully regenerated neuromasts (Fig. 5c,d). Importantly, comparison of polarity distributions across a horizontal midline showed distributions of 52/48% in each compartment, indicating no polarity distribution bias between the dorsal and ventral halves of parallel neuromasts (Fig. 5d). These observations support the possibility that the macula expands horizontally by a centrifugal movement of hair cells. During hair-cell development, there is a temporal hierarchy of gene expression along which cells transition as follows: SqET4<sup>-</sup>/Atoh1a<sup>weak+</sup> (prospective UHCPs) → SqET4<sup>+</sup>/Atoh1a<sup>strong+</sup>

(UHCPs and immature hair cells)  $\rightarrow$  SqET4<sup>+</sup>/Atoh1a<sup>-</sup> (mature hair cells) (Fig. 5e). We evaluated the expression of these markers in fully regenerated neuromasts using triple transgenics *Tg[atoh1a:TdTomato; SqET4; Cldnb:mGFP]* and found that the oldest hair cells (SqET4<sup>+</sup>/Atoh1a<sup>-</sup>) were located at the periphery of the neuromast furthest from the midline of bilateral symmetry, whereas the youngest pairs (SqET4<sup>+</sup>/Atoh1a<sup>strong+</sup>) were central and described the typical direction of regeneration that connects the dorsal and ventral polar compartments ( $n=9$ ) (Fig. 5f). DiASP incorporation experiments that discriminate between immature and mature (mechanotransducing) hair cells revealed that older cells described a line perpendicular to that of the direction of regeneration (Fig. 5g). Importantly, DiASP(+) cells were always excluded from the polar compartments where the UHCPs and immature hair cells are preferentially located (Fig. 5g). These results, together with the scarcity of UHCPs outside the polar compartments (Fig. 3d, Fig. 4c), indicate that the horizontal expansion of planar polarity is not caused by the ectopic development of UHCPs, and that it is likely to occur because older hair cells that maintain their original orientation move away from the midline of the neuromast towards its periphery.



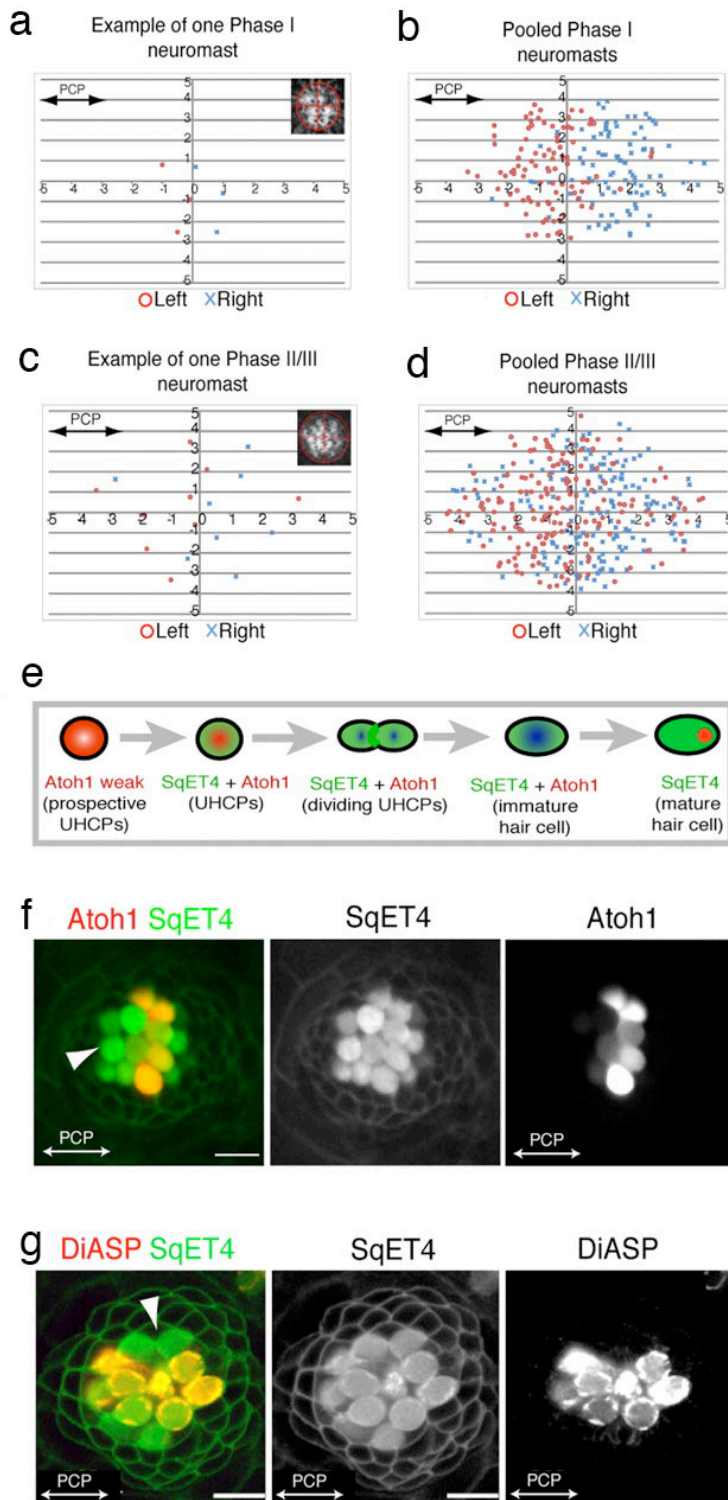


**Figure 5. Local and global planar polarization of the neuromast epithelium.** (a-d) Hair-cell planar polarity distribution in regenerating and mature neuromasts. Positional values of each polarity are plotted in a Cartesian plane. (a,b) Example of one neuromast (a) and 20 pooled neuromasts (b) in Phase I. (c,d) Example of one neuromast (c) and 22 pooled neuromasts (d) in Phase II/III. (e) Schematic transition of marker gene-expression in prospective UHCPs [weakly *Atoh1a*+ (pink)], UHCPs, immature and young hair cells [co-expressing *SqET4* and *Atoh1a* (green/red)], and mature hair cells [exclusively *SqET4*+ (green)]. (f) A *Tg[Atoh1a:TdTomato; SqET4]* neuromast exemplifies this transition [GFP(+) UHCPs and hair cells (green) and *Atoh1a*(+) cells (red)]. The white arrowhead indicates mature hair cells on the rostral part of this parallel neuromast. (g) DiASP incorporation into hair cells of *Tg[Cldnb:mGFP; SqET4]* neuromast, showing the exclusion of mature hair cells from the polar compartments. The white arrowhead indicates immature hair cells on the dorsal part of this parallel neuromast.

## 3.4 DISCUSSION

### 3.4.1 Hair-cell regeneration anisotropy and bilateral symmetry are functionally linked

During the initial phase of hair-cell regeneration in the zebrafish lateral line, a vertical midline bisects the neuromast epithelium into perfect mirror-symmetric plane-polarized halves. Each half contains hair cells of identical planar orientation but opposite to that of the confronting half. Hair-cell regeneration is strongly directional along the axis of bilateral symmetry. Our results explain the reason behind this reproducible behavior. It occurs because the development of UHCPs is spatially restricted to the dorsal or ventral polar compartments. The division of UHCPs into two hair cells, coupled with a consistent opposite planar orientation of the hair-cell siblings along a single axis, eventually defines the midline of mirror symmetry. Live imaging demonstrates that oriented progenitor divisions are not essential for regeneration anisotropy. Therefore, bilateral symmetry is sustained by a strongly anisotropic regeneration process that relies on the stabilization of

progenitor identity in permissive polar compartments. An additional important aspect of our results is that they conclusively demonstrate that the SqET4 transgenic line highlights bona fide hair-cell progenitors, the proliferation of which is essential for hair-cell regeneration in the lateral line. This conclusion is further supported by a recent publication reporting that the promoter element of the *atp2b1a* gene is responsible for the expression pattern of the GFP in the SqET4 transgenic line, and that a morpholino-mediated knockdown of *atp2b1a* negatively affected the division of the hair-cell progenitors (Go et al., 2010).

### **3.4.2 Regeneration anisotropy is not due to a localized stem-cell population**

One explanation for the compartmentalized acquisition of UHCP identity is that the polar compartments are stem cell niches. Live imaging indicates that this is unlikely because prospective UHCPs originate elsewhere in the neuromast. Thus, the polar compartments appear to be a permissive environment for the acquisition of UHCP identity by supporting cells. One possibility is that an intrinsic cell-fate determinant instructs some supporting cells to become UHCPs, and that intercellular signals prevent these cells from fully executing their differentiation until they reach a polar compartment. Previous results suggest that the source of hair-cell progenitors are the Sox2(+) cells that reside basally in the neuromast epithelium (Hernández et al., 2007). The observation that in the mouse, chick and zebrafish ears, the combinatorial activity of Sox2 and Notch control the development of pro-sensory patches, from where hair cells will eventually develop supports this proposition (Daudet et al., 2009; Millimaki et al., 2010). Future experiments involving loss- and gain-of-function of Sox2 in the lateral line will allow this possibility to be tested directly.

### **3.4.3 Regeneration anisotropy depends on compartmentalized Notch signaling**

What controls the spatiotemporal development of UHCP? When Notch activity was blocked in the whole organ by DAPT treatments, directional regeneration was broken, indicating that compartmentalized Notch signaling prevents the ectopic development of hair-cell progenitors. Using fluorescent sensors and live imaging, we demonstrate that the polar compartments have low levels of Notch signaling. Because the localization of the polar compartments does not change over time, a consequence of UHCP development within them is the anisotropic regeneration of the hair cells. We have observed that hair-cell regeneration is always progressive. Live imaging of SqET4 fish showed that UHCP development alternate between the dorsal and ventral aspects of the neuromast. One explanation for the progressive development of UHCPs is that Atoh1a in the UHCPs and in young hair cells activates the expression of Notch ligands cell-autonomously. In turn, lateral inhibition originating from these cells would prevent the surrounding supporting cells from becoming new progenitors until hair cells have matured and lost Atoh1a expression. This would decrease the number of cells expressing Notch ligands, allowing the organ to re-set and develop new UHCPs. It will be necessary to define the identity of the relevant Notch ligands and to manipulate their activity in a cell-specific manner to test this hypothesis.

### **3.4.4 The origin of axial references remains unknown**

One outstanding question is the origin of axial references and whether they rely on long-range signals. If this were the case, disruptions of regeneration

anisotropy should not affect epithelial planar polarity because hair cells would be properly oriented regardless of their position in the epithelium. It follows that disruptions of Notch that break regeneration anisotropy should not cause planar-polarity defects in the epithelium. However, loss of Notch signaling randomizes hair-cell orientation, arguing against a role of long-range cues in polarizing the epithelium. However, we cannot currently rule out the possibility that Notch signaling directly controls the establishment of axial references for planar polarity by affecting the expression, transport or interpretation of long-range polarizing cues. Future experiments using iterative cycles of hair-cell ablation and regeneration, with an intervening blockade of Notch signaling, may be able to provide evidence for or against a role of Notch in the control of polarizing cues. An alternative possibility that could reconcile the effect of loss of Notch with a role of long-range polarization is that Notch signaling controls the positioning of the organelle that defines planar polarity in this tissue, the kinocilium of the hair cell. Under this scenario, loss of Notch would not allow kinocilia to respond to external polarizing cues. However, we believe that this is not likely because loss of Notch signaling in the mouse and the zebrafish ears produce normally polarized hair cells, which align in similar directions to their neighbors (Haddon et al., 1998a; Lewis and Davies, 2002). In addition, a disruption of the internal machinery for planar polarity in the cell by loss of Notch should generate some hair cells with centrally located kinocilia, a phenotype that we have never observed. With our current knowledge, the most likely explanation for the planar polarity defects in neuromasts lacking Notch signaling is that supernumerary hair cells produce mechanical disturbances or packaging defects. Thus, a role for long-range polarizing signals at the origin of axial references remains a possibility.

### **3.4.5 Centrifugal hair-cell movement propagates planar polarity horizontally**

Although hair-cell regeneration remains strongly anisotropic, the macula eventually expands symmetrically. This could be due to the development of UHCPs outside the polar compartments during Phases II and III. Alternatively, polar compartments may themselves relocate or expand around the entire neuromast. Although these situations are possible, the weight of the evidence is against them. First, the majority of UHCPs develop within the dorsal or ventral aspect of neuromasts in all three phases of regeneration, and the small percentage of UHCPs that could not be unambiguously located within these compartments would be insufficient to account for the rapid and widespread symmetric expansion of planar polarity. Second, we observed that peripheral hair cells were negative for *Atoh1a*, indicating that they are older than those located centrally or nearby the polar compartments. Therefore, we conclude that planar polarity is likely to propagate symmetrically because hair cells move away from the midline towards the periphery of the neuromast. It follows that the hair cells located peripherally along a line perpendicular to that of regeneration should be the oldest. Our results on DiASP incorporation support this conclusion.

### **3.4.6 Planar cell inversions**

Live imaging demonstrates that oriented progenitor divisions are not essential for regeneration anisotropy. In addition, we observed that the majority of hair-cell sibling rotate around their contact point immediately after UHCP cytokinesis. To the best of our knowledge, our data is the first description of ‘planar cell inversions’. This remarkable cellular behavior could offer further mechanistic insights into the process that sustains bilateral symmetry during regeneration. It may reveal a general process that links epithelial polarity to external mechanical cues (Aigouy et al., 2010). It could also play a role in maintaining cellular orientation in plastic tissues with high cellular turnover, such as in the mammalian kidney, lung or brain

ventricles (Fischer et al., 2006; Mirzadeh et al., 2010; Saburi et al., 2008; Yates et al.).

### **3.5 Conclusion**

In this study we employed transgenic sensors and markers of hair-cell progenitors, combined with high-resolution long-term in toto continuous live imaging, to demonstrate that hair-cell regeneration is strongly anisotropic, and that regeneration anisotropy is regulated by Notch signaling. The model that emerges from our results (summarized in Fig. 6) suggests that bilateral symmetry is sustained by compartmentalized Notch activity, which governs regeneration anisotropy by permitting the stabilization of UHCP identity in the polar compartments. There are several examples of dynamic or stable compartments that allow cells to lose stemness and progress through a differentiation program (Mathur et al.; Voog et al., 2008). In the specific case of the lateral line, the polar compartments appear to oppose a niche by allowing supporting cells to become UHCPs. Further molecular dissection of this process in the zebrafish lateral line may provide deeper insights into the mechanisms that control the homeostasis of tissue architecture.

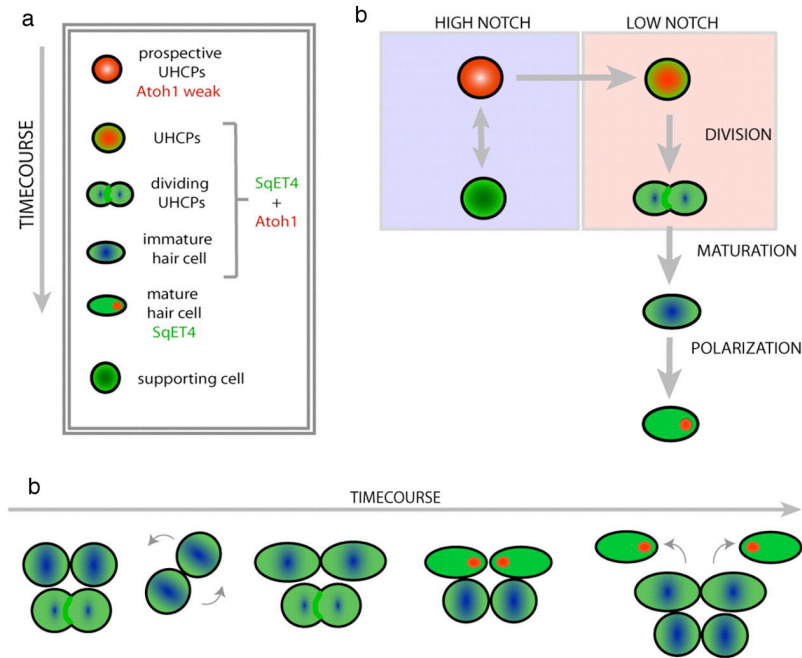


**Figure 6. Model of epithelial planar polarization in the neuromast. (a)** Scheme of the different cell types or cell status in the neuromast. Cellular identities are color coded and the expression profile of the different markers is placed next to the cells. A gray arrow indicates the temporal transition along the differentiation path. **(b)** The model of cell-fate acquisition in the neuromast, combining the temporal hierarchy of gene expression relative to the areas of high (purple) or low (pink) Notch activity. **(c)** The temporal transition of hair cells from the division of their progenitor, through the planar inversions indicated by two curved gray arrows on the second scheme from the left, and the eventual realignment of polarized hair cells, shown by the red dots that represent the kinocilia. Two small gray arrows show the centrifugal movement of mature hair cells in the right-most schematic, which propagates planar polarity across the epithelium.

### 3.6 Supplementary materials

**Supplementary Movie 1. Time lapse of a regenerating neuromast in the *SqET4* transgenic line treated with nocodazole.** GFP expression highlights UHCPs and hair cells. This neuromast has developed two hair cells a single UHCP that could never divide or produce hair cells.

**Supplementary Movie 2. Time lapse of a regenerating neuromast in the *SqET4* transgenic line.** GFP expression highlights a UHCP that divides mitotically giving rise to a pair of hair cells. The axis of cell division is oblique to the axis of epithelial planar polarity of the neuromast.



**Supplementary Movie 3. Time lapse of a regenerating neuromast in the double transgenic *TgCldnb:mGFP; SqET4* line, which expresses a membrane-targeted GFP in all supporting cells and a cytoplasmatic GFP in UHCPs and hair cells.** A UCHP appears at the dorsal aspect of the neuromast. Upon UCHP cytokinesis, the two sister hair cells invert positions, transiently and locally loosing their position on either side of the line of bilateral symmetry, and eventually they re-align along the axis of epithelial planar polarity.

**Supplementary Movie 4. Time lapse of a regenerating neuromast using a double transgenic *TgCldnb:mGFP; SqET4*.** Some individual supporting cells (back-tracked and identified with a red and a yellow dot) move within the plane of the epithelium to reach a polar compartment, where they subsequently become UHCPs, each dividing into a pair of hair cells.

**Supplementary Movie 5. Time lapse of a regenerating neuromast using a double transgenic *TgCldnb:mGFP;SqET4* under DAPT treatment.** Supporting cells that divided to generate hair cells were back-tracked and identified with colored dots. This shows that the inhibition of Notch signaling leads to excessive and ectopic formation of UHCPs that eventually divided generating pairs of hair cells.

**Supplementary Movie 6. Time lapse of a regenerating neuromast using a double transgenic *Tgato1a:TdTomato; SqET4*.** TdTomato (red) is expressed at low levels in supporting cells and strongly upregulated in a UCHP also SqET4(+) in green that develops within the dorsal polar compartment. This UCHP eventually divides into a pair of hair cells.

“Even an angel learns how to fly”

- *Fantasia Barrino* -

# Chapter 4

## The histone variant macroH2A is an epigenetic regulator of key developmental genes

(This chapter is only a part of published paper collaboration  
with Luciano Di Croce Group)

Marcus Buschbeck<sup>1,4</sup>, Iris Uribesalgo<sup>1</sup>, Indra Wibowo<sup>1</sup>, Pau  
Rué<sup>1,2</sup>, David Martín<sup>1</sup>, Arantxa Gutierrez<sup>1</sup>, Lluís Morey<sup>1,4</sup>,  
Roderic Guigó<sup>1</sup>, Hernán López-Schier<sup>1</sup> and  
Luciano Di Croce<sup>1,3</sup>

<sup>1</sup>*Laboratory of Sensory Cell Biology & Organogenesis, Centre de Regulació Genòmica, Doctor  
Aiguader 88, (08003) Barcelona, Spain*

<sup>2</sup>*Department de Física i Enginyeria Nuclear, Universitat Politècnica de Catalunya, Terrassa,  
Spain*

<sup>3</sup>*Institució Catalana de Recerca i Estudis Avançats (ICREA), Barcelona, Spain*

<sup>4</sup>*Present addresses: Institute for Predictive and Personalized Medicine of Cancer (IMPPC),  
Barcelona, Spain*

*Nature Structural and Molecular Biology 2009 16(10), 1074-1079*

## 4.1 Abstract

The histone variants macroH2A1 and macroH2A2 are associated with X chromosome inactivation in female mammals. However, the physiological function of macroH2A proteins on autosomes is poorly understood. Microarray-based analysis in human male pluripotent cells uncovered occupancy of both macroH2A variants at many genes encoding key regulators of development and cell fate decisions. On these genes, the presence of macroH2A1+2 is a repressive mark that overlaps locally and functionally with Polycomb repressive complex 2. We demonstrate that macroH2A1+2 contribute to the fine-tuning of temporal activation of *HOXA* cluster genes during neuronal differentiation. Furthermore, elimination of macroH2A2 function in zebrafish embryos produced severe but specific phenotypes. Taken together, our data demonstrate that macroH2A variants constitute an important epigenetic mark involved in the concerted regulation of gene expression programs during cellular differentiation and vertebrate development.

## 4.2 Introduction

The structural unit of chromatin is the nucleosome. It consists of DNA wrapped 1.75 times around an octamer of histone proteins. In addition to their structural role, histones are integration sites for various signals and are highly modified on their N-terminal tails (Kouzarides, 2007). These modifications serve as binding platforms for other proteins and are crucially involved in the regulation of all chromatin functions, such as DNA repair and transcriptional regulation.

The term 'epigenetic' has been coined for information that does not rely on DNA sequence but can still be transmitted from mother to daughter cells (Wolffe and Matzke, 1999). Histone modifications and DNA methylation constitute a large part of the epigenetic memory of the cell. A common form of epigenetic modification is the complete exchange of a canonical histone for a variant. Among all known histone variants, macroH2A differs most from its canonical counterpart, but its function is poorly understood (Sarma and Reinberg, 2005). In addition to a homologous histone domain, macroH2A has a large C-terminal domain of unknown activity, called the macro domain. This domain is about twice the size of the histone domain and protrudes out of the compact structure of the nucleosome (Chakravarthy et al., 2005). Thus, the macro domain is likely to serve as a binding interface for chromatin regulators. The vertebrate genome contains two closely related macroH2A variants, macroH2A1 and macroH2A2, which are enriched at the inactive X chromosome and centrosomes, suggesting their involvement in gene repression and heterochromatinization (Costanzi and Pehrson, 1998). MacroH2A1 can interfere with transcription factor binding, SWI/SNF-induced nucleosome sliding and initiation of RNA polymerase II (RNAP II) transcription *in vitro* (Angelov et al., 2003; Doyen et al., 2006). In Namalwa cells, a Burkitt lymphoma cell line, the presence of macroH2A1 in a positioned nucleosome on the proximal promoter rendered the interleukin-8 (*IL8*) gene inactive and insensitive to viral stress stimuli (Agelopoulos and Thanos, 2006). MacroH2A1 in complex with inactive poly (ADP-ribose) polymerase-1 (PARP1) contributes to the repression of heat shock-responsive *hsp70* genes (Ouararhni et al., 2006). Upon heat shock, macroH2A1 is released from the promoter, thus activating PARP1, which in turn stimulates transcription through ADP-ribosylation. The inhibition of PARP1 by macroH2A1 also contributes to X chromosome inactivation (Nusinow et al., 2007). Notably, the macro domain can bind ADP-ribose and some of its derivatives, but the

consequence of such metabolite binding is not known (Karras et al., 2005; Kustatscher et al., 2005). Despite these recent advances, the physiological and cellular function of macroH2A remains elusive, largely because of our limited knowledge about the genes that are regulated by this atypical histone variant.

Using NTera2/D1 (NT2) cells, a testicular cancer cell line that retains some stem cell characteristics such as pluripotency, we conducted an extended analysis of macroH2A targets. Here we describe more than 800 target genes identified by analyzing chromatin immunoprecipitations with human promoter arrays. Further analysis of these genes allowed us to describe the physiological function of macroH2A as an epigenetic regulator of development and cell fate decisions. This was validated *in vivo* by the generation of severe specific phenotypes upon disruption of macroH2A2 function in zebrafish embryos.

## **4.3 Results**

### **4.3.1 Genomic analysis of macroH2A target genes**

The genes encoding both macroH2A1 and macroH2A2 are expressed in NT2 cells (Supplementary Fig. 1a). To analyze their distribution in the genome, we first generated specific antibodies directed against the nonhistone regions of both forms (Supplementary Fig. 1a,b). Using these antibodies and a commercially available anti-macroH2A1 antibody, we performed a series of chromatin immunoprecipitations (ChIPs) in biological replicates (Fig. 1a). Although the commercial antibody had a weaker signal, it correlated positively with the other ChIPs (Spearman correlation coefficient 0.29). Input and pulled down DNA were labeled with different dyes and

hybridized together to human promoter arrays (ChIP-on-chip). Data were analyzed with respect to nonspecific IgG controls. We scored genes as macroH2A target genes if they had at least four significantly enriched probes within 5.5 kb upstream and 2.5 kb downstream of the transcriptional start site ( $P < 0.05$ ). To further validate our approach, we compared the list of macroH2A1 target genes calculated with nonspecific IgG samples as background controls to a list of target genes using macroH2A1 samples from cells treated with macroH2A-specific short hairpin RNA (shRNAs), denoted as shmacroH2A-treated, instead of with IgG (Supplementary Fig. 2a,b). As expected, when we used samples from shmacroH2A-treated cells, which retained residual macroH2A1 signal, for background subtraction, a smaller set of macroH2A1 target genes was yielded. Notably, this set of macroH2A1 target genes was almost fully represented in the set calculated with IgG (Supplementary Fig. 2c), thus validating the use of IgG as a negative control for our purposes.

Among the about 17,000 genes that were represented in our analysis, we identified 250 high-confidence macroH2A1 and 424 high-confidence macroH2A2 target genes (Fig. 1b). Both sets of target genes strongly overlapped with almost two-thirds of all macroH2A1 target genes that also scored positive for macroH2A2. Next, we had a closer look at those genes that scored positive for one macroH2A form but not the other. We observed that the very same probes that were significantly enriched for one macroH2A form often showed enrichment of the respective other macroH2A protein just below threshold levels ( $P < 0.05$ ). This suggested that our lists of target genes were an underestimation. Thus, we decided to perform a third analysis that treated all seven macroH2A variant samples as replicates. This approach yielded a set of 838 genes, which included more than 90% of both individual sets of target genes. This approach also led to the inclusion of 368 additional genes that showed a low but robust enrichment for both macroH2A forms.

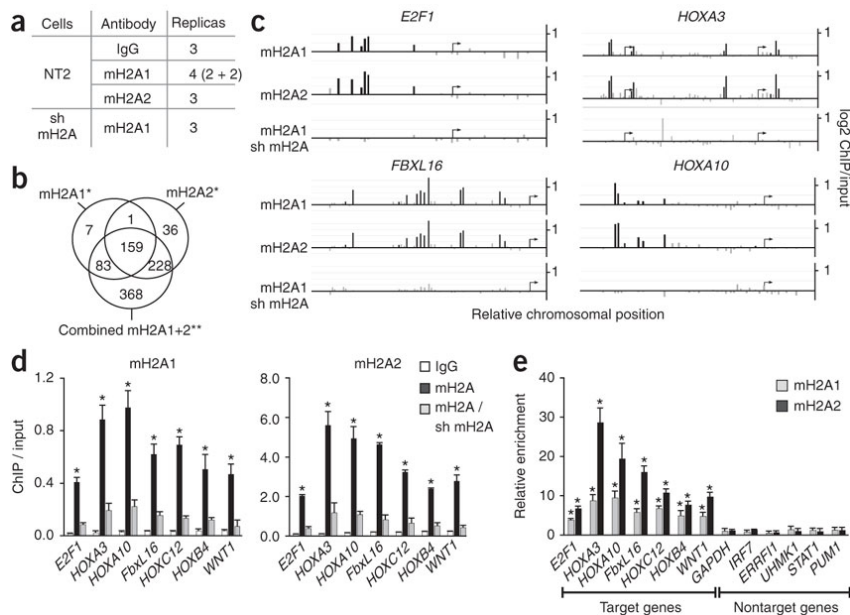


**Figure 1. Identification of macroH2A target genes by ChIP-on-chip analysis.** (a) Overview of ChIP-on-chip samples used. (b) Venn diagram showing the number and overlap of target genes calculated for macroH2A1 (mH2A1), macroH2A2 (mH2A2) and for the combined data set (\*,  $P < 0.05$ ; \*\*,  $P < 0.005$ ). (c) Enrichment plot of signals along four target genes. Significant signals are shown in black. Arrows indicate transcriptional start sites. (d) Standard ChIP analysis of identified target genes in control and shmacroH2A-treated cells (sh mH2A). Error bars indicate the s.d. of three independent experiments and asterisks indicate  $P$ -values of  $<0.05$  with respect to shRNA-treated control samples. (e) Enrichment on the same target genes with respect to the average enrichment on control genes. Asterisks indicate  $P$ -values of  $<0.05$  for both macroH2A1 and macroH2A2 compared to nontarget genes.

Enrichments of macroH2A1 and macroH2A2 were found at discrete gene regions, as indicated for *E2F1*, *FBXL16*, *HOXA3* and *HOXA10* (Fig. 1c). Signals replicated well in different biological samples (Supplementary Fig. 3) and were strongly reduced in cells treated with macroH2A shRNA (Fig. 1c, below). To validate these results, we first analyzed a set of target genes by conventional ChIP. Notably, macroH2A1



and macroH2A2 occupancy was confirmed in all cases, and the signal was strongly reduced in shmacroH2A-treated cells (Fig. 1d). Second, to exclude the effects of nonspecific co-precipitation, we confirmed that enrichment on target genes was several fold higher than on control genes (Fig. 1e). For the latter, we randomly selected a few nontarget genes and the two housekeeping genes *GAPDH* and *PUM1*.

### **4.3.2 MacroH2A variants are enriched at developmental genes**

Analysis of the largest set of macroH2A1+2 targets (GEO GSE17531) revealed that they were enriched for genes that control developmental processes (Fig. 2a). Notably, the same held true whether we calculated the sets of macroH2A1 or macroH2A2 target genes individually or used samples from shmacroH2A-treated cells instead of IgG as a background control (Supplementary Fig. 4a,b). Genes encoding proteins with homeobox domains and those containing other DNA-binding domains were overrepresented among the set of macroH2A target genes (Fig. 2b). Among these homeobox genes were almost all genes of the *HOXA*, *HOXB* and *HOXC* clusters, but also others belonging, for instance, to the *DLX*, *LHX* and *MEIS* families (Fig. 2c).

The role of macroH2A proteins in transcriptional regulation is not fully understood. The presence of both macroH2A forms on the inactive X chromosome suggested early on that they could function in repression. However, in some cases macroH2A1 was also found to be enriched upstream of highly transcribed genes such as Albumin1 (Changolkar and Pehrson, 2006). Hence, we asked how the presence of macroH2A correlates with the transcriptional activity of its target genes. For this purpose, we grouped genes into five categories based on their expression levels and then

analyzed the relative distribution of the set of macroH2A target genes. MacroH2A target genes were overrepresented in the group of genes with no detectable transcription and progressively underrepresented among groups of genes with increasing expression (Fig. 2d). Although this shows that macroH2A correlates with gene repression, its presence is not a strict indicator for transcriptional inactivity. We next aligned all target promoters at their transcriptional start site (TSS) and calculated the average distribution of macroH2A. Our results indicate that the presence of macroH2A is minimal in the direct vicinity of the transcription start site, but peaks at 2–3 kb upstream and, to a lesser extent, 2–3 kb downstream of the TSS (Fig. 2e). The reduction of the macroH2A signal at the TSS was confirmed for several target genes and was sustained after normalization for nucleosome density monitored by histone H3 ChIPs (Fig. 2f). These results suggest that macroH2A is a repressive mark that peaks at TSS distal regions, which in some cases allows transcription to occur.

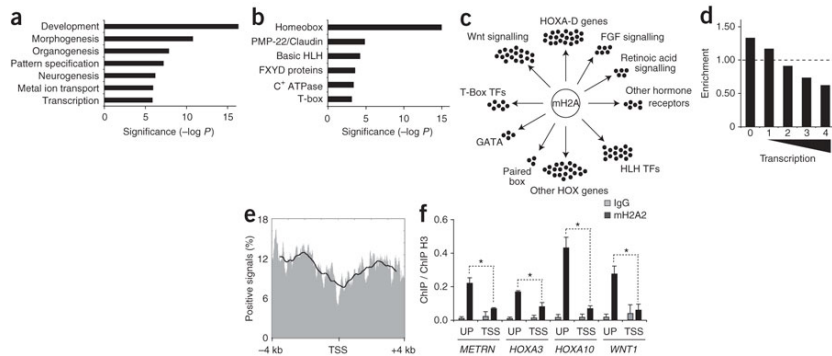


**Figure 2. Repressive macroH2A targets key developmental genes.** (a) Genes bound by macroH2A (mH2A) were compared to biological process gene ontologies. Only highly represented, nonredundant categories are shown. (b) mH2A target genes were analyzed for encoded protein domains. Significant categories including helix loop helix (HLH) proteins and cation transporter (C<sup>+</sup>) ATPases with a *P*-value < 0.001 are shown. (c) A selection of bound genes involved in developmental and transcriptional regulation. Small circles indicate number of genes. Genes were grouped according to pathways and families such as homeobox proteins (HOX),

fibroblast growth factor (FGF) signaling and HLH transcription factors (TFs). The names of genes included in the representation are detailed in Supplementary Figure 2b. **(d)** mH2A occupancy correlates with low transcriptional activity. Genes were grouped into five expression categories according to average probe intensities on Agilent Human Expression arrays (0 indicates no signal/expression and 1–4 indicates very low to high expression, respectively). Distribution of targets has been corrected for the distribution of all genes analyzed by ChIP-on-chip. **(e)** Distribution of mH2A2 bound probes within a 8-kb window centered on the TSS of its target genes. The black line represents smoothing over of the actual data. **(f)** ChIP analysis of macroH2A2 occupancy on TSS and upstream (UP) regions. Data have been normalized for H3 occupancy (\*,  $P < 0.05$ ). Results are expressed as the mean  $\pm$  s.e.m.

### 4.3.3 MacroH2A is required for proper zebrafish embryogenesis

To test the role of macroH2A *in vivo*, we decided to use zebrafish embryogenesis as a model system. The zebrafish genome possesses both a macroH2A1-encoding and a macroH2A2-encoding gene. The proteins are 70% identical to their human counterparts (Supplementary Fig. 5a). In contrast to many human cells, we found that zebrafish embryos predominantly expressed macroH2A2, whereas macroH2A1 was hardly detectable (Fig. 3a). MacroH2A2 was readily detectable by western blot (Supplementary Fig. 5b), and mRNA *in situ* hybridization indicated expression in various tissues, with particularly high levels in the developing brain (Fig. 3b).

We used specific morpholinos targeting the translational start site of the macroH2A2 mRNA to efficiently knock down macroH2A2 protein expression (Supplementary Fig. 5c,d). Injection of these inhibitors resulted in several developmental defects, the most obvious being severe deformations of the body structure (Fig. 3c and Supplementary Fig. 5e). As *in situ* hybridizations showed that macroH2A2 is highly expressed in the head region, we decided to analyze the developing brain in more detail using expression of different genes as markers.

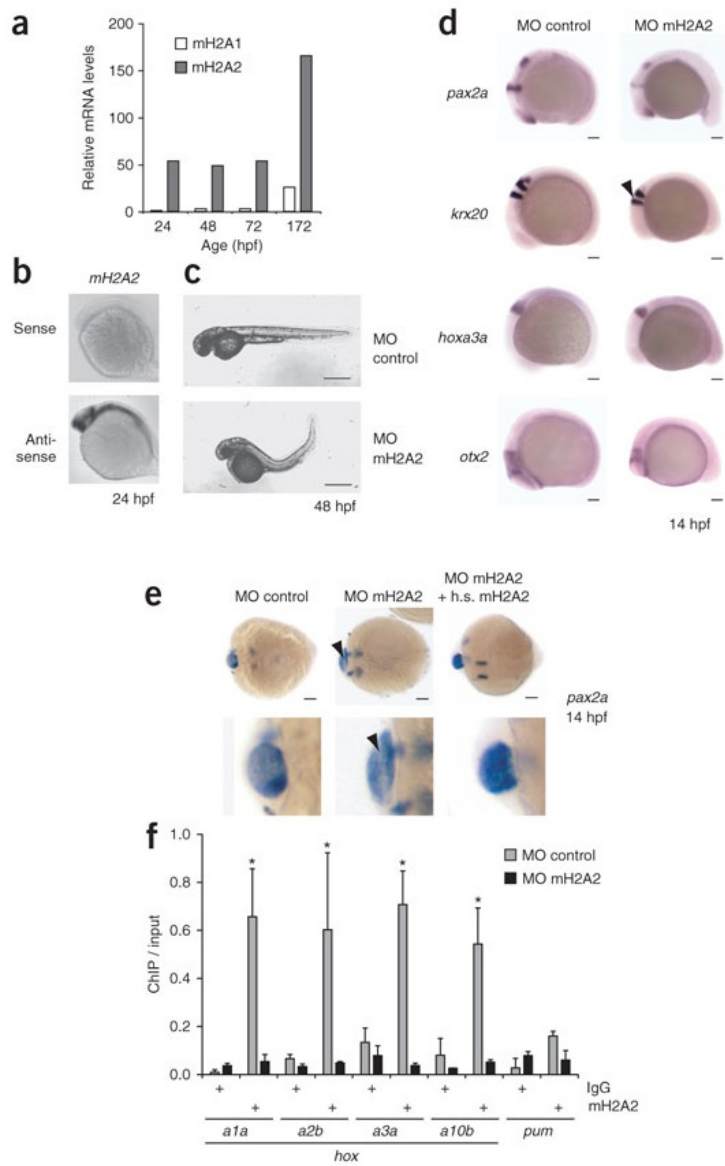


**Figure 3. MacroH2A is essential for normal zebrafish embryogenesis.** (a) MacroH2A (mH2A) expression in early zebrafish embryos. Quantitative RT-PCR analysis of both mH2A mRNAs in early zebrafish embryos at different time points (hours post fertilization (hpf)). Expression data were normalized to GAPDH expression, and data for different mH2A forms were normalized with identical amounts of corresponding plasmidic DNA. (b) Spatial expression of mH2A2 and negative control staining in the 24-hpf embryo is shown by *in situ* RNA hybridization. (c) Loss-of-function phenotype of a zebrafish embryo 48 h after injection of morpholinos (MO) directed against mH2A2 and control. Scale bars show 500  $\mu$ m. (d) Characterization of morphants and control embryos at the 11 somite stage by *in situ* RNA hybridization. Arrowheads indicate alterations in regions corresponding to rhombomere 4 and the MHB. Scale bars show 100  $\mu$ m. (e) Rescues were generated by injection of embryos with mH2A2 morpholino in combination with human (h.s.) mH2A2 mRNA. Dorsal views of embryos at the 11 somite stage are shown after *in situ* RNA hybridization for the MHB marker *pax2a*. Scale bars show 100  $\mu$ m. Below, further-magnified sections of the MHB. (f) Chromatin was prepared from MO control and MO macroH2A2-injected embryos 24 hpf. ChIP demonstrates that macroH2A2 is specifically enriched on several *box* genes (\*,  $P < 0.05$  with respect to IgG and MO macroH2A2-injected controls). Results are expressed as the mean  $\pm$  s.e.m.

MacroH2A2 morpholino-treated embryos displayed several malformations in the brain (Fig. 3d). For instance, rhombomere 4 of the hindbrain was reduced in size compared with the other rhombomeres, as indicated by staining of the neighboring rhombomeres with a *krox20* probe. Staining for *pax2a* further indicated a defect in the formation of the midbrain-hindbrain boundary (MHB). Notably, a combination of similar rhombomere 4 and MHB malformations has been observed upon miR-9 RNA overexpression (Leucht et al., 2008), suggesting developmental co-regulation of these regions. As further shown by *otx2* and *boxa3a* staining, the extension of the most anterior head region was also reduced in macroH2A2-deficient embryos compared with normal embryos (Fig. 3d).

Next, we decided to test whether human macroH2A2 can rescue the phenotype of the morphants. Therefore, we again turned to *pax2a* staining of the MHB: whereas control animals displayed the circular disc of an intact boundary in a dorsal view, macroH2A knockdown animals showed a cleft separating the structure into two halves (Fig. 3e). Notably, co-injection of

human macroH2A2 mRNA fully rescued this phenotype, thus revealing the functional conservation of macroH2A function across species. Finally, we found that macroH2A2 was specifically enriched on the promoters of several zebrafish *box* genes, suggesting that target genes of macroH2A are also shared between different species (Fig. 3f). Taken together, these results demonstrate that macroH2A function is required for proper zebrafish development and is enriched at *box* genes in this species too.

## 4.4 Discussion

The data presented here and elsewhere (Changolkar et al., 2007; Ouararhni et al., 2006) suggest that macroH2A1+2 occupies genes that need to be maintained in a chromatin state that is repressed but sensitive to signal-mediated activation. This would hold true for the many developmental regulators that we found to be macroH2A1+2 targets, which eventually need to be activated during cell fate switches in pluripotent cells. In NT2 cells, for instance, macroH2A1+2 target genes of the *HOXA* cluster were readily activated by administration of RA, which initiates the neuronal differentiation program. The fact that knockdown of macroH2A1+2 increased the sensitivity of *HOXA* genes to RA suggests that the macroH2A variants act as repressors in the fine-tuning of such developmental expression programs. *In vitro* data suggested that the presence of macroH2A in nucleosomes at the proximal promoter could interfere with transcription initiation (Doyen et al., 2006). However, our results indicate that macroH2A occupancy is minimal in the direct vicinity of the transcription start site, pointing toward an alternative mechanism of repression.

The spatial expression of macroH2A was not uniform in the zebrafish embryo, suggesting that macroH2A has specific functions for a subset of developmental processes or particular tissues. The defects observed upon elimination of macroH2A could be caused by the

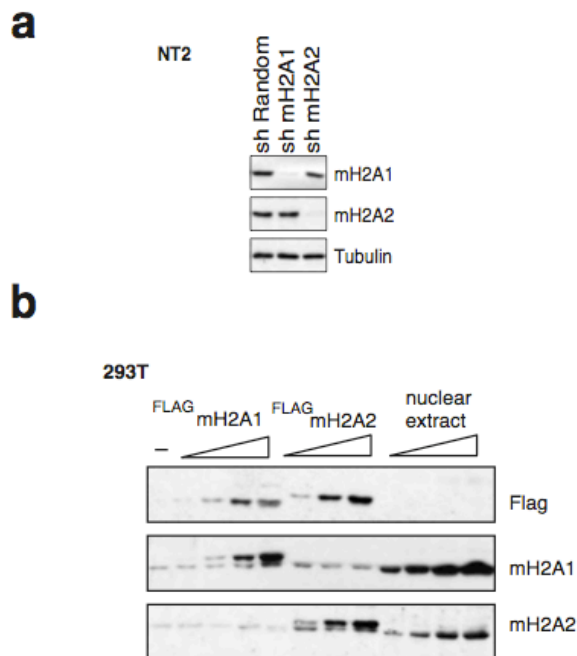
deregulation of a single pivotal key regulatory gene. However, taking into account that macroH2A targets many developmental genes, the loss-of-function phenotype is probably the consequence of alterations in the expression of several genes at once. In macroH2A-deficient animal, alterations in temporospatial gene expression patterns may not need to be strong to make them, in their sum, capable of perturbing the complex process of embryonic development. The generation of macroH2A-deficient embryos was technically facilitated by the fact that zebrafish embryos express only one of the two macroH2A forms. Otherwise, loss of a single macroH2A form might have been functionally compensated by the continuing presence of the other at the same chromatin regions. Knockout mice lacking only macroH2A1 developed normally (Changolkar et al., 2007); the slower development of mice compared to zebrafish might further allow for additional repressive pathways to compensate for loss of macroH2A function. It remains to be seen how a double knockout of both macroH2A forms will affect mammalian development, but on the basis of our results in zebrafish we would anticipate specific embryonic defects.

The presence of the histone variant macroH2A is a dynamic nucleosome modification. On the *HOXA* cluster, macroH2A is removed upon activation with RA and is re-incorporated following removal of RA. It is conceivable that several protein complexes are involved in these loading and unloading processes. Likely candidates are complexes formed around histone chaperones and chromatin remodelers, which have both been shown to be able to catalyze similar reactions with other histone proteins. The histone chaperone HIRA, for instance, was shown to specifically mediate H3.3-containing nucleosome assembly (Tagami et al., 2004). Conversely, SWI/SNF-related remodeling complexes can mediate the removal of H2A–H2B dimers from a promoter upon hormonal activation (Vicent et al., 2004). To fully understand the function of macroH2A, future work will have to thoroughly address both the regulation of macroH2A incorporation in

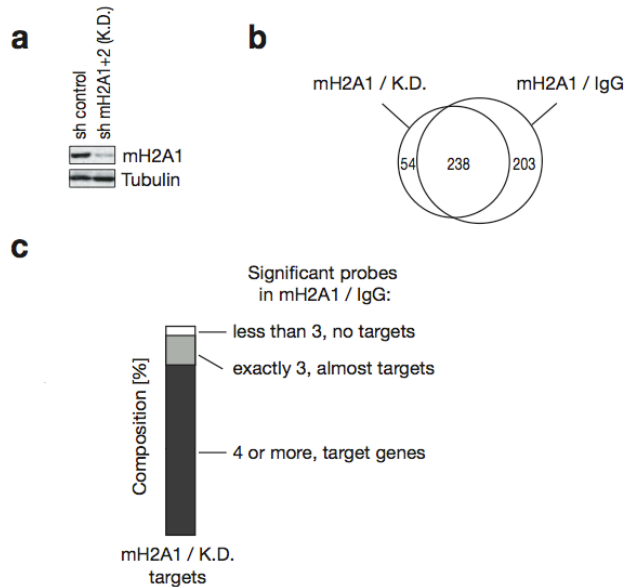
determined loci and the consequence of its presence for the function of the surrounding chromatin.



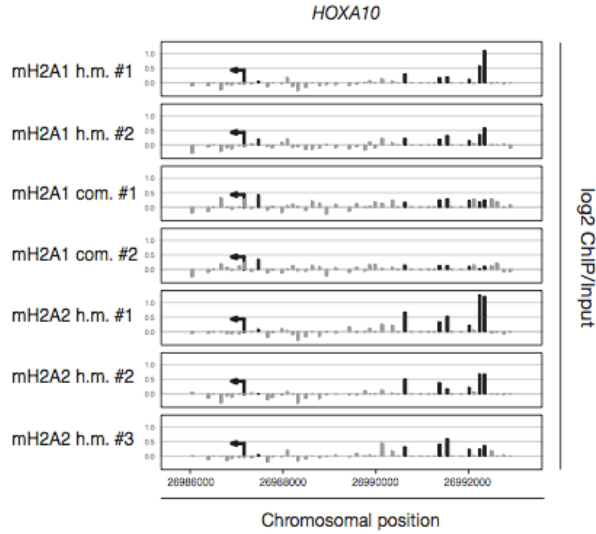
## 4.5 Supplementary Materials



**Supplementary Figure 1. Antibody specificity.** (a) NT2 cells interfered for either macroH2A1 (mH2A1) or macroH2A2 (mH2A2) were analyzed by western blot using antibodies generated against the macro domains of the respective mH2A forms. Anti-tubulin immunoblotting was used to control loading. (b) 293T cells expressing different amounts of exogenous FLAG-tagged mH2A1 or mH2A2 were analyzed by immunoblotting using anti-FLAG and the same mH2A antibodies described above.

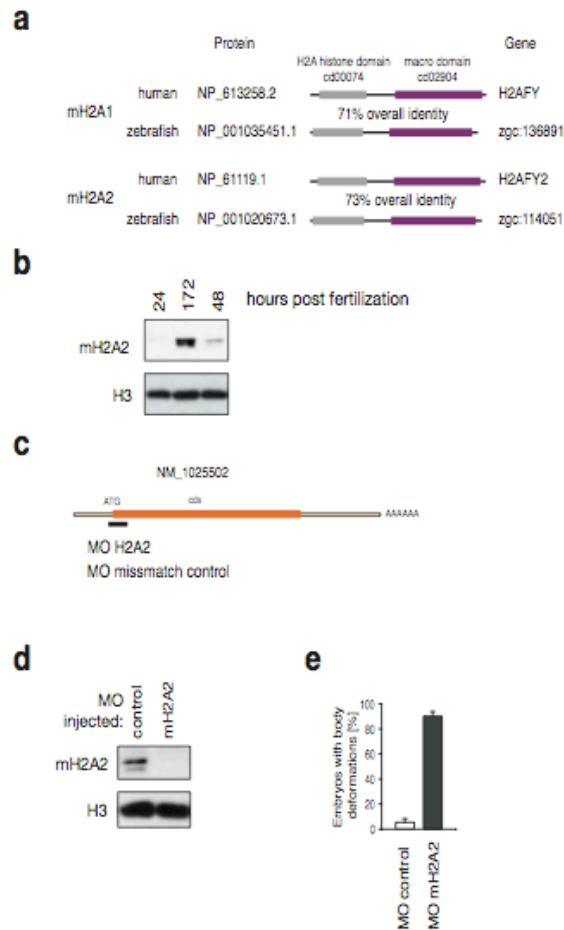


**Supplementary Figure 2. Comparison of macroH2A1 (mH2A1) target genes calculated in respect to IgG and knock-down samples.** (a) Crude cellular extracts from NT2 cells treated with shRNA targeting mH2A1+2 expression (K.D.) were analyzed by western blot using anti-macroH2A1 and Tubulin antibodies. (b) Venn diagram showing the overlap of mH2A1 target genes calculated with mH2A1 samples generated with anti-mH2A1 h.m. antibody and calculated either with respect to IgG (mH2A1/IgG) or samples generated with the same mH2A1 antibody and chromatin from K.D. cells (mH2A1/K.D.). Identification of probes with significantly enriched signal was carried out using the rank product nonparametric test. Statistically significant probes (raw p-value < 0.05) were assigned to genes if they were within -5.5kb upstream to +2.5kb downstream of its annotated TSS (by GeneSymbol and RefSeq). For the analysis, genes with probe sets with less than 5 probes were excluded. Genes were scored as target genes if they had four or more significant probes in their associated probe set. (c) Composition of mH2A1 / K.D. target genes set according to their number of significant probes in the mH2A1 / IgG data set.



**Supplementary Figure 3. ChIP-on-chip replicates.** Enrichment plots of signals along the *HOXA10* promoter are shown for all seven macroH2A (mH2A) replicates. Antibodies were either home made (h.m.) or commercially available (com.). Signals that scored significantly enriched with respect to IgG are depicted in black.





**Supplementary Figure 6. Zebrafish macroH2A orthologs and morpholino-mediated knock-down.** (a) The schematic representation of human and zebrafish macroH2A (mH2A) orthologs. Accession number for protein sequences and Gene symbols are indicated. (b) Total nuclei of zebrafish embryos were analyzed by anti-mH2A2 and anti-Histone H3 immunoblotting. (c) An inhibitory morpholino (MO) was designed against the translational start site of zebrafish mH2A2 mRNA. For the control mismatch morpholino we introduced a few base alterations. (d) Western blot of 48 h old embryos demonstrating efficient knock-down of mH2A2. (e) Quantification of embryos with body deformations (see Fig 3c).

“The world is three days: As for yesterday it has vanished along with all the  
was in it. As for tomorrow you may never see it. As for today, it is yours, so  
work on it”

- *Al-Hasan Al-Basri* -

# **Chapter 5**

## **General Discussion**

## 5.1 Eya: Seeing is not always believing

The Eyes absent (Eya) proteins possess dual functions as both protein tyrosine phosphatases and transcriptional co-activators, and are involved in cell-fate determination and organ development (Jemc and Rebay, 2007a). As transcriptional co-activator, Eya has been characterized to interact with So/Six proteins. Studies in mammals demonstrate the genetic interactions between *Eya1-4* and *Six* family genes that work together to control and regulate the development of many organs (Coletta et al., 2004; Ford et al., 1998; Xu et al., 1997a; Xu et al., 1997b). The mouse embryos of *Eya1* and *Six1* knockouts show defects in the proliferation/survival of the precursor cells of multiple organs, and die after at birth (Li et al., 2003; Xu et al., 1999; Xu et al., 2002; Zou et al., 2004). *Eya1* mutations cause Branchio-Oto-Renal syndrome (BOR) with sensorineural hearing loss, craniofacial and kidney defects (Abdelhak et al., 1997b), phenotypes that are largely recapitulated in *Eya1*<sup>-/-</sup> mice (Xu et al., 1999). Further study in mice demonstrates genetic relationship between *Six-Eya-Dach*. *Six1* can act as either an activator or a repressor when there are recruitments of cofactors, such as Eya co-activators and Dach co-repressors. Eya, in the other hand, can reverse Dach co-repressors function to become co-activator by recruiting the other co-activators, including CBP (Li et al., 2003). This is achieved on the basis of its intrinsic phosphatase activity. Other study on the development of eye disc in *Drosophila* suggests that the expression patterns and mutant phenotypes of Eya and So show similarity (Cheyette et al., 1994). Clonal analysis has showed that *so* mutant tissue undergoes cell death, explaining the loss of eye tissue in clones and suggesting a potential role for *eya* and *so* in regulating cell cycle genes (Cheyette et al., 1994; Pignoni et al., 1997).

Thus, studies on the genetic interaction between Six-Eya-Dach show a novel aspect of co-regulatory network that intricately involved co-



activator and co-repressor complexes to modulate transcription in a tissue- and promoter-specific manner (Figure 1, (Glass and Rosenfeld, 2000; Li et al., 2003; McKenna and O'Malley, 2002; McKinsey et al., 2001). The Eya-Six-Dach complexes might be able to function as transcriptional repressors through association with the Groucho (Gro) family of corepressors (Kobayashi et al., 2001; López-Ríos et al., 2003). This is based on the studies that have shown that zebrafish Six2 and Six4 and *Drosophila* So, were able to interact both with Eya and Gro family corepressors (Kobayashi et al., 2001; Silver et al., 2003). However, the interaction between Six1 and Gro was abrogated by co-transfection with Eya, suggesting Six proteins may function as corepressors independently of Eya (Silver et al., 2003). Interestingly, it has been predicted that Eya possesses a Gro-binding engrailed homology 1 (eh1) domain (Goldstein et al., 2005). Although this interaction has yet to be demonstrated in vivo, these data suggest that Eya may function as both a coactivator and a corepressor in a context-dependent manner.

Eya tyrosine phosphatase activity is important for normal eye development in *Drosophila* (Rayapureddi et al., 2003; Tootle et al., 2003). Although recent reports link the nuclear tyrosine phosphatase activity of Eya with DNA damage repair (Cook et al., 2009; Krishnan et al., 2009), the Eya tyrosine phosphatase activity has also been linked to a cytoplasmic-cellular function (Xiong et al., 2009). Phosphorylation of *Drosophila* Eya by Abelson (Abl) shuttles it to the cytoplasm in which it carries out an, as yet unidentified, essential function (Xiong et al., 2009). However, how the dual function of Eya is coordinated and coregulated during development and if these two functions are independent or interdependent still need to be study extensively.

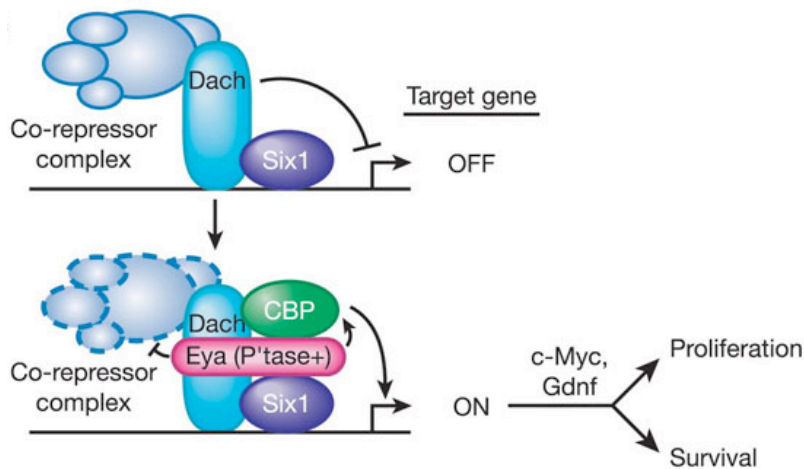
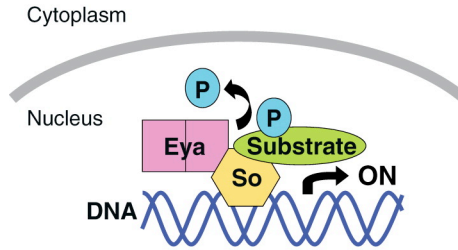


**Figure 1. Schematic model of Six–Eya–Dach complex that regulates target gene activation.** In the absence of functional Eya, Six1-Dach complex recruits a co-repressor complex and inhibits the expression of the target gene. Upon binding to the Eya protein, Six1-Dach complex recruits other co-activators, including CBP, to allow the expression of the target genes essential for precursor cell proliferation and survival (Source of this figure is from Li et al., 2003).

There are two different models proposed by Jemc and Rebay (Figure 2, (Jemc and Rebay, 2007b)). The first model depicts the Eya phosphatase activity that closely link to the transcription domain. These two functions are interconnected and cannot be separated. Eya acting as transcriptional coactivator will also act to dephosphorylate substrate in the nucleus. The second model explains the independency of transcription and phosphatase activities. Eya as transcription factor will work in the nucleus as transcriptional coactivator while Eya as phosphatase will do its function in the cytoplasm.

**a Model 1: PTP and TA linked**



**b Model 2: PTP and TA independent**

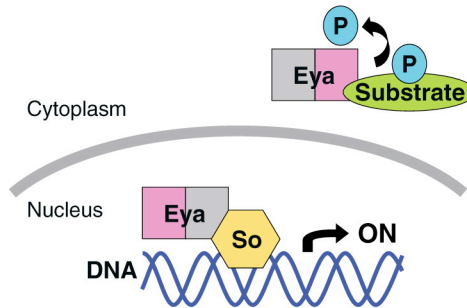


**Figure 2. Schematic models showing the relationship between Eya phosphatase and transcription factor activities.** Eya is divided in half, with the left side representing transcription activity and the right side representing phosphatase activity. Pink shading indicates which function(s) are active, whereas gray indicates inactive function(s). **(a)** Model 1: Eya phosphatase and transcription factor activities are tightly linked in that Eya both acts as a transcription factor in the nucleus and dephosphorylates substrates in the nucleus. Substrate dephosphorylation can affect transcriptional output in a variety of ways. For example, the substrate could be a cofactor that when dephosphorylated associates with Eya and Sine oculis (So) to increase transactivation of targets. **(b)** Model 2: Eya phosphatase and transcription factor functions are independent. Eya functions as a transcription factor in the nucleus but functions as a phosphatase in the cytoplasm. Many possible permutations exist for both models, some of which are alluded to in the text. Abbreviations: P, phosphate group; PTP, protein tyrosine phosphatase; TA, transcriptional activation (Source of this figure is from Jemc and Rebay, 2007b).

In zebrafish, there are at least two well-studied *eya* genes, *eya1* and *eya4* (Kozlowski et al., 2005; Nica et al., 2006; Schonberger et al., 2005; Wang et al., 2008). In zebrafish, *eya1* gene mutations cause the *dog-eared* phenotype (Whitfield et al., 1996), which is characterized by small otic vesicles,

malformed semicircular canals, reduced numbers of hair cells in the otic vesicle and the lateral line neuromasts, and very small jaw structure (Kozłowski et al., 2005). In *eya1* mutants and morphants the otic vesicle and neuromast malformations are similar to those found in *eya4* morphant fish, indicating the involvement *eya1* and *eya4* in a common regulatory network during development of the zebrafish sensory system. However, in the otic vesicle *eya1* gene is expressed in a broader domain at 24 hpf (Sahly et al., 1999), in contrast to the restricted focal domain of *eya4* expression, implied that each of these molecules had specific roles in otic vesicle development (Wang et al., 2008). The expression patterns of these two genes in the neuromasts are still to be determined. Moreover, unlike *eya1* morphants or mutants, *eya4* morphants did not show ectopic cell death in the developing otic vesicle. Particular functions by these transcriptional co-activators during zebrafish development are further evident from the studies that involve the heart (*eya4*) (Schonberger et al., 2005) or mandible (*eya1*) (Kozłowski et al., 2005).

We investigated the participation of Eya1 in migration of lateral line primordium by using genetic and pharmacological approaches. We created the dominant-negative Eya1 (dnEya1) protein that contains WRPW motif found in Her6 protein (Pasini et al., 2001; Pasini et al., 2004). This motif will recruit the repressor complex, thus, inhibiting the transcription of target genes. With this approach, we try to disrupt the transcription factor activity of Eya1 but leave the phosphatase domain intact. Although we obtained the phenotypic similarity between dnEya1-injected embryos and *dog* mutants, suggesting that phosphatase domain is dispensable for the phenotype of *dog* mutants, more detail experiments are required to show that the transcription factor and phosphatase functions of Eya1 are required independently and in parallel. The potential experiments that we could think of is by creating “phosphatase-dead” Eya transgenes that mimic the mutation if BOR or BO syndrome.

## 5.2 Eya in development and disease

There has been studied on the Eya functions as a transcriptional coactivator in correlation with Six family proteins. The interaction between these two proteins generates the activation of target genes that involve in cell cycle progression and differentiation in several tissues (Bonini et al., 1997; Coletta et al., 2004; Kriebel et al., 2007; Li et al., 2003; Yu et al., 2006). Apparently, overexpression of Eya promotes cell proliferation *in vitro* that is not dependent on the phosphatase activity (Pandey et al., 2010). Supporting this observation, *Xenopus* Eya3 overexpression exhibited an enlarge brain structures and eyes at the tailbud stage (Kriebel et al., 2007). Overexpression of Eya in *Drosophila* also resulted in tissue enlargement (Bonini et al., 1997; Pignoni et al., 1997). The studies on the Eya target genes, indeed, showed that Eya transcription factor, but not phosphatase activity, regulates cyclin D1 and cyclin A1 (Coletta et al., 2004; Yu et al., 2006) and proto-oncogene cMyc (Li et al., 2003). Thus, Eya, together with Six, may involve in tumorigenesis via different mechanisms. Although poorly studied, Dach family proteins also contribute to the tumor metastasis. The malignancy of ovarian and breast tumors and malignant peripheral sheath tumors showed de-regulation of Eya-Six-Dach complexes (Miller et al., 2010; Wu et al., 2006).

The relationship of Eya phosphatase activity and tumorigenesis is also under extensive study since the inhibition of phosphates activity in Eya could be an attractive approach for anti-cancer therapy.

Brachio-oto-renal (BOR) syndrome is an autosomal-dominant disease characterized by ear, branchial arch and kidney defects (Abdelhak et al., 1997a). This syndrome is caused by mutations in Eya and/or Six proteins (Azuma et al., 2000). The some of the mutations observed are affected the phosphatase activity (Li et al., 2003; Mutsuddi et al., 2005)5). However,

studies showed that BOR-type mutations appeared to disrupt both the phosphatase and transcriptional coactivator domains. Several data support that Eya missense mutations both in EyaBOR and EyaHAD exhibited reduced transactivation ability, suggesting that phosphatase activity contributes to Eya's transcriptional activity (Li et al., 2003; Mutsuddi et al., 2005). Several mutations in *Xenopus* Eya1 showed similar phenotypes observed in BOR syndrome, suggesting functional conservation of phosphatase active sites across species (Li et al., 2010).

As its name suggests, Eya is required for proper eye formation in *Drosophila*; however, the role in the eye development of vertebrate is still questionable. In BOR and BO syndromes eye defects are absent as well as in the Eya1 knockout mice (Azuma et al., 2000; Jemc and Rebay, 2007a; Xu et al., 1997b).

### **5.3 Eya and Other Aspects of Biological Processes**

Notch signaling is important for cell fate determination. Cell fate between two daughter cells can be determined by asymmetric distribution of Notch signaling. The difference Notch activity can be a result of different localization and inheritance of Numb, a negative regulator of Notch pathway (Cayouette et al., 2001; Petersen et al., 2002; Shen et al., 2002). In correlation with Eya1 function, localization of Numb protein is affected upon *eya1* knockout/knockdown (El-Hashash et al., 2011). This result confirmed the finding that Eya1 functions as a phosphatase to regulate aPKC $\zeta$  phosphorylation, which in turn important for asymmetric Numb localization since aPKC $\zeta$  phosphorylates Numb (Dho et al., 2006; Smith et al., 2007).

Other studies show the link between Eya1 and DNA damage repair in mammals (Cook et al., 2009; Krishnan et al., 2009). The phosphatase activity of Eya has novel role in mammalian organogenesis, acting by directing a cell's decision either to undergo apoptosis or the process of DNA

repair. This process is achieved by dephosphorylation of tyrosin 142 (Tyr-142) of H2AX (Xiao et al., 2009). In mammalian cells, histone H2A.X possesses a tyrosyl residue at its C terminus (Tyr-142), which is constitutively phosphorylated under normal growth conditions. Following DNA damage, such as in response to ionizing radiation, this residue becomes dephosphorylated, mediated by Eya phosphatase activity, while  $\gamma$ H2A.X, the Ser-139-phosphorylated form, appears. The phosphorylation of Tyr-142 blocked the recruitment of repair complexes to phosphorylate serine 139 of  $\gamma$ -H2AX, which is mediated by MDC1, whereas recruitment of pro-apoptotic factors, including JNK1, is activated (Figure 3, (Cook et al., 2009; Krishnan et al., 2009). Further characterization of the functional interaction between EYA and H2A.X will yield new insights into links between DNA damage, repair, apoptosis, and carcinogenesis

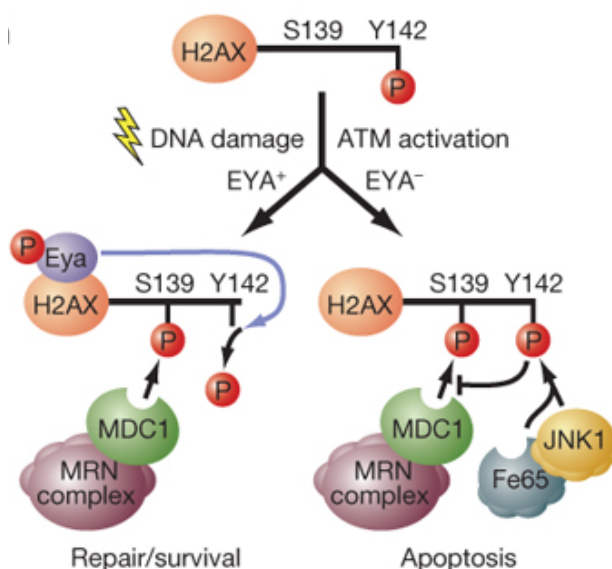


**Figure 3. Schematic model for Y142 phosphorylation status of H2AX in regulation of apoptotic versus repair response.** In the presence of Y142 phosphorylation, binding of repair factors to phosphorylated serine 139, which is mediated by MDC1, is inhibited, while recruitment of pro-apoptotic factors, including JNK1, is promoted (Source of this figure is from Cook et al., 2009).

## 5.4 Interplay among Signaling Pathways during posterior lateral line migration

Signaling molecules that are secreted by cells, part of developing and remodeling tissues, are powerful developmental regulators and modulators. These molecules must be tightly controlled in term of their expressions in spatial and temporal manners. One example of tissue remodeling in developing embryos is the migration of primordium in posterior lateral line system of zebrafish (Aman and Piotrowski, 2008; Lecaudey et al., 2008; Nechiporuk and Raible, 2008). While primordium is migrating, the successive changes occur. The cells at the front of the primordium show the characteristic of mesenchymal-like behavior that are loosened and showing processus, like lamellopodia and filopodia (Lecaudey et al., 2008).

It has been shown that long-range migration events in the lateral-line primordium are regulated by the interaction between chemokine, *sdf1a*, and its receptors, *cxc4b* and *cxc7b* (Dambly-Chaudiere et al., 2007; Haas and Gilmour, 2006; Valentin et al., 2007; Villablanca et al., 2006). The antagonistic interactions between *cxc7b* and *cxc4b/sdf1a* have been studied extensively in migrating primordium of zebrafish (Dambly-Chaudiere et al., 2007; Gamba et al., 2010). The *sdf1* gene is expressed in the trunk of the wild-type fish along the horizontal myoseptum (Dambly-Chaudiere et al., 2007; David et al., 2002; Haas and Gilmour, 2006; Valentin et al., 2007). During the development of zebrafish embryos, Sdf1/CXCR4/CXCR7 signaling is required to guide multiple migratory events, such as germ cells migration (Boldajipour et al., 2008), terminal sensory neuron migration (Knaut and Schier, 2008), interneuron (Wang et al., 2011), posterior lateral line primordium (David et al., 2002), arterial vasculature (Siekmann et al., 2009) and endoderm cells (Nair and Schilling, 2008). The spatial restriction of expression domains occurs in these events mention above. The separation



of these domains restricts one type of cell to follow its own path without intended to follow the path for another cell type (Staton et al., 2011). For example, the expression of CXCR4 is found in germ cells and the CXCR7 in the adjacent somatic cells (Boldajipour et al., 2008). In lateral line primordium, CXCR4 is expressed in the leading zone while CXCR7 is expressed in the trailing (David et al., 2002; Haas and Gilmour, 2006). It has been suggested that CXCR7 functions as CXCL12 receptor sink to generate a gradient of CXCL12 via ligand sequestration so that PGCs will migrate (Boldajipour et al., 2008). Another proposal using cell culture shows that cells transfected with both CXCR4 and CXCR7 display the heterodimers of CXCR7 with CXCR4. With this way, CXCR7 lowered the CXCR4 signaling (Levoye et al., 2009; Sierro et al., 2007). Our results showed that the expression of CXCR4 in *dog* mutant is similar to that of wildtype suggesting that Eya1 is not necessary for the expression of CXCR4. CXCR7 expression, however, is obviously affected by the loss of Eya1. This finding suggests that Eya1 functions in the migration of primordium through the expression of CXCR7. Our result is also in agreement with others that show the migration defects due to the loss of CXCR7 expression in primordium (Haas and Gilmour, 2006; Valentin et al., 2007). Our data also showed that sometime the tip cells of primordium in *dog* mutant is detached from the rest of the cells in primordium. This phenotype is reminiscence that of CXCR7 loss of function (Valentin et al., 2007). Cells that migrate individually displays at least two different behaviors that can interchange each other: run and tumble (Polin et al., 2009; Potdar et al., 2009). The run behavior correlates with the directionality movement while the tumbling one correlates with a change of orientation that results in random oriented movement and/or in circle. Interestingly, these two behaviors are observed in the tip cells of *dog* mutant primordium and sometime are accompanied by pulling back this group of cells towards the neighbouring cells. These observations strongly indicate that the trailing cells of the primordium loss the ability to migrate properly in

*dog* mutant. Thus, *Eya1* is suggested to be required for “fine-tuning” of the movement of primordium and the precise arrival of primordium at the target site.

It has been shown in neural crest migration that cell-cell contacts play important role in cell migration, although the mechanisms underlying this cell behavior and particularly those involving directionality during collective migration is still needed to be elucidated (Theveneau et al., 2010). We realized that the migration of neural crest cells can not be compared directly to the migration of lateral line primordium but from the study on neural crest migration, one can be considered that even if CXCL12 signaling is working at the single cell level, the information has to be translated into the directionality of cells that have cadherin-dependent interactions (Theveneau et al., 2010). Study in neural crest cells also suggests that cadherin-mediated cell interactions are essential for proper collective migration of a highly mesenchymal and invasive cell population. This is achieved by integrating cell interactions and external cues. In other words, the local environment has to be coupled with the interaction of each cell on the invasive cell migration (Theveneau et al., 2010).

As mentioned in chapter 2, that primordium is defined by morphogenetic territories since there are two signaling pathways involved in the formation of these regions. These territories have to be maintained throughout migration to enable primordium to perform periodic changes from mesenchymal-to-epithelial transition to the deposition of neuromast. There is much to be learnt to understand how the dynamically periodic changes in primordium is controlled at morphogenetic territories. The migratory movement of lateral-line primordium is regulated by two signaling pathways (Aman and Piotrowski, 2008; Aman and Piotrowski, 2009; Ma and Raible, 2009). These two well-known signaling centers are a Wnt/ $\beta$ -catenin signaling that is activated in few numbers of cells in leading zone and a Fgf

signaling that is activated in the trailing zone. Wnt/ $\beta$ -catenin and Fgf signaling show complex genetic interaction that restricts each other so that one signaling occupies one polarity in the primordium. Wnt/ $\beta$ -catenin signaling induces the expression of secreted Fgf3 and Fgf10 ligands in the tip cells of leading zone. At the same time, Wnt/ $\beta$ -catenin signaling also induces the Fgf signaling inhibitor *sef* in leading cells. Thus, Fgf pathway activation is inhibited in leading cells. Even though leading cells express Fgf ligand, only target genes in the trailing zone are activated because *fgfr1* is only expressed in trailing cells. Fgf ligands reach their receptor by diffusion. Fgf signaling in trailing cells activates the Wnt/ $\beta$ -catenin signal inhibitor *dkek1*, which restricts Wnt/ $\beta$ -catenin pathway activation to cells residing the leading zone of the primordium (Figure 4, (Aman and Piotrowski, 2008)). This study has demonstrated that Wnt/ $\beta$ -catenin activation represses *cxc7b* expression in leading cells. Furthermore, ectopic activation of Wnt/ $\beta$ -catenin signaling in the trailing portion of the primordium abolishes expression of *cxc7b* in these cells. As a result the primordium stops migrating, showing similar phenotype that is observed in *cxc7b*-depleted embryos (Aman and Piotrowski, 2008; Dambly-Chaudiere et al., 2007; Valentin et al., 2007). However, our study showed contrasting results. By applying pharmacological approaches, we obtained that upon inhibition of Wnt/ $\beta$ -catenin signaling, the expression of *cxc7b* in both *apc* and *dog* mutants can be restored suggesting that the loss of *cxc7b* expression in both mutants is not consequence of expanded Wnt/ $\beta$ -catenin signal.

The important question now is what triggers the activation of Wnt/ $\beta$ -catenin signaling in the tip cells of leading zone? We hypothesis here that Wnt ligands are likely the messenger for this activation although we can not rule out the possibility that other factors also take part in this process. This assumption comes from other studies done in cell cultures that showed Wnt5 or Wnt11 triggers Wnt signaling and cell motility by binding to the

Frizzled receptor and co-receptor ROR2, a receptor Tyr kinase (Nishita et al., 2006). This complex activates c-Jun N-terminal kinase (JNK) and leads to Rho-family GTPase activation, cell polarization, cytoskeletal remodeling and cell migration (Nishita et al., 2006). Although Wnt5 and Wnt11 are part of noncanonical Wnt signaling, the possibility that Wnt receptor is affecting distinct intracellular response, for example Wnt/ $\beta$ -catenin signaling, is one alternative (Figure 4, (van Amerongen and Nusse, 2009)).

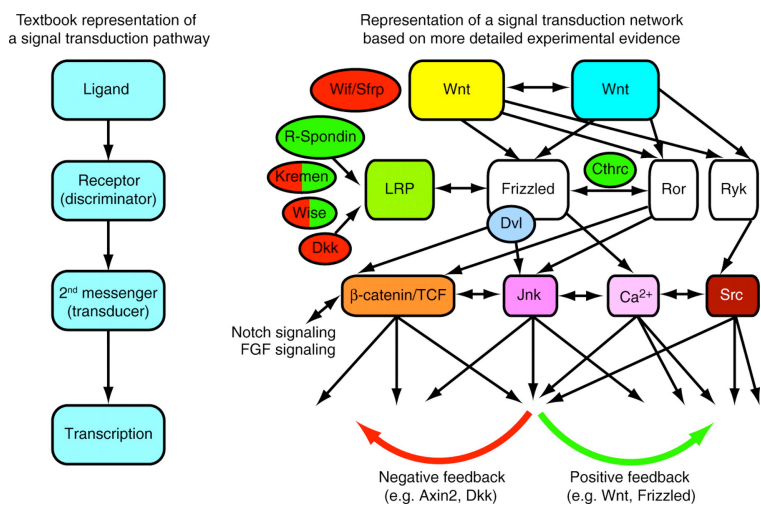


**Figure 4. Signal transduction networks.** Textbook molecular biology assigns that a signal transduction cascade begins with the binding of an extracellular ligand to a membrane receptor, after which cytoplasmic second messengers transduce the signal to the nucleus, resulting in the transcription of a given set of target genes. In reality, the situation is not that simple, and complications exist at practically every level. A wide variety of ligands exists. In reality, biology does not follow a straight line. Signals can branch off at virtually every step, modifiers can represent a parallel input that affects the outcome of signal transduction independently of extracellular ligand stimulation, intense cross-talk (depicted by double-headed arrows) exists between different signaling cascades, and feedback mechanisms provide an additional layer of control. (Source of this figure is from van Amerongen and Nusse, 2009).

The repression of Wnt/ $\beta$ -catenin signaling in the trailing cells is mediated by the Dkk1, located in the transition zone, that is activated by Fgf signaling. How this Dkk1 expression is controlled in the dynamic remodeling primordium? Why the expression of Dkk1 is restricted to the transition zone while the Fgf signaling is expressed in almost the whole trailing cells? The answers are still opened to debate. We, however, hypothesize that both Fgf and Wnt/ $\beta$ -catenin signaling take part in the regulation of Dkk1 expression at the transition zone. The model that we propose includes the combination of concentration-dependent Fgf and time-dependent Wnt/ $\beta$ -catenin signaling signals. The Fgf signaling in the trailing zone is activated in a concentration-dependent manner to control the activation of Dkk1 expression in the trailing zone. While the Wnt/ $\beta$ -catenin signaling is only activated in the leading zone by factors that are not yet determined, the time-dependent effect of Wnt/ $\beta$ -catenin signaling is influenced by the Dkk1 activity. The intriguing situation is that when the Wnt/ $\beta$ -catenin signaling reaches the threshold by the time the Fgf signaling also reaches the threshold, this is the condition where Dkk1 expression is initiated and maintained.

In conclusion, our studies have revealed the involvement of extensive cross-talk between numerous ligands, receptors, co-receptors, and transcriptional regulators as well as between downstream intracellular messengers.

## **5.5 Making use of polarity: rosette formation**

Cell adhesion is very important for proper migration of a tissue to form an organ. Cadherins are cell surface proteins that have been known to play a role in cell adhesion. During the migration of primordium, periodic

morphological alterations occur that include the formation of rosette or pro-neuromast formation and pro-neuromast deposition (Hava et al., 2009; Matsuda and Chitnis, 2010). There are two known cadherins that are expressed in lateral-line system, *epithelial cadherin* or *cadherin 1 (cdh1)* and *neural cadherin* or *cadherin 2 (cdh2)* (Kerstetter et al., 2004; Liu et al., 2003). The knock down of *cdh2* in the zebrafish showed reduced number of neuromasts in the anterior and posterior lateral line as well as some neuromasts were deposited too close to each other (Liu et al., 2003). Also, tight junctions, including claudins 1 and 4, occludin and zona occludens; ZO1, are present in the lateral line primordium of zebrafish, as well as desmosome (Lecaudey et al., 2008). All these three cell-cell junctions are enriched at the apical constriction of forming rosettes in primordium. Apical constriction is an important feature for tissue bending, invagination and epithelization in several developmental contexts, such as *Drosophila* mesoderm invagination, neurulation in vertebrate and mesenchymal-to-epithelial transition in rosette formation in lateral line primordium (Biswas et al., 2010; Dambly-Chaudiere et al., 2007; Nikolaidou and Barrett, 2004; Valentin et al., 2007). Apical constriction required apical positioning of an acto-myosin ring system at all junctions that increases surface tension locally (Lecuit and Lenne, 2007). Apical constriction is also accompanied by an expansion of the basal-lateral surface that produces bottle-shaped cells in cross section (Hardin and Keller, 1988; Kimberly and Hardin, 1998; Lecaudey et al., 2008). Study of rosette formation is also done in *Drosophila*. This rosette formation can be found in the extension of germband (Blankenship et al., 2006). In this tissue there are five to six cells or even seven cells that take part. However, the mechanisms that control this tissue to form rosette is still unclear. It might be that rosette-specific pathway controls their number, structure and position. What about rosette formation in zebrafish lateral line primordium? The well-known signaling pathway that could control rosetogenesis is Fgf signaling (Aman and Piotrowski, 2008; Lecaudey et al., 2008; Nechiporuk and Raible,

2008). Upon Fgf signaling removal either by SU5402, inhibitor of Fgf signaling, or overexpression of dnFgfr1, rosette formation is lost which in turn abolished the migration. These studies draw a conclusion that rosette formation is necessary for migration of primordium (Lecaudey et al., 2008; Nechiporuk and Raible, 2008). However, another study shows different outcome regarding relationship between rosetogenesis and migration (Aman and Piotrowski, 2008). The later demonstrates that loss of Wnt/ $\beta$ -catenin signaling by overexpression of Dkk1 or deleted form of TCF completely eliminates proneuromast formation and deposition but not the migration. This suggests that rosetogenesis is uncoupled with migration in lateral line primordium (Aman and Piotrowski, 2008).

## **5.6 The lateral line primordium connects collective migration and differentiation and/or cell fate specification**

Previous studies have shown that during the development of lateral-line system in zebrafish Notch signaling is required to control hair-cell differentiation together with pro-neural gene, *atoh1* (Haddon et al., 1998b; Itoh and Chitnis, 2001; Itoh et al., 2003; Matsuda and Chitnis, 2010). The studies on Notch signaling in zebrafish lateral line system have been carried out using *mind bomb* (*mib*) mutant that exhibits supernumerary hair cells due to loss of Notch activation, i.e. lateral inhibition function. The mutation is found in a gene encoding a RING E3 ligase (Itoh et al., 2003). Several components of Notch signaling have been studied to compare between wildtype and *mib* mutants. Those genes are the *notch3* ligand, and two Notch receptors, *deltaA* and *deltaB*, that belong to members of neurogenic genes (Haddon et al., 1998b). One pro-neural gene, *atoh1a*, is also extensively

studied in hair-cell differentiation (Itoh and Chitnis, 2001; Lecaudey et al., 2008; Matsuda and Chitnis, 2010; Nechiporuk and Raible, 2008). Recent study has reported that Notch signaling participates in controlling the expression of *atob1* gene expression by restricting its expression (Matsuda and Chitnis, 2010). This restricted expression of *atob1* is important for establishment a focal Fgf signaling centre in rosetogenesis and moreover in maturing proneuromast. The mechanism proposed is that upon activation of Wnt/ $\beta$ -catenin signaling that will activate Fgf signaling, the expression of *atob1* and *deltaA* are initiated under the control of Fgf signaling. Delta will activate Notch activity in neighboring cells which in turn will restrict *atob1a* expression to central cell. While *atob1a* drives the expression of *deltaD* and *fgf10*, it inhibits the expression of *fgfr1* and creates Fgf signaling focal activation. In the case of no Notch signaling, unregulated and broadened expression domain of *atob1a* drives the expression of *fgf10* but inhibit that of *fgfr1*. As a result, Fgf signaling is shut off, *dkk1* expression is lost and Wnt/ $\beta$ -catenin signaling is expanded (Figure 5, (Matsuda and Chitnis, 2010). Attenuated Fgf signaling will result in elimination of rosette formation and halted of the migration (Lecaudey et al., 2008; Nechiporuk and Raible, 2008).

## 5.7 Notch signaling and hair cell regeneration

Notch signaling is famous for its function for establishing cell-fate specification and differentiation throughout animal kingdom (Artavanis-Tsakonas et al., 1999; Lewis, 1998). The Notch receptors are cell-surface transmembrane proteins. They bind to their ligands, including Delta, Serrate and Jagged, that are located on the surface of adjacent cells (for review see (Kopan and Ilagan, 2009). The complex formed transduces a signal that influences cell fate choices. Several evidences show that Notch signaling is involved in regulating hair cell development and regeneration in sensory



systems of several vertebrates (Daudet et al., 2009; Hori et al., 2007; Ma et al., 2008). In the zebrafish lateral line, Notch activity limits the proliferation of supporting cells during regeneration but has no effect in a steady-state situation, indicating that an additional mechanism maintains quiescence (Ma et al., 2008). In avian auditory, similar situation occurs showing that Notch activity is not required for supporting cell quiescence in undisturbed auditory epithelium since DAPT treatments,  $\gamma$ -secretase inhibitor or Notch activity inhibitor, exhibited no effect on the conversion of supporting cells into hair cells (Daudet et al., 2009). However, upon hair cell ablation DAPT treatment triggered overproduction of hair cells via mitotic and non-mitotic events without showing direct effect on the supporting cell division (Daudet et al., 2009). Therefore, these results suggests that Notch signaling is not required for supporting cells in quiescence state or to trigger hair cell regeneration after damage. Instead, Notch activity is required for supporting cells to produce hair cells in a correct number after damage (Daudet et al., 2009).

Hair cell regeneration in zebrafish lateral line resembled the developing neuromasts as hair cells are emerging (Itoh and Chitnis, 2001; Ma et al., 2008). These two processes can be linearized by the fact that the embryonic pattern of expression of Notch pathway components is reconstituted, and Notch signaling is reactivated (Itoh and Chitnis, 2001; Ma et al., 2008). During this process, Atoh1a acts upstream of DeltaD, while Notch activity inhibits expression of Atoh1 and DeltaD (Matsuda and Chitnis, 2010). Cells that express Atoh1a and DeltaD become hair cells, and by activating Nocth in neighboring cells, they remain as progenitor cells or differentiate as supporting cells (Matsuda and Chitnis, 2010). A similar process occurs during hair cell regeneration in neuromast upon hair cell ablation. Expression levels of Atoh1a are increased, followed by DeltaA/D upregulation (this thesis and Ma et al., 2008). As mentioned above, that blockage of Notch activity resulted in overproduction of hair cells at the expense of supporting cells in the auditory epithelium of avian (Daudet et al.,



As also mentioned above, Notch is not required for the quiescence cells either in chick or zebrafish sensory systems. Likewise, Notch blockade does not reactivate the entire radial glia population (Chapouton et al., 2010) proposing that the existence of additional signaling pathways maintaining quiescence at the VZ. It has been suggested that one important player in quiescence is the family of *Hes* or their *her* orthologs in zebrafish genes (Curry et al., 2006; Sang et al., 2008). In the brain of the zebrafish, nondividing radial glia showed to express members of the *her* family (Chapouton et al., 2006; Chapouton et al.). Indeed, in the avian auditory epithelium, *Her5* is expressed in the region where there is no division suggesting that Notch signaling has an inhibitory effect (Daudet et al., 2009). However, the involvement of *her* gene family in the neuromast development and regeneration needs to be performed.

## 5.7 Notch-ing tissue on and off

Study in the retina of zebrafish, in term of neurogenesis, has shown that Notch prevents progenitors from leaving the cell cycle and differentiating prematurely (Del Bene et al., 2008). Similar process happens during the neurogenesis in the adult telencephalon of zebrafish. This study showed that Notch signaling activity triggers progenitors into quiescence, whereas blockage of Notch activity triggers neural stem cell division and thus differentiation into neurons (Chapouton et al., 2010). Apparently, there is a participation of Notch and no Notch regions in these two systems (Chapouton et al., 2010; Del Bene et al., 2008). A Notch gradient has been found along the apical-basal axis of the neuroepithelium that is likely to play a key role in neurogenesis in zebrafish retina. Higher expression Notch mRNA is found on the apical side, whereas Delta mRNA and protein are higher basally. Thus, this gradient creates neuroepithelial polarity (Del Bene

et al., 2008). They have demonstrated that when the progenitor nucleus stays close to the apical side, it will receive high levels of Notch activity, and both of its daughters are likely to remain proliferative. On the other hand, if the nucleus is translocated more basally, progenitor will receive less Notch activity then the progenitor will produce one or two daughter neurons during its subsequent mitosis (Del Bene et al., 2008).

Similarly, the fluctuation of Notch activity is found in zebrafish adult telencephalon (Chapouton et al., 2010). Notch activity or Notch receptor is found in the ventricular region where nondividing radial glia cells populate. This region is in close proximity to cycling cells. Notch signaling is endogenously active in progenitors or nondividing radial glia and that activation of the pathway results in a transition from dividing radial glial cells to nondividing ones. Inasmuch as blocking endogenous Notch activity induces a transition from nondividing radial glial cells to dividing ones. Therefore, these results suggest that there is a maintenance mechanism for the equilibrium between quiescent and proliferating progenitors and that Notch activity regulates neuronal production during adulthood by oscillation mechanism (Chapouton et al., 2010).

In our study, we reported the relocation of some individual supporting cells to the areas defined by the polar compartment. In other word, the quiescence supporting cells are maintained by high Notch activity while when supporting cells are translocated into the area where Nocth activity is reduced, they will become UHCPs. Our data and others suggest that there will be always dynamic and stable compartments that allow cells to loose stemness and progress through a differentiation program (Mathur et al., 2010; Voog et al., 2008).

## **5.8 Vertebrate development and epigenetics: macroH2Ax on zebrafish development**

Vertebrate development relies on the specification of several hundreds unique cell types from a zygote. These cells carry the same genetic information but are able to establish and maintain the specific gene expression profile that gives rise to its cellular identity. The phenomenon where the heritable changes in cellular phenotype or gene expression caused by mechanisms other than the underlying DNA sequence are referred to as epigenetics. The efforts to understand the epigenetic mechanisms, their interactions and alteration in health and disease, have become a priority in biomedical research. Differentiated cells are able to retain epigenetic memory to transmit and maintain gene expression patterns (Banaszynski et al., 2010; Hemberger et al., 2009). This epigenetic memory is transmitted through trans-acting factors such as Polycomb and Trithorax proteins, DNA methylation, noncoding RNAs, histone modifications and histone variants (Guttman et al., 2009; Henikoff, 2008; Rando and Chang, 2009). Several histone variants have been studied extensively; one of them is macroH2A. Among all known histone variants, macroH2A has significant structural dissimilarity but its function is poorly understood (Sarma and Reinberg, 2005).

Here, we demonstrate the role of macroH2A incorporation into autosomal chromosomes. This study has shown that mH2A1 and mH2A2 nucleosomes in a human pluripotent cell line occupied the promoter regions of developmental genes, including homeobox genes, significantly overlapping with Polycomb repressive complex 2. These results support the hypothesis that macroH2As plays a role in transcriptional repression. In vivo validation on the function of macroH2A has been done by using zebrafish as a model. Our results showed that zebrafish possess two macroH2A

isoforms, macroH2A1 and macroH2A2. However, macroH2A2 is the dominant gene that is expressed in the developing zebrafish embryos, especially in the brain region. Using several marker genes for the developing brain and hox genes, our results showed that there are developmental defects with prominent malformation in the brain upon morpholino injection targeting transcriptional start site of macroH2A2. The conservation of macroH2A2 across species was also tested by injecting human macroH2A2 mRNA into zebrafish eggs. The result indicated that human macroH2A2 could rescue the phenotype of injected embryos with morpholino suggesting the functional conservation.

## **5.9 Future directions:**

1. How are Eya's dual functions as transcription factor and protein phosphatase coordinated and coregulated during development? Are the two functions dependent or independent?
2. Identification of biological relevant substrates of Eya1 phosphatase activity will be crucial to elucidating the functional importance of this activity in both normal development and human disease.
3. Elucidating of the complete list of targets activated by Eya1-Six transcription factor will provide insight into how Eya1 and the retinal determination gene network (RDGN) interface with a variety of signaling pathways to regulate patterns of gene expression important for cell cycle control, cell fate specification, differentiation, and morphogenesis.
4. Regeneration can be seen as recapitulating development; thus many of the genes involved in hair-cell development are being investigated

both to gain insights and to use as tools for initiating formation of hair cells.

5. The availability of transgenic fish that expresses Gal4 in neuromast, i.e. in hair cells, have allowed us to create transgenic fishes that contain UAS promoter in their genome that drives gene of interest fused to fluorescent protein. This will ease the study of certain gene in specific cell in neuromast.
6. The loss- and gain-of-function of Sox2 in the lateral line will allow to test the possibility for the combinatorial activity between Sox2 and Notch signaling to control the development of pro-sensory patches.
7. The hypothesis is that decreased number of cells expressing Notch ligands, allowing the organ to re-set and develop new UHCPs. It will be necessary to define the identity of the relevant Notch ligands and to manipulate their activity in a cell-specific manner.

# APPENDIX 1: MATERIALS AND METHODS

## TRANSGENIC FISH AND HUSBANDRY

### Zebrafish animals and strains

Fish used were maintained under standardized conditions and experiments were performed in accordance with protocols approved by the PRBB Ethical Committee of Animal Experimentation. Eggs were collected from natural spawning and maintained at 28.5°C, embryos were staged by hour post-fertilization (hpf) or day post-fertilization (dpf).

Table 1. Zebrafish strains and transgenics using in this study.

Zebrafish	Note	Publication
<i>aal</i> <sup>22744</sup>	nonsense mutation (TCG→TAG), resulting in a premature termination deleting the last 29 amino acid residues of Eya1 protein	Nica <i>et al.</i> , 2006; Herzog <i>et al.</i> , 2004b
<i>dpg</i> <sup>m90</sup>	a GT→GG transition in a splice donor site of the <i>eya1</i> gene. During processing of mutant pre-mRNA, an intronic GT is used as splice donor, which leads to a 4-bp insertion (GGAG) and a frame shift and more severe truncation of the resulting protein, removing most of the Eya domain, including two of the three conserved noncontiguous sequence motifs that form the catalytic phosphatase core of Eya proteins	Kozłowski <i>et al.</i> , 2005; Whitfield <i>et al.</i> , 1996
<i>apc</i> <sup>m90</sup>	A premature stop codon corresponding to amino acid (a.a.) 1318 of human APC	Haramis <i>et al.</i> , 2006; Hurlstone <i>et al.</i> , 2003
<i>SqET4</i>	Enhancer trap line with EGFP reporter marked mature hair cells and hair cell progenitors of neuromast	Parinov <i>et al.</i> , 2004
<i>SqET10</i>	Enhancer trap line with EGFP reporter marked supporting cells	Parinov <i>et al.</i> , 2004
<i>SqET20</i>	Enhancer trap line with EGFP reporter marked external mantle cells of the neuromast	Parinov <i>et al.</i> , 2004
<i>Tg(cldB:lynEGFP)</i>	8 kb cldB promoter fused to	Haas & Gilmour,



	lynEGFPpA. Expression of GFP in every cell of the migrating pLLP, as well as the neuromast organs, the progenitors of which can be identified as 2–3 rosette-like structures in the migrating primordium, and a chain of interneuromast cells.	2006
<i>Tg(hsp70:ca-FGFR1)</i>	Heat-shocked inducible expression of a constitutively active form of <i>Xenopus</i> Fgfr1. A point mutation in the Fgfr1 kinase domain (K562E) results in autophosphorylation of the receptor in the absence of bound ligand (Neilson and Friesel, 1996).	Marques <i>et al.</i> , 2008
<i>Tg(hsp70:EGFP-Dkk1)</i>	mmGFP5 (Siemering <i>et al.</i> , 1996) was fused to the C-terminus of zebrafish <i>dkk1</i> (Genbank accession # AB023488). Dkk1 fusion proteins were cloned downstream zebrafish hsp70-4 promoter and upstream of the SV40 polyadenylation signal of the vector pCS2+.	Stoick-Cooper <i>et al.</i> , 2007
<i>Tg(erm:Gal4;UAS:Kaede)</i>	5 kb upstream to the ATG start site of translation of <i>erm</i> gene fused to gal4-vp16 coding sequences.	Esain <i>et al.</i> , 2010
<i>Tg(atoh1a:tdTomato)</i>		
<i>Tp1(bglob:hmgb1-mCherry)</i>	A <i>tp1bglob</i> element consisting of 6 copies of the TP1 promoter (12 Rbp-Jκ binding sites), upstream of the rabbit β-globin minimal promoter, fused to zebrafish <i>high-mobility group box 1(hmgb1)</i> gene, which encodes a nuclear factor associated with chromatin. Using standard fusion PCR protocols, this sequence (minus the termination codon) was fused <i>mCherry</i> .	Parsons <i>et al.</i> , 2009
<i>Tg(hsp70:Gal4;UAS:Nicd-myc)</i>	Over-expression of the Notch intra-cellular domain (NICD), from Notch 1a, was carried	A gift from P. Chapouton; Scheer and Campos-

	out using fish transgenic for both <i>Tg(hsp70l:Gal4)</i> and <i>Tg(UAS:myc-Notch1a-intra)</i>	Ortega, 1999
--	--	--------------

**Heat-shocked treatments on the transgenic zebrafish that possess hsp70 promoter.**

All the embryos obtained from crossing transgenic fish that bear hsp70 promoter were incubated at 39 °C for 20-30 min in groups of 30-40 in 2 ml Eppendorfs tubes containing a total volume of 1000 µl E3 medium. Following incubation embryos were returned to 10 cm petri dishes containing E3 at 28°C or RT.

**GENOTYPING OF *aal*<sup>22744</sup> and *dog*<sup>tm90b</sup>**

Individual *aal*<sup>22744</sup> mutant larvae and wild-type siblings were genotyped taking advantage of a restriction fragment length polymorphism generated by the mutation. The last exon of the *eya1* gene and flanking intron sequences were amplified via PCR from genomic DNA with primers CGA GAG AGT AAT CCA GAG GTT TG (sense) and ACA CTT GCT ACG TGT CTA GAA AAT G (antisense), followed by restriction digest of the PCR product with *TaqI* for 2 h at 65°C. In the mutant DNA, the *TaqI* site is destroyed by the mutation, and the amplified fragment remains uncleaved (260 bp), whereas the wild-type fragment is cut, yielding two bands of 180 and 80 bp. *dog*<sup>tm90b</sup> was genotyped as described in Kozlowski et al. (2005). A novel *MnI* RFLP is present in the *dog*<sup>tm90b</sup> *eya1* allele. PCR amplification of the genomic region using exon primer F7 (5'-CCAACGTCGGTGTTCATTTGGGAC-3') and intron primer R7 (5'-CGGTGAGCTTTGTAGGGGGTGAGG-3') yields an amplified product of 173-bp that, following digestion with *MnI*, yields several smaller products including a diagnostic *dog*<sup>tm90b</sup> allele-specific 82-bp product.

**DNA CONSTRUCTS**

To make dominant negative Eya1, *Danio* Eya1 cDNA was amplified using forward primer: (Eya1\_KOZAK\_NotI\_Fw):  
CGGCGGCCGCTGCCACCATGGAAATGCAGGATCTAGC  
and reverse primer: (Eya1\_her6WRPWstop\_XhoI\_Rv):  
CCTGGAGCTACCAAGGCCGCCACACCAAGGCCGCCACAAATACTCCAG  
GTCCAG. The 5' end of the amplicon was cloned between NotI and XhoI restriction sites in pCS2+ vector for synthetic cRNA production.

**RNA SYNTHESIS FOR INJECTION**

For injection, plasmid containing gene of interest was linearized with proper restriction enzymes. The linearized plasmid were used as a template for *in vitro* transcription to synthesize capped RNA. This procedure was done by using mMESSAGE mMACHINE T7/SP6/T3 Kit (Ambion). RNA polymerases used were according to the direction of open reading frame of the template.

## MORPHOLINOS

All morpholinos used in this study were diluted in sterile miliQ water and were prepared and injected in 1–4 cell stage embryos. When two MOs were injected in the same embryo, we carried out both separate injections of the different MOs and single injections of MO mixtures, with very similar results. List of morpholinos are found in Table 2.

Table 2. Morpholino oligos that are used in this thesis.

Morpholinos	Sequences (5' → 3')	Concentration	Source
Control	CTTGTTCCTGCACCACTCGAGATC	5 ng/nl	This study
<i>mH2A2</i>	TTTCTTTTCCTCCTCTGGCTGACATC	5 ng/nl	This study
<i>eya1</i>	AAACAAAGATGATAGACCTACTTCC	8 ng/nl	Kozłowski <i>et al.</i> , 2005
<i>six1b</i>	CGAAAGAAGGCAACATTGACATGAC		Bessarab <i>et al.</i> , 2004
<i>p53</i>	AGAATTGATTTTGCCGACCTCCTCT	0.025-0.1 mM	

## NEOMYCIN TREATMENTS

Selected larvae for fixation and live imaging were treated in E3 medium containing 250  $\mu$ M neomycin for 1 hour at room temperature. After treatments, larvae were washed several times using small diameter strainer to wash off residual neomycin. Larvae were allowed to recover from neomycin treatment for couple of hours before live imaging and treatments with other drugs to avoid high mortality.

## VITAL DYE AND PHALLOIDIN STAINING

For vital labeling of hair cells, larvae were immersed in 5  $\mu$ g/ml of DiASP (Invitrogen, Carlsbad, CA, USA) in E3 medium for 2 minutes at room temperature and then washed several times to remove the excess of dye. For phalloidin staining, samples were fixed in 4% PFA overnight at 4°C then washed several times in 0.1% PBST and incubated in phalloidin-Alexa 568 or Alexa 488 (Invitrogen) diluted 1:20 in 0.1% PBST overnight at 4°C. Samples were washed several times in 0.1% PBST before being mounted.

## ALKALINE PHOSPHATASE STAINING

Zebrafish neuromasts have endogenous phosphatase (AP) activity, detectable after 48 hpf. This makes it easy for rapid visualization of neuromasts. Larvae were fixed in 4%PFA for 1-4 hours at RT. Then they were washed 3 x 10 minutes in PBST. They were finally stained in a staining buffer solution (see procedure above for Alkaline Tris buffer) for *in situ* hybridization until purple color appears. This can vary from

sample to sample, from 1 minute to 15 minutes. The color reaction were stopped by washing 3 x 10 minutes in PBST and stored at 4°C.

## WHOLE-MOUNT *IN SITU* HYBRIDIZATION

### High resolution in situ hybridization (ISH) to whole-mount zebrafish embryos (updated from Thisse and Thisse, 2008)

There are several ways to perform each step required for whole mount ISH. We choose to describe here an experimental procedure that optimizes the conditions to perform high throughput analysis and to get a high-resolution analysis of gene expression. Nevertheless, this protocol is also appropriate for analysis of the expression of a single gene at one particular developmental stage.

#### A - Probe synthesis

Component	Amount per reaction	Final
Linear Template DNA	2.5µl	100-200 ng
5x Transcription buffer	1µl	1X
DTT 0.1M	0.5µl	10 mM
DIG-RNA labeling mix (UTP)	0.5 µl	
RNAse in (40U/µl)	0.25 µl	10 U
T3 or T7 RNA polymerase (20U/µl)	0.25 µl	5U

1. Mix and incubate 2 h at 37°C.
2. Add 2 µl RNAse free DNase I and 18 µl sterile water. Mix and incubate for 30 min at 37°C.
3. Stop the reaction by adding 1 µl sterile 0.5 M EDTA and 9 µl sterile water.
4. Place a SigmaSpin Post Reaction Purification column on top of a microfuge tube. Centrifuge 15 s at 750 g.
5. Break the base of the column and discard lid. Spin 2 min at 750 g.
6. Place the column on a new microfuge tube. Add the RNA template on top of the resin.
7. Centrifuge 4min at 750 g. Discard the column.
8. Add 1 µl sterile EDTA 0.5M and 9 µl of RNAlater to the sample; this protects the RNA from degradation . Test 1/10 of the synthesis on agarose gel.

#### B – Embryo / Larva collection, chorion removal, fixation, storage

1. Collect the eggs.
2. Place embryos in a 100 ml beaker, covered with a minimal amount of water (10 ml).
3. Pour 3 ml Pronase (1/100 wt/vol, warmed to 28.5°C) into the beaker and incubate for 1 min.
4. Gently rinse the eggs 3 times with fish water.
5. Place the embryos in large Petri dishes (50 embryos maximum for a 94 mm Petri dish, 600 embryos for a 145 mm Petri dish) coated with 2% agarose.

6. Let the embryos develop at 28.5°C until the most of the chorions have been removed.
7. Collect the dechorionated embryos by pouring them in a new Petri dish.
8. Continue to incubate the embryos at 28.5°C in Petri dishes containing fish water until the desired developmental stage is reached. If post-gastrulation stages are to be examined, the formation of melanin pigment needs to be prevented. This can be achieved by replacing regular fish water with 0.0045% 1-Phenyl-2-Thiourea (PTU) solution prepared in 0.3 x Danieau medium at the end of gastrulation. For larva and embryos older than 24 hours post fertilization (hpf) change this medium once a day.
9. Fix dechorionated embryos of the appropriate developmental stage(s) in 4% (wt/vol) paraformaldehyde in 1 x PBS overnight at 4°C into Petri dishes. (Alternatively, embryos can be dechorionated, after fixation in PFA, by hand using sharpened forceps – Dumond 5 Switzerland).
10. The next day, dehydrate the embryos in 100% methanol for 15 min at room temperature.
11. Place the eggs at -20°C in 100 % methanol for at least two hours before use. Embryos can be kept at -20°C in methanol for several months.

## C – In situ hybridization

### *Step 1: Permeabilization of Embryos*

#### 1. Rehydration.

- |              |                               |
|--------------|-------------------------------|
| - 1 x 5 min  | 100% Methanol                 |
| - 1 x 5 min  | 75% Methanol -25% PBST        |
| - 1 x 5 min  | 50% Methanol -50% PBST        |
| - 1 x 5 min  | 25% Methanol -75% PBST        |
| - 3 x 10 min | PBST (PBS 1 x / tween20 0.1%) |

#### 2. Permeabilization of embryos.

1. Digestion with proteinase K (PK)
2. Final solution at 10 µg/ml in PBT (test appropriate time for every new batch of PK)

For embryos at 75 % epiboly (Gastrula)	0 - 30 sec
For embryos from 5-6 somites (ES)	1 min
For embryos from 18-20 somites (MS)	3 min
For embryos of 24 h	10 min
For embryos of 36 h	20 min
For embryos of 48 h and later	30 min

3. Postfixation (stop the proteinase K digestion):

- 20 mn in 4% PFA-PBS

washes:

- 3 x 10 min in PBT

4. Transfer embryos into 2 ml sterile eppendorf tubes

#### 3. Prehybridization of embryos

Incubation from 2 to 5 h at 70°C in 0.6 to 1 ml of hybridization mix (HM). For 50 ml:

	volume	final
--	--------	-------

Formamide	25,0 ml	50% formamide
20 x SSC	12,5 ml	5 x SSC
Heparin 5 mg/ml	0,5 ml	50 µg/ml
tRNA 50 mg/ml	0,5 ml	500 µg/ml
Tween 20 20%	0,25 ml	0,1%
Acide citrique 1M	0,46 ml	-> pH 6
H2O	to 50 ml	

For strong probes that don't require long labelling incubation time, heparin and tRNA are not essential and can be omitted.

Possible storage in HM for weeks at -20°C or at + 4°C for a day

### ***Step 2: Hybridization***

Add the antisense DIG labelled RNA:

Remove the HM use for prehybridization

add 200 µl of HM containing 30 - 100 ng of probe (1 - 2 µl of probe synthesis)

Incubate O/N at 70°C in a waterbath

### ***Step 3: Washes/Preincubation – Incubation with Antibody***

1 x quickly with HM (without tRNA and heparin) at 70°C

10 mn 75% HM + 25% 2xSSC à 70°C

10 mn 50% HM + 50% 2xSSC à 70°C

10 mn 25% HM + 75% 2xSSC à 70°C

10 mn 2xSSC à 70°C

**2 x 30 mn in 0.2 x SSC at 70°C**

10 mn 75 % 0.2xSSC + 25% PBT at RT (room temperature)

10 mn 50 % 0.2xSSC + 50% PBT at RT

10 mn 25 % 0.2xSSC + 75% PBT at RT

10 mn PBT at RT

### ***Preincubation of embryos for Ab labelling***

Incubate embryos several hours under agitation in

BSA 2 mg/ml - 2% Sheep serum in PBT

### ***Incubation with Alkaline phosphatase anti DIG antibody***

Dilute anti-DIG Ab to 1/5,000 - 10,000

Incubate overnight at 4°C with agitation

### ***Step 4 – Washes/labeling reaction***

#### **Washes (remove unbound Antibodies)**

1 quick wash in PBT at room temperature

6 x 15 mn in PBT at room temperature under gentle agitation

(dry on paper before moving in the next solution)  
3 x 5 mn at room temperature in alkaline tris buffer

**Alkaline Tris buffer :**

	volume	final
Tris HCl pH 9,5 1M	10 ml	100 mM
MgCl <sub>2</sub> 1	5 ml	50 mM
NaCl 5M	2 ml	100 mM
Tween 20 20%	0,5 ml	0,1%
H <sub>2</sub> O	to 50 ml	

**Labelling**

Move embryo in eppendorf tubes (remove them first from baskets in a 6 cm petri dish filled with alkaline tris buffer)  
remove the excess of alkaline tris buffer and replace with 700 µl of labelling mix freshly prepared

**Labelling mix :**

225 µl NBT + 50 ml Alkaline Tris buffer + 175 µl BCIP

To decrease background and perform long labelling incubation (24h incubation time at room temperature) NBT solution can be decreased 10x (22.5 µl for 50 ml Alkaline Tris buffer).

22.5 µl NBT + 50 ml Alkaline Tris buffer + 175 µl BCIP

**Stock Solutions :**

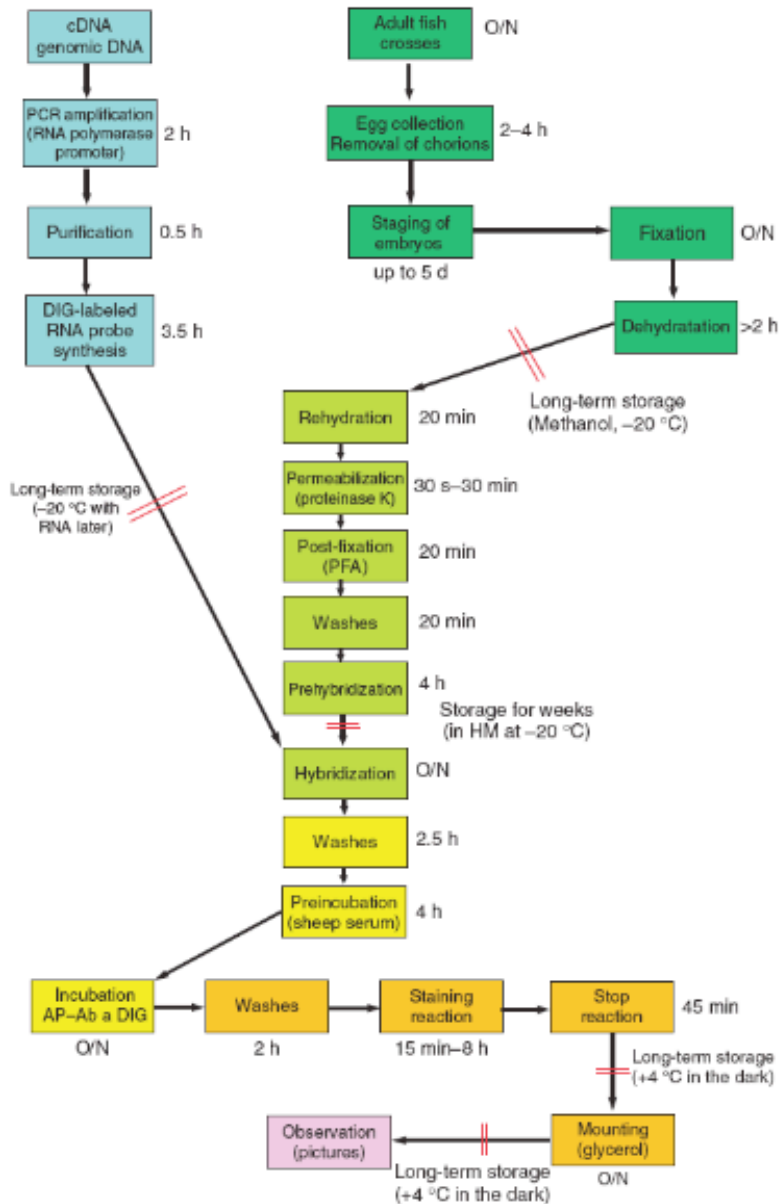
**NBT :** 50 mg Nitro Blue Tetrazolium dissolved in 0.7 ml de N,N-dimethylformamide anhydrous and 0.3 ml of water (store at -20°C)

**BCIP :** 50 mg of 5-Bromo 4-Chloro 3-indolyl Phosphate dissolved in 1 ml of N,N-dimethylformamide anhydrous (store at -20°C)

Move embryos with labelling mix into 12 well ceramic plates. Let the reaction occuring in the dark, looking under dissecting scope every 15 min for the first hour then every ½ h or 1h after the first hour of reaction.

Stop labelling in PBS pH 5,5 EDTA 1 mM (3 washes, 1 quick and 2 under gentle agitation)

Store at 4°C in PBS pH 5,5 EDTA 1 mM in the dark (labelled embryos can be kept for years)



### Flow diagram

The different steps of the ISH protocol are indicated into boxes linked by arrows and colored in blue for steps corresponding to synthesis of the probe, in dark green for preparation of embryos, in light green for Day 1 of in situ procedure, in yellow for Day 2, in orange for Day 3 and in pink for the final step. Time required for each step is indicated near the box (O/N: over night). Pause points are indicated in the diagram by two red lines across arrows. Information about the length and conditions of storage is indicated (from Thisse and Thisse, 2008).



## MATERIALS – REAGENTS

### REAGENTS

- cDNA or genomic DNA
- PCR master mix (Promega, cat. No. M7505)
- Sterile double distilled water
- Trizma® base (Sigma, cat. no. T1503)
- Ethylenediaminetetraacetic acid (EDTA) (Eurobio, cat. no. GAUEDT00-66)
- Boric acid (Sigma, cat. no. B7901)
- Agarose (Sigma, cat. no. A9539)
- Transcription buffer (Promega, cat. no. P118B)
- DL-Dithiothreitol (DTT) (Promega, cat. no. P117B)
- DIG RNA Labeling Mix (UTP) (Roche, cat. no. 1277073)
- RNasein (Promega, cat. no. N251X)
- T3 RNA-Polymerase (Promega, cat. no. P207C)
- T7 RNA-Polymerase (Promega, cat. no. P207B)
- RNase free DNase I (Roche, cat. no. 776785)
- NaOH (Sigma, cat. no. S8045)
- RNAlater (Sigma, cat. no. R-0901)
- Paraformaldehyde (PFA) (Sigma, cat. no. P-6148) see REAGENT

### SETUP

- **CAUTION** Noxious substance. Avoid inhalation and contact with the eye and skin. Use protective clothes during preparation and application.
- Methanol (Technisolv, cat. no. prol83809-360) **CAUTION** Avoid inhalation and contact with the eye and skin.
- 1-phenyl-2-thiourea (PTU) (Sigma, cat. no. P7629) **CAUTION** Poison. Highly toxic, may be fatal if swallowed or inhaled. Experimental teratogen. Irritant. Safety glasses, gloves, good ventilation, dust mask if powdered product may get into the atmosphere.
- NaCl (Sigma, cat. no. S3014)
- KCl (Sigma, cat. no. P9541)
- MgSO<sub>4</sub> (Sigma, cat. no. M2643)
- Ca(NO<sub>3</sub>) (Sigma, cat. no. C1396)
- HEPES (Sigma, cat. no. H3375)
- H<sub>2</sub>O<sub>2</sub> (Sigma, cat. no. 31642)
- KOH (Sigma, cat. no. P1767)
- Tween20 (Sigma, cat. no. P-1379)
- Proteinase K (Roche Diagnostics, cat. no. 1092766) Prepare 10 mg/ml stock solution in PBT and store at -20°C in 100µl aliquots. Final concentration for embryo permeabilisation is 10µg/ml.
- Formamide high purity grade (Carlo Erba, cat. no. 452286)
- Citric acid trisodium salt (Sigma cat. no. C3674)
- Citric acid monohydrate (Sigma, cat. no. C1909)
- Heparin sodium salt (Sigma, cat. no. H-3393)
- tRNA from wheat germ Type V, lyophilized powder (Sigma, R7876)
- Phenol solution Saturated with 0.1 M citrate buffer, pH 4.3 (Sigma, P4682)
- Chloroform (Carlo erba, cat. no. 438603)
- Sodium acetate (Merck, cat. no. 0095096B)

- Ethanol absolute (Technisolv, cat. no. PROL83813-360)
- Sheep serum ( Interchim SA, cat. no. 013-000-121). Resuspend in 10 ml of sterile water, aliquot and store at -20°C
- Albumin from bovine serum, further purified Fraction V, 99% pure (BSA) (Sigma, A3059)
- Sheep anti Digoxigenin-AP Fab fragments (Roche Diagnostic, cat. no. 1093274)
- HCl (Sigma, cat. no. H1758)
- MgCl<sub>2</sub> (Sigma, cat. no. 63068)
- Nitro Blue Tetrazolium (NBT, Sigma, N6639). Dissolve 50 mg of Nitro Blue Tetrazolium in 0.7 ml N, N-dimethylformamide and 0.3 ml sterile water and store at -20°C.
- 5-bromo 4-chloro 3-indolyl phosphate ( BCIP, Sigma, B-8503). Dissolve 50 mg of 5-Bromo 4-Chloro 3-Indolyl Phosphate in 1 ml of N, N-dimethylformamide anhydrous and store at -20°C.
- N, N-Dimethylformamide anhydrous, 99.8% (Aldrich, cat. no. 227056)
- Na<sub>2</sub>HPO<sub>4</sub>, 12H<sub>2</sub>O (Fluka, 71650)
- NaH<sub>2</sub>PO<sub>4</sub> (Merck, cat. no. 1,06346,1000)
- Glycerol ≥99% (Sigma, G6279)
- Stop solution: 1 x PBS pH5.5, 1mM EDTA, 0.1% Tween 20 (vol/vol)
- 10 x PBS pH5.5 stock solution: 10.8 g of Na<sub>2</sub>HPO<sub>4</sub>, 65g of NaH<sub>2</sub>PO<sub>4</sub>, 80g NaCl, 2g KCl are dissolved into 1 l of water.
- PBT: 1 x PBS, 0.1% Tween20 (vol/vol)
- 20x SSC stock solution: NaCl 175.3 g, Citric acid trisodium salt 88.2g dissolved in 1l of water.
- Blocking buffer: 1 x PBT, 2% sheep serum (vol/vol), 2mg/ml BSA.
- 0.3 x Danieau medium: 17 mM NaCl, 2 mM KCl, 0.12 mM MgSO<sub>4</sub>, 1.8 mM Ca(NO<sub>3</sub>)<sub>2</sub>, 1.5 mM HEPES, pH 7.6
- Alkaline Tris buffer: 100 mM Tris HCl pH 9.5, 50 mM MgCl<sub>2</sub>, 100 mM NaCl, 0.1% Tween 20
- Tris HCl pH 9.5

**Mounting embryos:** To mount the embryos, 3 (for embryos after 24 hpf) or 4 (for embryos before 24h) cover slips of thickness 1.5 are glued together using a drop of super glue (cyanoacrylate) to make a bridge. A drop of glycerol containing the embryo is placed in the middle of the slide between two coverslip bridges and covered with a larger cover slip (24 x 40 mm, thickness 1). Using this mounting system, embryos can be rolled in all positions (for embryos younger than the 16 somite stage) by gently moving the upper cover slip. For older embryos, elongation of the tail limits the rotation possibilities to rotation around the antero-posterior axis only.

## WHOLE-MOUNT FLUORESCENT *IN SITU* HYBRIDIZATION

Modification from

Zebrafish Whole Mount High-Resolution Double Fluorescent In Situ Hybridization

Tim Brend, Scott A. Holley

Department of Molecular, Cellular and Developmental Biology, Yale University

### **1. Fixation**

1. Fix embryos overnight at 4°C with 4% paraformaldehyde (PFA) in PBS.
2. Remove fix and wash 3 x PBS, 10 minutes each at room temperature (RT).
3. Manually dechorionate embryos in PBS in a glass depression plate using watchmaker forceps. After dechoriation, embryos are transferred using a fire-polished glass Pasteur pipette as they may stick to polypropylene pipettes.
4. Transfer embryos through a series of 25%, 50% and 75% methanol in PBS for 5 minutes each.
5. Replace liquid with 100% methanol, incubate 5 minutes and then replace with fresh methanol.
6. Place embryos at -20°C for a minimum of one hour. (We typically incubate the embryos overnight. Standard in situ hybridization will work on embryos stored for more than a year, but we have not examined whether the high-resolution of the fluorescent in situ hybridization is lost by prolonged storage.)
7. Wash embryos for 5 minutes each in 75%, 50%, 25% methanol in PBST at RT. Wash twice for 5 minutes each in PBST at RT.
8. Fix again for 20 minutes in 4% PFA in PBS at RT.
9. Wash 3 x 10 minutes each in PBST at RT.

#### **NOTE REGARDING PFA:**

We store 4% PFA in aliquots at -20°C (see table of reagents). For the initial fixation, we only use PFA that has never been previously thawed. For subsequent fixations, we often use PFA that has been previously thawed. The initial fixation appears to be critical for successful staining with this protocol.

### **2. Proteinase and Postfixation**

1. Digest with proteinase K (10 µg/ml in PBST) at RT for 3 to 12 minutes to permeabilize the embryos. (The incubation time depends on the age of the embryos as younger stages are more sensitive. It also depends on the batch of enzyme.) For somitogenesis stage embryos, we typically permeabilize for 3-4 minutes. For larvae, we permeabilize for 20 min. During this incubation, we lay the microcentrifuge tube on its side.
2. Rinse briefly in PBST and wash once for 5 minutes in PBST.
3. Fix again for 20 minutes in 4% PFA in PBS at RT.
4. Wash twice, for 5 minutes each, in PBST at RT.

### **3. Prehybridization**

1. Prehybridize at 65 °C for at least 1 hour in HYB+.

### **4. Hybridization**

1. Remove all but 50 µl of the preHYB, but make sure to keep the embryos completely submerged.
2. Add 1-2 µl of each riboprobe (digoxigenin- and fluorescein-labeled riboprobes) to the embryos and mix by gently flicking the tube. The amount of probe is typically 1-2µl from a 20µl probe synthesis reaction.
3. Given that fluorescein is light-sensitive, the tubes should be wrapped in aluminum foil or otherwise exposed to minimal light from this point forward.

4. Incubate the embryos overnight at 65 °C.

#### **5. Probe removal**

Note that the solutions from this point forward lack detergent. Elimination of detergent appears to help the staining reactions but does cause the embryos to become rather sticky.

1. Remove the riboprobe.
2. Wash 1 x 30 min at 65 °C in HYB-
3. Wash for 15 minutes at 65 °C in 75% HYB-/25% 2xSSC.
4. Wash for 15 minutes at 65 °C in 50% HYB-/50% 2xSSC.
5. Wash for 15 minutes at 65 °C in 25% HYB-/75% 2xSSC.
6. Wash for 15 minutes at 65 °C in 2xSSC.
7. Wash for 30 minutes 65 °C in 0.2 x SSC.

#### **6. Anti-Fluorescein antibody incubation**

1. Block for at least 1 hour at RT in 500µl of a solution of 1x maleic acid buffer plus 2% blocking reagent (see table of reagents).
2. Add the anti-Fluorescein-POD antibody, as supplied by Roche, at a 1:500 dilution in the blocking solution.
3. Incubate overnight at 4°C. During this incubation, we lay the microcentrifuge tube on its side.
4. Wash 4 x 20 minutes in 1x maleic acid buffer. Wash twice for 5 minutes each in PBS.

#### **7. Detection of fluorescein-labelled probe**

1. Incubate 30-60 minutes in TSA Plus Fluorescein Solution. (Spin down TSA substrate before making staining solution. For the reaction, dilute tyramide reagent 1:50 in Perkin Elmer amplification diluent buffer.) During this incubation, we lay the microcentrifuge tube on its side. Reaction time must be determined empirically for each probe. Unfortunately, the staining reaction cannot be visually monitored as the substrate is fluorescent, and one will see ubiquitous green fluorescence throughout the staining reaction.
2. Wash for 10 minutes each in 30%, 50%, 75% and 100% methanol in PBS.
3. Incubate in a solution of 1% H2O2 in methanol for 30 minutes to inactivate the first peroxidase.
4. Wash 10 minutes each in 75%, 50% and 30% methanol in PBS. Then wash twice for 10 minutes each in PBS. It is important that all of the methanol be removed.

#### **NOTES ON THE TYRAMIDE SIGNAL AMPLIFICATION:**

We have been using the Perkin Elmer TSA Kits. We find that the Alexa-Tyramide substrates stain well using the Perkin Elmer amplification diluent buffer, but we have not had success using the staining buffer provided with the Invitrogen/Molecular Probes Kits. Lastly, we have found that Cy5 fluorescence is eliminated by subsequent Methanol/H2O2 treatment while fluorescein and Alexa-647 are unaffected. Cy3 may also be adversely affected by the Methanol/H2O2 treatment as it is structurally related to Cy5. For this reason, Cy3 and Cy5 TSA reactions should only be used for the second staining reaction in a double fluorescent in situ protocol.

### **8. Anti-digoxigenin antibody incubation**

1. Block the embryos again for at least 1 hour at RT in a solution of 1x maleic acid buffer plus 2% blocking reagent.
2. Add the anti-DIG POD antibody as supplied by Roche at a 1:1000 dilution in above blocking solution
3. Incubate overnight at 4°C. During this incubation, we lay the microcentrifuge tube on its side.
4. Wash 4 x 20 minutes in 1x maleic acid buffer. Wash twice for 5 minutes each in PBS.

### **9. Detection of digoxigenin-labelled probe**

1. Incubate 30-60 minutes in TSA Plus Cy5 Solution (Spin down TSA substrate before making staining solution. For the reaction, dilute tyramide reagent 1:50 in amplification diluent buffer) During this incubation, we lay the microcentrifuge tube on its side. Reaction time must be determined empirically for each probe.
2. Wash three times for 10 minutes each in PBST.

### **10. DAPI staining**

1. Incubate the embryos with DAPI solution as required.

### **11. Mounting**

1. Incubate the embryos for 10 minutes each in 25% and 50% glycerol in PBST. Clear overnight in 75% glycerol at 4°C.
2. We dissect and deyolk the embryos and flat mount them on a microscope slide. The yolk can produce significant background fluorescence. Dissection is much easier after the embryos have cleared overnight in glycerol.  
(Alternatively) We add Fluorescent Mounting Medium Vectashield and analyze the embryos the day after.

#### **SOLUTIONS:**

PBST PBS plus 0.1% Tween

SSCT SSC plus 0.1% Tween

1 x maleic acid buffer: 150mM maleic acid, 100mM NaCl (pH 7.5)

HYB- 50% formamide

5xSSC

0.1% Tween-20

HYB+ HYB-

5mg/ml torula (yeast) RNA

50µg/ml heparin

### **CELL CYCLE INHIBITOR TREATMENTS**

Compounds for cell cycle inhibitors were used as described before (Murphey *et al.*, 2006). Larva were treated for the desired period with the drugs in E3 medium in Table 2 in the presence of 1% DMSO at 28.5 °C. Zebrafish strains used were SqET4 and *Tg(Brn3c:GFP)* to quantify the number of hair cells. For statistical analysis, at least 10 larvae were used and around 70 neuromasts were analyzed. For

time-lapse confocal, larvae we mounted in a 1% low melting point agarose (see Imaging procedures)

Table 2. Comparison of minimum effective doses of known cell cycle inhibitors.

Compounds	NIH3T3 cells	AB9 cells	Zebrafish embryos	Zebrafish larvae
Aphidicolin (DMSO)	7.4 $\mu$ M	7.4 $\mu$ M	259 $\mu$ M	100 $\mu$ M
Genistein (DMSO)	47 $\mu$ M	93 $\mu$ M	93 $\mu$ M	25 $\mu$ M
Nocodazole (DMSO)	150 nM	ND	150 nM	150 nM
Mimosine (10% NaHCO <sub>3</sub> )	200 $\mu$ M	200 $\mu$ M	-2000 $\mu$ M	-2000 $\mu$ M
Okadaic acid (DMSO)	0.06 $\mu$ M	6 $\mu$ M	-6 $\mu$ M	-6 $\mu$ M
Taxol (DMSO)	10 $\mu$ M	10 $\mu$ M	-100 $\mu$ M	-100 $\mu$ M
Colchicine (H <sub>2</sub> O)	200 $\mu$ M	ND	1000 $\mu$ M	1000 $\mu$ M

\* All compounds were purchased from Calbiochem (San Diego, CA, USA)

## WHOLE MOUNT ASSAY FOR CELL PROLIFERATION

1. Dechorionate embryo of desired age, and place in 10mM BrdU, made up in Embryo Medium with 15% DMSO at 6 to 8 degrees for 20 minutes or put the petri dish resting on top of ice. For larvae, use 1% DMSO instead of 15% and incubate larvae until the desired stages.

2. Allow embryos to develop to desired age.

3. Fix in 4% PFA, several hours at RT, or ON in the cold.

4. Remove PFA, wash embryos 2X in methanol. Put embryos in fresh methanol, place

at -20°C, for at least overnight. Indefinite storage at -20°C is fine.

5. Rehydrate using a graded Methanol/PBST series: 75%, 50%, 25% and wash 3x10 min in PBST.

6. Incubate at RT in 2N HCl for 1 hour.
  8. Rinse 3 x 10 minutes in PBST.
  9. Incubate at least 2 hours in blocking solution, rocking or shaking gently.
  10. Incubate 4 hours, or more (RT), in anti-BrdU, 1:150, (ON in cold is fine), rocking or shaking gently.
  11. Rinse several times, then wash 4 x 30 minutes each in PBST, rocking or shaking gently.
  12. Incubate at least 2 hours in blocking solution, rocking or shaking gently.
  13. Incubate 2 hours or more with fluorescent labeled secondary antibody, 1:150, in PBST (ON in cold is also fine).
  14. Rinse several times, then wash 4 x 30 minutes each in PBST, rocking or shaking.
  15. Store embryo or larvae in PBST plus mounting medium, Vectashield with or without DAPI.
- 
- A. PBS-D-Tw: PBS + 1% DMSO + 0.1% Tween-20
  - B. 4% PF: 4% paraformaldehyde, 50 mM NaPO<sub>4</sub>, pH 7.4.
  - C. 10mM BrdU: made up in embryo medium with 1% or 15% DMSO according to the stages of the embryos or larvae.
  - D. 2 N HCl, in water.
  - E. 10 mg/ml proteinase K stock.
  - F. Anti-BrdU antibody and appropriate secondary antibody and detection system.
  - G. Blocking Solution: PBST + 1% BSA + 2% Normal Goat Serum.

## **TUNEL ASSAYS**

### **1. Fixation**

1. Fix embryos overnight at 4°C with 4% paraformaldehyde (PFA) in PBS.
2. Remove fix and wash 3 x PBS, 10 minutes each at room temperature (RT).
3. Manually dechorionate embryos in PBS in a glass depression plate using

watchmaker forceps. After dechoriation, embryos are transferred using a fire-polished glass Pasteur pipette as they may stick to polypropylene pipettes.

4. Transfer embryos through a series of 25%, 50% and 75% methanol in PBS for 5 minutes each.

5. Replace liquid with 100% methanol, incubate 5 minutes and then replace with fresh methanol.

6. Place embryos at -20°C for a minimum of one hour. (We typically incubate the embryos overnight. Standard in situ hybridization will work on embryos stored for more than a year, but we have not examined whether the high-resolution of the fluorescent in situ hybridization is lost by prolonged storage.)

7. Wash embryos for 5 minutes each in 75%, 50%, 25% methanol in PBST at RT. Wash twice for 5 minutes each in PBST at RT.

8. Fix again for 20 minutes in 4% PFA in PBS at RT.

9. Wash 3 x 10 minutes each in PBST at RT.

## **2. Proteinase and Postfixation**

1. Digest with proteinase K (10 µg/ml in PBST) at RT for 3 to 12 minutes to permeabilize the embryos. (The incubation time depends on the age of the embryos as younger stages are more sensitive. It also depends on the batch of enzyme.) For somitogenesis stage embryos, we typically permeabilize for 3-4 minutes. For larvae, we permeabilize for 20 min. During this incubation, we lay the microcentrifuge tube on its side.

2. Rinse briefly in PBST and wash once for 5 minutes in PBST.

3. Fix again for 20 minutes in 4% PFA in PBS at RT.

4. Wash twice, for 5 minutes each, in PBST at RT.

## **3. TUNEL reaction mix**

1. Incubate embryos for 60 minutes in TUNEL buffer at RT.

2. Replace TUNEL buffer with TUNEL reaction mix, a 9:1 ratio of TUNEL buffer-TUNEL enzyme for 3 hours at 37°C in darkness.

3. Positive control: incubate embryos with DNase solution (1 µl DNase, 5 µl DNase buffer, 44 µl miliQ for 15 min at 37°C). Rinse briefly in PBST and wash once for 5 min in PBST. Incubate embryos in TUNEL reaction mix.

4. Negative control: incubate embryos only in TUNEL buffer.

5. Wash embryos three times 30 minutes in PBST at RT.

## **4. DAPI staining**

1. Incubate embryos in DAPI staining solution (1:500 in PBST) for 15 min at RT.

2. Wash embryos or larva 3 x 30 minutes in PBST and store embryos in PBST with vectashield at 4°C. NOTE: DAPI staining can also be done in this stage by adding Vectashield with DAPI (Vector Labs).



## **DAPT TREATMENTS**

(adapted from Geling *et al.*, 2002)

1. Prepare 10 mM DAPT stock solution in 100% DMSO.
2. Dechorionate embryo or larvae.
3. Set up the treatments and control solutions. Add the DAPT stock solution into E3 medium to get 50-100  $\mu$ M final solutions. NOTE: DAPT will precipitate if not warmed at RT.
4. Swirl dishes to thoroughly mix.
5. Transfer embryo or larvae to the treatment dishes and incubate until the desired developmental stages.
6. Wash briefly and fix embryo or larvae in 4% PFA overnight at 4°C. For time lapse movie, mount larvae in 1% low melting point agarose in the presence of 10  $\mu$ M DAPT solution and tricaine.

## **MOUNTING EMBRYOS OR LARVAE FOR TIME-LAPSE VIDEOMICROSCOPY**

1. Prepare a 1-1.2% solution of low melting point agarose in Embryo Medium by heating in a boiling water bath or in a microwave oven. This solution remains liquid at 37-40°C, but quickly hardens when cooled.
2. Keep a small amount of solution (5 ml) liquid in a test tube in a 42°C water bath.
3. Quickly suck up the embryo or larvae in a small drop of E3 medium and transfer it onto the imaging disk.
4. Using a fine minuten hair mounted on a needle holder, position the embryo at the appropriate angle in the agar and allow the agar to harden.
5. After the agar hardens, place a 3 ml of E3 medium containing tricaine over the agar block.

## **WHOLE-MOUNT ANTIBODY STAINNING**

### **Procedure**

1. Remove chorions for embryos older than 18 somites.
2. Fix embryos in 4% formaldehyde in PBS 1-2 hours 25°C, or 4-12 hours 4 °C.
3. Dechorionate embryos that are younger than 18 somites.
4. Transfer embryos into 100% methanol and store them at -20 °C (2 hours to several months).

5. Rehydration. Transfer embryos into microfuge tubes and rehydrate them by successive incubations in the following solutions (25°C, ~750 µL/tube):  
75% MeOH/25% PBS for 5 minutes (no agitation)  
50% MeOH/50% PBS for 5 minutes (no agitation)  
25% MeOH/75% PBS for 5 minutes (no agitation)  
PBX (PBS containing 0.1-1.0% Triton X-100) for 4 x 5 minutes (rocking agitation; percentage of detergent will depend on antibody and embryo stage used).
6. Blocking. Block in antibody blocking buffer (650 µL/tube; 10% sheep serum, in PBX containing 0.5% BSA, and 1% DMSO (optional)) for several hours at room temperature, or overnight at 4 °C, with rocking agitation.
7. Primary antibody staining. Dilute primary antibody to desired concentration in antibody blocking buffer. Remove blocking buffer from embryos and replace with diluted antibody solution. Incubate overnight at 4 °C with rocking agitation.
8. Washes at room temperature with rocking agitation:  
PBX, very brief wash  
PBX for 5 minutes, 5 times  
PBX for 20 minutes, 3 times
9. Blocking. Block in antibody blocking buffer (650 µL/tube; 10% sheep serum, in PBX containing 0.5% BSA) for 1-2 hours at room temperature with rocking agitation.
10. Secondary antibody staining. Dilute secondary antibody 1/200 in antibody blocking buffer or PBST. Remove blocking buffer from embryos and replace with diluted antibody solution. Incubate room temperature for 2-3 hours with rocking agitation.
11. Washes at room temperature with rocking agitation:

PBX, very brief wash

PBX for 5 minutes, 5 times

PBX for 20 minutes, 3 times

8. Embryos may then be transferred to a 1:1 PBS/glycerol solution for documentation or mounting.

## Reagents

Paraformaldehyde

10X PBS

Triton X-100

Primary antibody

Alexa-Fluor conjugated secondary antibody

BSA

DMSO (optional)

Methanol

Normal Sheep Serum (heat inactivated at 56 °C for 30 minutes)

Methylcellulose

## IMAGING

For whole-mount ISH, embryos were mounted in 75% glycerol and photographed on a Olympus BX61 microscope using 4X or 20X dry objectives with transmission light. Whole embryo images were acquired on a Leica MZ10 stereomicroscope. Fluorescent images were acquired using either a Leica SP5 or SPE microscope using 20X dry objective or 40X oil immersion objective. Images were processed using Imaris and/or ImageJ software packages, and assembled with Adobe Photoshop CS2, Adobe Illustrator CS2, and Macromedia FreeHand MX. For time-lapse imaging, staged and dechorionated embryos were anesthetized with tricaine and mounted in 0.8-1% low-melting-point agarose on a glass-bottom culture dish (MatTek). Z-stack series were acquired every 2-10 min intervals using either 20X dry objective or 40X oil of Leica SPE or SP5 confocal microscope. All movies were processed by using Imaris or ImageJ softwares.



## APPENDIX 2: ABBREVIATIONS

<b>A</b>		cldB	claudinB
Abl	Abelson	cRNA	complementary ribonucleic acid
Ag	<i>Anopheles gambiae</i> str. PEST	CXCL12	c-x-c chemokine ligand type 12
ALL	anterior lateral line	CXCR4	c-x-c chemokine receptor type 4
APC	adenomatous polyposis coli	CXCR7	c-x-c chemokine receptor type 7
At	<i>Arabidopsis thaliana</i>	<b>D</b>	
Atp2b1a	adenosine triphosphate type 2b1a	Dach	Dachsund
<b>B</b>		DiASP	4-(4-Diethylaminostyryl)-1-methylpyridinium iodide
bHLH	basic helix-loop-helix	Dkk	dickkopf
BO	brachio-oto syndrome	Dm	<i>Drosophila melanogaster</i>
BOR	brachio-oto-renal syndrome	DNA	deoxyribonucleic acid
BrdU	Bromo-deoxy-uridine	Dr	<i>Danio rerio</i>
Bt	<i>Bos Taurus</i>	<b>E</b>	
<b>C</b>		e-cdh	epithelial-cadherin
CBP	CREB-binding protein	ED	eya domain
Cdh	cadherin	eGFP	enhanced green fluorescent protein
Cf	<i>Canis familiaris</i>		

Erβ2	estrogen receptor β2	met	MNNG HOS Transforming gene
Ey	eyeless		
Eya	eyes absent	MET	mesenchymal-to-epithelial transition
<b>F</b>			
Fgf	fibroblast growth factor	mib	mind bomb
Fgfr	fibroblast growth factor receptor	MRN	Mre11, Rad50 and Nbs1
		mRNA	messenger ribonucleic acid
<b>G</b>			
GAL4	galactosidase 4	<b>N</b>	
GFP	green frulorescent protein	n-cdh	neuronal-cadherin
Gg	<i>Gallus gallus</i>	NICD	Notch intracellular domain
Gro	Groucho	<b>O</b>	
<b>H</b>		Os	<i>Oryza sativa</i>
H2AX	histone H2A	<b>P</b>	
HAD	Haloacid dehalogenase	P	phosphate group
Hs	<i>Homo sapiens</i>	PLL	posterior lateral line
<b>J</b>		Pt	<i>Pan troglodytes</i>
JNK1	c-Jun N-terminal kinase 1	PTP	protein tyrosine phosphatase;
<b>M</b>		<b>R</b>	
MDC1	Mediator of DNA damage checkpoint protein 1	RDGN	retinal determination gene network
		RFP	red fluorescent protein

Rn	<i>Rattus norvegicus</i>	Tmie	transmembrane inner ear
<b>S</b>			
SDF1	stromal cell- derived factor 1	Toy	Twin of eyeless
		<b>U</b>	
SqET10	enhancer type 10 transgenic	UAS	upstream activation sequence
SqET20	enhancer trap 20 transgenic	UHCP	unipotent hair cell progenitor
SqET4	enhancer trap 4 transgenic	<b>W</b>	
<b>T</b>		Wnt	wingless integration site
TA	transcriptional activation	WRPW	Tryptopan- Arginine-Proline- Tryptopan motif
<i>tacstd</i>	tumor-associated calcium signal transducer gene		

## References

- Abdelhak, S., Kalatzis, V., Heilig, R., Compain, S., Samson, D., Vincent, C., Levi-Acobas, F., Cruaud, C., Le Merrer, M., Mathieu, M. et al. (1997a). Clustering of mutations responsible for branchio-oto-renal (BOR) syndrome in the eyes absent homologous region (eyaHR) of EYA1. *Hum Mol Genet* **6**, 2247-55.
- Abdelhak, S., Kalatzis, V., Heilig, R., Compain, S., Samson, D., Vincent, C., Weil, D., Cruaud, C., Sahly, I., Leibovici, M. et al. (1997b). A human homologue of the *Drosophila* eyes absent gene underlies branchio-oto-renal (BOR) syndrome and identifies a novel gene family. *Nat Genet* **15**, 157-64.
- Agelopoulos, M. and Thanos, D. (2006). Epigenetic determination of a cell-specific gene expression program by ATF-2 and the histone variant macroH2A. *EMBO J* **25**, 4843-53.
- Aigouy, B., Farhadifar, R., Staple, D. B., Sagner, A., Roper, J. C., Julicher, F. and Eaton, S. (2010). Cell flow reorients the axis of planar polarity in the wing epithelium of *Drosophila*. *Cell* **142**, 773-86.
- Aman, A. and Piotrowski, T. (2008). Wnt/beta-catenin and Fgf signaling control collective cell migration by restricting chemokine receptor expression. *Dev Cell* **15**, 749-61.
- Aman, A. and Piotrowski, T. (2009). Multiple signaling interactions coordinate collective cell migration of the posterior lateral line primordium. *Cell Adh Migr* **3**, 365-8.
- Angelov, D., Molla, A., Perche, P. Y., Hans, F., Cote, J., Khochbin, S., Bouvet, P. and Dimitrov, S. (2003). The histone variant macroH2A interferes with transcription factor binding and SWI/SNF nucleosome remodeling. *Mol Cell* **11**, 1033-41.
- Artavanis-Tsakonas, S., Rand, M. D. and Lake, R. J. (1999). Notch signaling: cell fate control and signal integration in development. *Science* **284**, 770-6.
- Aulehla, A., Wiegraebe, W., Baubet, V., Wahl, M. B., Deng, C., Taketo, M., Lewandoski, M. and Pourquie, O. (2008). A beta-catenin gradient links the clock and wavefront systems in mouse embryo segmentation. *Nat Cell Biol* **10**, 186-93.
- Axelrod, J. D. (2009). Progress and challenges in understanding planar cell polarity signaling. *Semin Cell Dev Biol* **20**, 964-71.
- Azuma, N., Hirakiyama, A., Inoue, T., Asaka, A. and Yamada, M. (2000). Mutations of a human homologue of the *Drosophila* eyes absent gene (EYA1) detected in patients with congenital cataracts and ocular anterior segment anomalies. *Hum Mol Genet* **9**, 363-6.



- Baena-López, L. A., Baonza, A. and Garcia-Bellido, A.** (2005). The orientation of cell divisions determines the shape of *Drosophila* organs. *Curr Biol* **15**, 1640-4.
- Banaszynski, L. A., Allis, C. D. and Lewis, P. W.** (2010). Histone variants in metazoan development. *Dev Cell* **19**, 662-74.
- Behra, M., Bradsher, J., Sougrat, R., Gallardo, V., Allende, M. L. and Burgess, S. M.** (2009). Phoenix is required for mechanosensory hair cell regeneration in the zebrafish lateral line. *PLoS Genet* **5**, e1000455.
- Bessarab, D. A., Chong, S. W. and Korzh, V.** (2004). Expression of zebrafish *six1* during sensory organ development and myogenesis. *Dev Dyn* **230**, 781-6.
- Biswas, S., Emond, M. R. and Jontes, J. D.** (2010). Protocadherin-19 and N-cadherin interact to control cell movements during anterior neurulation. *J Cell Biol* **191**, 1029-41.
- Blankenship, J. T., Backovic, S. T., Sanny, J. S., Weitz, O. and Zallen, J. A.** (2006). Multicellular rosette formation links planar cell polarity to tissue morphogenesis. *Dev Cell* **11**, 459-70.
- Blechinger, S. R., Kusch, R. C., Haugo, K., Matz, C., Chivers, D. P. and Krone, P. H.** (2007). Brief embryonic cadmium exposure induces a stress response and cell death in the developing olfactory system followed by long-term olfactory deficits in juvenile zebrafish. *Toxicol Appl Pharmacol* **224**, 72-80.
- Boldajipour, B., Mahabaleswar, H., Kardash, E., Reichman-Fried, M., Blaser, H., Minina, S., Wilson, D., Xu, Q. and Raz, E.** (2008). Control of chemokine-guided cell migration by ligand sequestration. *Cell* **132**, 463-73.
- Bonini, N. M., Bui, Q. T., Gray-Board, G. L. and Warrick, J. M.** (1997). The *Drosophila* eyes absent gene directs ectopic eye formation in a pathway conserved between flies and vertebrates. *Development* **124**, 4819-26.
- Bonini, N. M., Leiserson, W. M. and Benzer, S.** (1993). The eyes absent gene: genetic control of cell survival and differentiation in the developing *Drosophila* eye. *Cell* **72**, 379-95.
- Borsani, G., DeGrandi, A., Ballabio, A., Bulfone, A., Bernard, L., Banfi, S., Gattuso, C., Mariani, M., Dixon, M., Donnai, D. et al.** (1999). EYA4, a novel vertebrate gene related to *Drosophila* eyes absent. *Hum Mol Genet* **8**, 11-23.
- Bouzaffour, M., Dufourcq, P., Lecaudey, V., Haas, P. and Vríz, S.** (2009). Fgf and Sdf-1 pathways interact during zebrafish fin regeneration. *PLoS One* **4**, e5824.
- Bricaud, O., Chaar, V., Dambly-Chaudiere, C. and Ghysen, A.** (2001). Early efferent innervation of the zebrafish lateral line. *J Comp Neurol* **434**, 253-61.
- Brignull, H. R., Raible, D. W. and Stone, J. S.** (2009). Feathers and fins: non-mammalian models for hair cell regeneration. *Brain Res* **1277**, 12-23.

- Cayouette, M., Whitmore, A. V., Jeffery, G. and Raff, M.** (2001). Asymmetric segregation of Numb in retinal development and the influence of the pigmented epithelium. *J Neurosci* **21**, 5643-51.
- Ceol, C. J., Pellman, D. and Zon, L. I.** (2007). APC and colon cancer: two hits for one. *Nat Med* **13**, 1286-7.
- Chakravarthy, S., Gundimella, S. K., Caron, C., Perche, P. Y., Pehrson, J. R., Khochbin, S. and Luger, K.** (2005). Structural characterization of the histone variant macroH2A. *Mol Cell Biol* **25**, 7616-24.
- Chamorro, M. N., Schwartz, D. R., Vonica, A., Brivanlou, A. H., Cho, K. R. and Varmus, H. E.** (2005). FGF-20 and DKK1 are transcriptional targets of beta-catenin and FGF-20 is implicated in cancer and development. *EMBO J* **24**, 73-84.
- Changolkar, L. N., Costanzi, C., Leu, N. A., Chen, D., McLaughlin, K. J. and Pehrson, J. R.** (2007). Developmental changes in histone macroH2A1-mediated gene regulation. *Mol Cell Biol* **27**, 2758-64.
- Changolkar, L. N. and Pehrson, J. R.** (2006). macroH2A1 histone variants are depleted on active genes but concentrated on the inactive X chromosome. *Mol Cell Biol* **26**, 4410-20.
- Chapouton, P., Adolf, B., Leucht, C., Tannhauser, B., Ryu, S., Driever, W. and Bally-Cuif, L.** (2006). her5 expression reveals a pool of neural stem cells in the adult zebrafish midbrain. *Development* **133**, 4293-303.
- Chapouton, P., Skupien, P., Hesl, B., Coolen, M., Moore, J. C., Madelaine, R., Kremmer, E., Faus-Kessler, T., Blader, P., Lawson, N. D. et al.** (2010). Notch activity levels control the balance between quiescence and recruitment of adult neural stem cells. *J Neurosci* **30**, 7961-74.
- Chapouton, P., Webb, K. J., Stigloher, C., Alunni, A., Adolf, B., Hesl, B., Topp, S., Kremmer, E. and Bally-Cuif, L.** (2011). Expression of hairy/enhancer of split genes in neural progenitors and neurogenesis domains of the adult zebrafish brain. *J Comp Neurol*.
- Chen, B., Dodge, M. E., Tang, W., Lu, J., Ma, Z., Fan, C. W., Wei, S., Hao, W., Kilgore, J., Williams, N. S. et al.** (2009). Small molecule-mediated disruption of Wnt-dependent signaling in tissue regeneration and cancer. *Nat Chem Biol* **5**, 100-7.
- Chen, R., Amoui, M., Zhang, Z. and Mardon, G.** (1997). Dachshund and eyes absent proteins form a complex and function synergistically to induce ectopic eye development in *Drosophila*. *Cell* **91**, 893-903.
- Chen, W. Y., John, J. A., Lin, C. H. and Chang, C. Y.** (2007). Expression pattern of metallothionein, MTF-1 nuclear translocation, and its dna-binding activity in zebrafish (*Danio rerio*) induced by zinc and cadmium. *Environ Toxicol Chem* **26**, 110-7.
- Cheyette, B. N., Green, P. J., Martin, K., Garren, H., Hartenstein, V. and Zipursky, S. L.** (1994). The *Drosophila* sine oculis locus encodes a homeodomain-containing protein required for the development of the entire visual system. *Neuron* **12**, 977-96.

- Chezar, H. H.** (1930). Studies on the lateral-line system of amphibia. II. Comparative cytology and innervation of the lateral-line organs in the Urodela. *J. Comp. Neurol.* **50**.
- Chiu, L. L., Cunningham, L. L., Raible, D. W., Rubel, E. W. and Ou, H. C.** (2008). Using the zebrafish lateral line to screen for ototoxicity. *J. Assoc. Res. Otolaryngol* **9**, 178-90.
- Choo, B. G., Kondrichin, I., Parinov, S., Emelyanov, A., Go, W., Toh, W. C. and Korzh, V.** (2006). Zebrafish transgenic Enhancer TRAP line database (ZETRAP). *BMC Dev Biol* **6**, 5.
- Coffin, A. B., Ou, H., Owens, K. N., Santos, F., Simon, J. A., Rubel, E. W. and Raible, D. W.** (2010). Chemical screening for hair cell loss and protection in the zebrafish lateral line. *Zebrafish* **7**, 3-11.
- Coletta, R. D., Christensen, K., Reichenberger, K. J., Lamb, J., Micomonaco, D., Huang, L., Wolf, D. M., Muller-Tidow, C., Golub, T. R., Kawakami, K. et al.** (2004). The Six1 homeoprotein stimulates tumorigenesis by reactivation of cyclin A1. *Proc Natl Acad Sci U S A* **101**, 6478-83.
- Coletta, R. D., McCoy, E. L., Burns, V., Kawakami, K., McManaman, J. L., Wysolmerski, J. J. and Ford, H. L.** (2010). Characterization of the Six1 homeobox gene in normal mammary gland morphogenesis. *BMC Dev Biol* **10**, 4.
- Collado, M. S., Burns, J. C., Hu, Z. and Corwin, J. T.** (2008). Recent advances in hair cell regeneration research. *Curr Opin Otolaryngol Head Neck Surg* **16**, 465-71.
- Collet, J. F., Stroobant, V., Pirard, M., Delpierre, G. and Van Schaftingen, E.** (1998). A new class of phosphotransferases phosphorylated on an aspartate residue in an amino-terminal DXDX(T/V) motif. *J Biol Chem* **273**, 14107-12.
- Cook, P. J., Ju, B. G., Telese, F., Wang, X., Glass, C. K. and Rosenfeld, M. G.** (2009). Tyrosine dephosphorylation of H2AX modulates apoptosis and survival decisions. *Nature* **458**, 591-6.
- Corwin, J. T. and Cotanche, D. A.** (1988). Regeneration of sensory hair cells after acoustic trauma. *Science* **240**, 1772-4.
- Costanzi, C. and Pehrson, J. R.** (1998). Histone macroH2A1 is concentrated in the inactive X chromosome of female mammals. *Nature* **393**, 599-601.
- Curry, C. L., Reed, L. L., Nickoloff, B. J., Miele, L. and Foreman, K. E.** (2006). Notch-independent regulation of Hes-1 expression by c-Jun N-terminal kinase signaling in human endothelial cells. *Lab Invest* **86**, 842-52.
- Dahmann, C., Oates, A. C. and Brand, M.** (2011). Boundary formation and maintenance in tissue development. *Nat Rev Genet* **12**, 43-55.
- Dambly-Chaudiere, C., Cubedo, N. and Ghysen, A.** (2007). Control of cell migration in the development of the posterior lateral line: antagonistic

interactions between the chemokine receptors CXCR4 and CXCR7/RDC1. *BMC Dev Biol* **7**, 23.

**Daudet, N., Gibson, R., Shang, J., Bernard, A., Lewis, J. and Stone, J.** (2009). Notch regulation of progenitor cell behavior in quiescent and regenerating auditory epithelium of mature birds. *Dev Biol* **326**, 86-100.

**David, N. B., Sapede, D., Saint-Etienne, L., Thisse, C., Thisse, B., Dambly-Chaudiere, C., Rosa, F. M. and Ghysen, A.** (2002). Molecular basis of cell migration in the fish lateral line: role of the chemokine receptor CXCR4 and of its ligand, SDF1. *Proc Natl Acad Sci U S A* **99**, 16297-302.

**Del Bene, F., Wehman, A. M., Link, B. A. and Baier, H.** (2008). Regulation of neurogenesis by interkinetic nuclear migration through an apical-basal notch gradient. *Cell* **134**, 1055-65.

**Dessaud, E., Yang, L. L., Hill, K., Cox, B., Ulloa, F., Ribeiro, A., Mynett, A., Novitch, B. G. and Briscoe, J.** (2007). Interpretation of the sonic hedgehog morphogen gradient by a temporal adaptation mechanism. *Nature* **450**, 717-20.

**Dho, S. E., Trejo, J., Siderovski, D. P. and McGlade, C. J.** (2006). Dynamic regulation of mammalian numb by G protein-coupled receptors and protein kinase C activation: Structural determinants of numb association with the cortical membrane. *Mol Biol Cell* **17**, 4142-55.

**Dijkgraaf, S.** (1963). The functioning and significance of the lateral-line organs. *Biol Rev Camb Philos Soc* **38**, 51-105.

**Dodé, C., Levilliers, J., Dupont, J. M., De Paepe, A., Le Du, N., Soussi-Yanicostas, N., Coimbra, R. S., Delmaghani, S., Compain-Nouaille, S., Baverel, F. et al.** (2003). Loss-of-function mutations in FGFR1 cause autosomal dominant Kallmann syndrome. *Nat Genet* **33**, 463-5.

**Donner, A. L. and Maas, R. L.** (2004). Conservation and non-conservation of genetic pathways in eye specification. *Int J Dev Biol* **48**, 743-53.

**Doyen, C. M., An, W., Angelov, D., Bondarenko, V., Mietton, F., Studitsky, V. M., Hamiche, A., Roeder, R. G., Bouvet, P. and Dimitrov, S.** (2006). Mechanism of polymerase II transcription repression by the histone variant macroH2A. *Mol Cell Biol* **26**, 1156-64.

**Drake, K. M., Ruteshouser, E. C., Natrajan, R., Harbor, P., Wegert, J., Gessler, M., Pritchard-Jones, K., Grundy, P., Dome, J., Huff, V. et al.** (2009). Loss of heterozygosity at 2q37 in sporadic Wilms' tumor: putative role for miR-562. *Clin Cancer Res* **15**, 5985-92.

**Eddison, M., Le Roux, I. and Lewis, J.** (2000). Notch signaling in the development of the inner ear: lessons from *Drosophila*. *Proc Natl Acad Sci U S A* **97**, 11692-9.

**El-Hashash, A. H., Turcatel, G., Al Alam, D., Buckley, S., Tokumitsu, H., Bellusci, S. and Warburton, D.** (2011). *Eya1* controls cell polarity, spindle orientation, cell fate and Notch signaling in distal embryonic lung epithelium. *Development* **138**, 1395-407.

**Esain, V., Postlethwait, J. H., Charnay, P. and Ghislain, J.** FGF-receptor signaling controls neural cell diversity in the zebrafish hindbrain by regulating *olig2* and *sox9*. *Development* **137**, 33-42.

**Faucherre, A., Pujol-Marti, J., Kawakami, K. and Lopez-Schier, H.** (2009). Afferent neurons of the zebrafish lateral line are strict selectors of hair-cell orientation. *PLoS One* **4**, e4477.

**Fischer, E., Legue, E., Doyen, A., Nato, F., Nicolas, J. F., Torres, V., Yaniv, M. and Pontoglio, M.** (2006). Defective planar cell polarity in polycystic kidney disease. *Nat Genet* **38**, 21-3.

**Ford, H. L., Kabingu, E. N., Bump, E. A., Mutter, G. L. and Pardee, A. B.** (1998). Abrogation of the G2 cell cycle checkpoint associated with overexpression of HSI1: a possible mechanism of breast carcinogenesis. *Proc Natl Acad Sci U S A* **95**, 12608-13.

**Forge, A. and Schacht, J.** (2000). Aminoglycoside antibiotics. *Audiol Neurotol* **5**, 3-22.

**Froehlicher, M., Liedtke, A., Groh, K., Lopez-Schier, H., Neuhauss, S. C., Segner, H. and Eggen, R. I.** (2009). Estrogen receptor subtype beta2 is involved in neuromast development in zebrafish (*Danio rerio*) larvae. *Dev Biol* **330**, 32-43.

**Gamba, L., Cubedo, N., Ghysen, A., Lutfalla, G. and Dambly-Chaudiere, C.** (2010). Estrogen receptor ESR1 controls cell migration by repressing chemokine receptor CXCR4 in the zebrafish posterior lateral line system. *Proc Natl Acad Sci U S A* **107**, 6358-63.

**Ghysen, A. and Dambly-Chaudiere, C.** (2007). The lateral line microcosmos. *Genes Dev* **21**, 2118-30.

**Glass, C. K. and Rosenfeld, M. G.** (2000). The coregulator exchange in transcriptional functions of nuclear receptors. *Genes Dev* **14**, 121-41.

**Go, W., Bessarab, D. and Korzh, V.** (2010). *atp2b1a* regulates Ca(2+) export during differentiation and regeneration of mechanosensory hair cells in zebrafish. *Cell Calcium* **48**, 302-13.

**Gobba, F.** (2003). Occupational exposure to chemicals and sensory organs: a neglected research field. *Neurotoxicology* **24**, 675-91.

**Goessling, W., North, T. E., Loewer, S., Lord, A. M., Lee, S., Stoick-Cooper, C. L., Weidinger, G., Puder, M., Daley, G. Q., Moon, R. T. et al.** (2009). Genetic interaction of PGE2 and Wnt signaling regulates developmental specification of stem cells and regeneration. *Cell* **136**, 1136-47.

**Goldstein, R. E., Cook, O., Dinur, T., Pisante, A., Karandikar, U. C., Bidwai, A. and Paroush, Z.** (2005). An eh1-like motif in odd-skipped mediates recruitment of Groucho and repression in vivo. *Mol Cell Biol* **25**, 10711-20.

**Grigoryan, T., Wend, P., Klaus, A. and Birchmeier, W.** (2008). Deciphering the function of canonical Wnt signals in development and disease: conditional loss- and gain-of-function mutations of beta-catenin in mice. *Genes Dev* **22**, 2308-41.

- Guttman, M., Amit, I., Garber, M., French, C., Lin, M. F., Feldser, D., Huarte, M., Zuk, O., Carey, B. W., Cassady, J. P. et al.** (2009). Chromatin signature reveals over a thousand highly conserved large non-coding RNAs in mammals. *Nature* **458**, 223-7.
- Haas, P. and Gilmour, D.** (2006). Chemokine signaling mediates self-organizing tissue migration in the zebrafish lateral line. *Dev Cell* **10**, 673-80.
- Haddon, C., Jiang, Y. J., Smithers, L. and Lewis, J.** (1998a). Delta-Notch signaling and the patterning of sensory cell differentiation in the zebrafish ear: evidence from the mind bomb mutant. *Development* **125**, 4637-44.
- Haddon, C., Smithers, L., Schneider-Maunoury, S., Coche, T., Henrique, D. and Lewis, J.** (1998b). Multiple delta genes and lateral inhibition in zebrafish primary neurogenesis. *Development* **125**, 359-70.
- Haines, L., Neyt, C., Gautier, P., Keenan, D. G., Bryson-Richardson, R. J., Hollway, G. E., Cole, N. J. and Currie, P. D.** (2004). Met and Hgf signaling controls hypaxial muscle and lateral line development in the zebrafish. *Development* **131**, 4857-69.
- Haramis, A. P., Hurlstone, A., van der Velden, Y., Begthel, H., van den Born, M., Offerhaus, G. J. and Clevers, H. C.** (2006). Adenomatous polyposis coli-deficient zebrafish are susceptible to digestive tract neoplasia. *EMBO Rep* **7**, 444-9.
- Hardin, J. and Keller, R.** (1988). The behaviour and function of bottle cells during gastrulation of *Xenopus laevis*. *Development* **103**, 211-30.
- Hava, D., Forster, U., Matsuda, M., Cui, S., Link, B. A., Eichhorst, J., Wiesner, B., Chitnis, A. and Abdelilah-Seyfried, S.** (2009). Apical membrane maturation and cellular rosette formation during morphogenesis of the zebrafish lateral line. *J Cell Sci* **122**, 687-95.
- Hawkins, R. D., Bashiardes, S., Powder, K. E., Sajan, S. A., Bhonagiri, V., Alvarado, D. M., Speck, J., Warchol, M. E. and Lovett, M.** (2007). Large scale gene expression profiles of regenerating inner ear sensory epithelia. *PLoS One* **2**, e525.
- Hemberger, M., Dean, W. and Reik, W.** (2009). Epigenetic dynamics of stem cells and cell lineage commitment: digging Waddington's canal. *Nat Rev Mol Cell Biol* **10**, 526-37.
- Henikoff, S.** (2008). Nucleosome destabilization in the epigenetic regulation of gene expression. *Nat Rev Genet* **9**, 15-26.
- Hernández, P. P., Moreno, V., Olivari, F. A. and Allende, M. L.** (2006). Sub-lethal concentrations of waterborne copper are toxic to lateral line neuromasts in zebrafish (*Danio rerio*). *Hear Res* **213**, 1-10.
- Hernández, P. P., Olivari, F. A., Sarrazin, A. F., Sandoval, P. C. and Allende, M. L.** (2007). Regeneration in zebrafish lateral line neuromasts: expression of the neural progenitor cell marker *sox2* and proliferation-dependent and-independent mechanisms of hair cell renewal. *Dev Neurobiol* **67**, 637-54.

- Herzog, W., Sonntag, C., Walderich, B., Odenthal, J., Maischein, H. M. and Hammerschmidt, M.** (2004). Genetic analysis of adenohipophysis formation in zebrafish. *Mol Endocrinol* **18**, 1185-95.
- Hisano, T., Hata, Y., Fujii, T., Liu, J. Q., Kurihara, T., Esaki, N. and Soda, K.** (1996). Crystal structure of L-2-haloacid dehalogenase from *Pseudomonas* sp. YL. An alpha/beta hydrolase structure that is different from the alpha/beta hydrolase fold. *J Biol Chem* **271**, 20322-30.
- Hori, R., Nakagawa, T., Sakamoto, T., Matsuoka, Y., Takebayashi, S. and Ito, J.** (2007). Pharmacological inhibition of Notch signaling in the mature guinea pig cochlea. *Neuroreport* **18**, 1911-4.
- Hudspeth, A. J.** (1985). The cellular basis of hearing: the biophysics of hair cells. *Science* **230**, 745-52.
- Itoh, M. and Chitnis, A. B.** (2001). Expression of proneural and neurogenic genes in the zebrafish lateral line primordium correlates with selection of hair cell fate in neuromasts. *Mech Dev* **102**, 263-6.
- Itoh, M., Kim, C. H., Palardy, G., Oda, T., Jiang, Y. J., Maust, D., Yeo, S. Y., Lorick, K., Wright, G. J., Ariza-McNaughton, L. et al.** (2003). Mind bomb is a ubiquitin ligase that is essential for efficient activation of Notch signaling by Delta. *Dev Cell* **4**, 67-82.
- Jaeger, J. and Martinez-Arias, A.** (2009). Getting the measure of positional information. *PLoS Biol* **7**, e81.
- Jemc, J. and Rebay, I.** (2007a). Identification of transcriptional targets of the dual-function transcription factor/phosphatase eyes absent. *Dev Biol* **310**, 416-29.
- Jemc, J. and Rebay, I.** (2007b). The eyes absent family of phosphotyrosine phosphatases: properties and roles in developmental regulation of transcription. *Annu Rev Biochem* **76**, 513-38.
- Johnson, A., Carew, E. and Sloman, K. A.** (2007). The effects of copper on the morphological and functional development of zebrafish embryos. *Aquat Toxicol* **84**, 431-8.
- Karras, G. I., Kustatscher, G., Buhecha, H. R., Allen, M. D., Pugieux, C., Sait, F., Bycroft, M. and Ladurner, A. G.** (2005). The macro domain is an ADP-ribose binding module. *EMBO J* **24**, 1911-20.
- Kerstetter, A. E., Azodi, E., Marrs, J. A. and Liu, Q.** (2004). Cadherin-2 function in the cranial ganglia and lateral line system of developing zebrafish. *Dev Dyn* **230**, 137-43.
- Kimberly, E. L. and Hardin, J.** (1998). Bottle cells are required for the initiation of primary invagination in the sea urchin embryo. *Dev Biol* **204**, 235-50.
- Knaut, H. and Schier, A. F.** (2008). Clearing the path for germ cells. *Cell* **132**, 337-9.
- Kobayashi, M., Nishikawa, K., Suzuki, T. and Yamamoto, M.** (2001). The homeobox protein Six3 interacts with the Groucho corepressor and acts as a transcriptional repressor in eye and forebrain formation. *Dev Biol* **232**, 315-26.

- Kochhar, A., Fischer, S. M., Kimberling, W. J. and Smith, R. J.** (2007). Branchio-oto-renal syndrome. *Am J Med Genet A* **143A**, 1671-8.
- Kopan, R. and Ilagan, M. X.** (2009). The canonical Notch signaling pathway: unfolding the activation mechanism. *Cell* **137**, 216-33.
- Kouzarides, T.** (2007). Chromatin modifications and their function. *Cell* **128**, 693-705.
- Kozlowski, D. J., Whitfield, T. T., Hukriede, N. A., Lam, W. K. and Weinberg, E. S.** (2005). The zebrafish dog-eared mutation disrupts *eya1*, a gene required for cell survival and differentiation in the inner ear and lateral line. *Dev Biol* **277**, 27-41.
- Kriebel, M., Muller, F. and Hollemann, T.** (2007). Xeya3 regulates survival and proliferation of neural progenitor cells within the anterior neural plate of *Xenopus* embryos. *Dev Dyn* **236**, 1526-34.
- Krishnan, N., Jeong, D. G., Jung, S. K., Ryu, S. E., Xiao, A., Allis, C. D., Kim, S. J. and Tonks, N. K.** (2009). Dephosphorylation of the C-terminal tyrosyl residue of the DNA damage-related histone H2A.X is mediated by the protein phosphatase eyes absent. *J Biol Chem* **284**, 16066-70.
- Kustatscher, G., Hothorn, M., Pugieux, C., Scheffzek, K. and Ladurner, A. G.** (2005). Splicing regulates NAD metabolite binding to histone macroH2A. *Nat Struct Mol Biol* **12**, 624-5.
- Lahiri, S. D., Zhang, G., Dunaway-Mariano, D. and Allen, K. N.** (2002). Caught in the act: the structure of phosphorylated beta-phosphoglucosyltransferase from *Lactococcus lactis*. *Biochemistry* **41**, 8351-9.
- Lanford, P. J., Lan, Y., Jiang, R., Lindsell, C., Weinmaster, G., Gridley, T. and Kelley, M. W.** (1999). Notch signaling pathway mediates hair cell development in mammalian cochlea. *Nat Genet* **21**, 289-92.
- Langheinrich, U., Hennen, E., Stott, G. and Vacun, G.** (2002). Zebrafish as a model organism for the identification and characterization of drugs and genes affecting p53 signaling. *Curr Biol* **12**, 2023-8.
- Lecaudey, V., Cakan-Akdogan, G., Norton, W. H. and Gilmour, D.** (2008). Dynamic Fgf signaling couples morphogenesis and migration in the zebrafish lateral line primordium. *Development* **135**, 2695-705.
- Lecaudey, V. and Gilmour, D.** (2006). Organizing moving groups during morphogenesis. *Curr Opin Cell Biol* **18**, 102-7.
- Lecuit, T. and Le Goff, L.** (2007). Orchestrating size and shape during morphogenesis. *Nature* **450**, 189-92.
- Lecuit, T. and Lenne, P. F.** (2007). Cell surface mechanics and the control of cell shape, tissue patterns and morphogenesis. *Nat Rev Mol Cell Biol* **8**, 633-44.
- Lee, Y., Grill, S., Sanchez, A., Murphy-Ryan, M. and Poss, K. D.** (2005). Fgf signaling instructs position-dependent growth rate during zebrafish fin regeneration. *Development* **132**, 5173-83.
- Leiserson, W. M., Benzer, S. and Bonini, N. M.** (1998). Dual functions of the *Drosophila* eyes absent gene in the eye and embryo. *Mech Dev* **73**, 193-202.



- Leucht, C., Stigloher, C., Wizenmann, A., Klafke, R., Folchert, A. and Bally-Cuif, L.** (2008). MicroRNA-9 directs late organizer activity of the midbrain-hindbrain boundary. *Nat Neurosci* **11**, 641-8.
- Levoye, A., Balabanian, K., Baleux, F., Bachelier, F. and Lagane, B.** (2009). CXCR7 heterodimerizes with CXCR4 and regulates CXCL12-mediated G protein signaling. *Blood* **113**, 6085-93.
- Lewis, J.** (1998). Notch signaling and the control of cell fate choices in vertebrates. *Semin Cell Dev Biol* **9**, 583-9.
- Lewis, J. and Davies, A.** (2002). Planar cell polarity in the inner ear: how do hair cells acquire their oriented structure? *J Neurobiol* **53**, 190-201.
- Li, X., Oghi, K. A., Zhang, J., Krones, A., Bush, K. T., Glass, C. K., Nigam, S. K., Aggarwal, A. K., Maas, R., Rose, D. W. et al.** (2003). Eya protein phosphatase activity regulates Six1-Dach-Eya transcriptional effects in mammalian organogenesis. *Nature* **426**, 247-54.
- Li, X., Perissi, V., Liu, F., Rose, D. W. and Rosenfeld, M. G.** (2002). Tissue-specific regulation of retinal and pituitary precursor cell proliferation. *Science* **297**, 1180-3.
- Li, Y., Manaligod, J. M. and Weeks, D. L.** (2010). EYA1 mutations associated with the branchio-oto-renal syndrome result in defective otic development in *Xenopus laevis*. *Biol Cell* **102**, 277-92.
- Linbo, T. L., Stehr, C. M., Incardona, J. P. and Scholz, N. L.** (2006). Dissolved copper triggers cell death in the peripheral mechanosensory system of larval fish. *Environ Toxicol Chem* **25**, 597-603.
- Liu, Q., Kerstetter, A. E., Azodi, E. and Marrs, J. A.** (2003). Cadherin-1, -2, and -11 expression and cadherin-2 function in the pectoral limb bud and fin of the developing zebrafish. *Dev Dyn* **228**, 734-9.
- López-Ríos, J., Tessmar, K., Loosli, F., Wittbrodt, J. and Bovolenta, P.** (2003). Six3 and Six6 activity is modulated by members of the groucho family. *Development* **130**, 185-95.
- López-Schier, H. and Hudspeth, A. J.** (2005). Supernumerary neuromasts in the posterior lateral line of zebrafish lacking peripheral glia. *Proc Natl Acad Sci U S A* **102**, 1496-501.
- López-Schier, H. and Hudspeth, A. J.** (2006). A two-step mechanism underlies the planar polarization of regenerating sensory hair cells. *Proc Natl Acad Sci U S A* **103**, 18615-20.
- López-Schier, H., Starr, C. J., Kappler, J. A., Kollmar, R. and Hudspeth, A. J.** (2004). Directional cell migration establishes the axes of planar polarity in the posterior lateral-line organ of the zebrafish. *Dev Cell* **7**, 401-12.
- Ma, E. Y. and Raible, D. W.** (2009). Signaling pathways regulating zebrafish lateral line development. *Curr Biol* **19**, R381-6.
- Ma, E. Y., Rubel, E. W. and Raible, D. W.** (2008). Notch signaling regulates the extent of hair cell regeneration in the zebrafish lateral line. *J Neurosci* **28**, 2261-73.

- Mathur, D., Bost, A., Driver, I. and Ohlstein, B.** (2010). A transient niche regulates the specification of *Drosophila* intestinal stem cells. *Science* **327**, 210-3.
- Matsuda, M. and Chitnis, A. B.** (2010). *Atoh1a* expression must be restricted by Notch signaling for effective morphogenesis of the posterior lateral line primordium in zebrafish. *Development* **137**, 3477-87.
- McKenna, N. J. and O'Malley, B. W.** (2002). Combinatorial control of gene expression by nuclear receptors and coregulators. *Cell* **108**, 465-74.
- McKinsey, T. A., Zhang, C. L. and Olson, E. N.** (2001). Control of muscle development by dueling HATs and HDACs. *Curr Opin Genet Dev* **11**, 497-504.
- Metcalf, W. K.** (1985). Sensory neuron growth cones comigrate with posterior lateral line primordial cells in zebrafish. *J Comp Neurol* **238**, 218-24.
- Metcalf, W. K., Kimmel, C. B. and Schabtach, E.** (1985). Anatomy of the posterior lateral line system in young larvae of the zebrafish. *J Comp Neurol* **233**, 377-89.
- Micalizzi, D. S., Farabaugh, S. M. and Ford, H. L.** (2010). Epithelial-mesenchymal transition in cancer: parallels between normal development and tumor progression. *J Mammary Gland Biol Neoplasia* **15**, 117-34.
- Miller, S. J., Lan, Z. D., Hardiman, A., Wu, J., Kordich, J. J., Patmore, D. M., Hegde, R. S., Cripe, T. P., Cancelas, J. A., Collins, M. H. et al.** (2010). Inhibition of Eyes Absent Homolog 4 expression induces malignant peripheral nerve sheath tumor necrosis. *Oncogene* **29**, 368-79.
- Millimaki, B. B., Sweet, E. M. and Riley, B. B.** (2010). Sox2 is required for maintenance and regeneration, but not initial development, of hair cells in the zebrafish inner ear. *Dev Biol* **338**, 262-9.
- Mirzadeh, Z., Han, Y. G., Soriano-Navarro, M., Garcia-Verdugo, J. M. and Alvarez-Buylla, A.** (2010). Cilia organize ependymal planar polarity. *J Neurosci* **30**, 2600-10.
- Montgomery JC, B. C., Carton AG.** (1997). The lateral line can mediate rheotaxis in fish. *Nature* **389**.
- Murphey, R. D., Stern, H. M., Straub, C. T. and Zon, L. I.** (2006). A chemical genetic screen for cell cycle inhibitors in zebrafish embryos. *Chem Biol Drug Des* **68**, 213-9.
- Mutsuddi, M., Chaffee, B., Cassidy, J., Silver, S. J., Tootle, T. L. and Rebay, I.** (2005). Using *Drosophila* to decipher how mutations associated with human branchio-oto-renal syndrome and optical defects compromise the protein tyrosine phosphatase and transcriptional functions of eyes absent. *Genetics* **170**, 687-95.
- Nagiel, A., Patel, S. H., Andor-Ardo, D. and Hudspeth, A. J.** (2009). Activity-independent specification of synaptic targets in the posterior lateral line of the larval zebrafish. *Proc Natl Acad Sci U S A* **106**, 21948-53.
- Nair, S. and Schilling, T. F.** (2008). Chemokine signaling controls endodermal migration during zebrafish gastrulation. *Science* **322**, 89-92.

- Nechiporuk, A. and Raible, D. W. (2008). FGF-dependent mechanosensory organ patterning in zebrafish. *Science* **320**, 1774-7.
- Nguyen, D. X., Chiang, A. C., Zhang, X. H., Kim, J. Y., Kris, M. G., Ladanyi, M., Gerald, W. L. and Massague, J. (2009). WNT/TCF signaling through LEF1 and HOXB9 mediates lung adenocarcinoma metastasis. *Cell* **138**, 51-62.
- Nica, G., Herzog, W., Sonntag, C., Nowak, M., Schwarz, H., Zapata, A. G. and Hammerschmidt, M. (2006). Eya1 is required for lineage-specific differentiation, but not for cell survival in the zebrafish adeno-hypophysis. *Dev Biol* **292**, 189-204.
- Nicolson, T. (2005). The genetics of hearing and balance in zebrafish. *Annu Rev Genet* **39**, 9-22.
- Nikolaidou, K. K. and Barrett, K. (2004). A Rho GTPase signaling pathway is used reiteratively in epithelial folding and potentially selects the outcome of Rho activation. *Curr Biol* **14**, 1822-6.
- Nishita, M., Yoo, S. K., Nomachi, A., Kani, S., Sougawa, N., Ohta, Y., Takada, S., Kikuchi, A. and Minami, Y. (2006). Filopodia formation mediated by receptor tyrosine kinase Ror2 is required for Wnt5a-induced cell migration. *J Cell Biol* **175**, 555-62.
- Nusinow, D. A., Hernandez-Munoz, I., Fazzio, T. G., Shah, G. M., Kraus, W. L. and Panning, B. (2007). Poly(ADP-ribose) polymerase 1 is inhibited by a histone H2A variant, MacroH2A, and contributes to silencing of the inactive X chromosome. *J Biol Chem* **282**, 12851-9.
- Ohto, H., Kamada, S., Tago, K., Tominaga, S. I., Ozaki, H., Sato, S. and Kawakami, K. (1999). Cooperation of six and eya in activation of their target genes through nuclear translocation of Eya. *Mol Cell Biol* **19**, 6815-24.
- Ou, H. C., Raible, D. W. and Rubel, E. W. (2007). Cisplatin-induced hair cell loss in zebrafish (*Danio rerio*) lateral line. *Hear Res* **233**, 46-53.
- Ouararhni, K., Hadj-Slimane, R., Ait-Si-Ali, S., Robin, P., Mietton, F., Harel-Bellan, A., Dimitrov, S. and Hamiche, A. (2006). The histone variant mH2A1.1 interferes with transcription by down-regulating PARP-1 enzymatic activity. *Genes Dev* **20**, 3324-36.
- Owens, K. N., Santos, F., Roberts, B., Linbo, T., Coffin, A. B., Knisely, A. J., Simon, J. A., Rubel, E. W. and Raible, D. W. (2008). Identification of genetic and chemical modulators of zebrafish mechanosensory hair cell death. *PLoS Genet* **4**, e1000020.
- Pai, R., Dunlap, D., Qing, J., Mohtashemi, I., Hotzel, K. and French, D. M. (2008). Inhibition of fibroblast growth factor 19 reduces tumor growth by modulating beta-catenin signaling. *Cancer Res* **68**, 5086-95.
- Pandey, R. N., Rani, R., Yeo, E. J., Spencer, M., Hu, S., Lang, R. A. and Hegde, R. S. (2010). The Eyes Absent phosphatase-transactivator proteins promote proliferation, transformation, migration, and invasion of tumor cells. *Oncogene* **29**, 3715-22.

- Parinov, S., Kondrichin, I., Korzh, V. and Emelyanov, A.** (2004). Tol2 transposon-mediated enhancer trap to identify developmentally regulated zebrafish genes in vivo. *Dev Dyn* **231**, 449-59.
- Parsons, M. J., Pisharath, H., Yusuff, S., Moore, J. C., Siekmann, A. F., Lawson, N. and Leach, S. D.** (2009). Notch-responsive cells initiate the secondary transition in larval zebrafish pancreas. *Mech Dev* **126**, 898-912.
- Pasini, A., Henrique, D. and Wilkinson, D. G.** (2001). The zebrafish Hairy/Enhancer-of-split-related gene *her6* is segmentally expressed during the early development of hindbrain and somites. *Mech Dev* **100**, 317-21.
- Pasini, A., Jiang, Y. J. and Wilkinson, D. G.** (2004). Two zebrafish Notch-dependent hairy/Enhancer-of-split-related genes, *her6* and *her4*, are required to maintain the coordination of cyclic gene expression in the presomitic mesoderm. *Development* **131**, 1529-41.
- Petersen, P. H., Zou, K., Hwang, J. K., Jan, Y. N. and Zhong, W.** (2002). Progenitor cell maintenance requires *numb* and *numblike* during mouse neurogenesis. *Nature* **419**, 929-34.
- Pignoni, F., Hu, B., Zavitz, K. H., Xiao, J., Garrity, P. A. and Zipursky, S. L.** (1997). The eye-specification proteins *So* and *Eya* form a complex and regulate multiple steps in *Drosophila* eye development. *Cell* **91**, 881-91.
- Polin, M., Tuval, I., Drescher, K., Gollub, J. P. and Goldstein, R. E.** (2009). *Chlamydomonas* swims with two "gears" in a eukaryotic version of run-and-tumble locomotion. *Science* **325**, 487-90.
- Potdar, A. A., Lu, J., Jeon, J., Weaver, A. M. and Cummings, P. T.** (2009). Bimodal analysis of mammary epithelial cell migration in two dimensions. *Ann Biomed Eng* **37**, 230-45.
- Rando, O. J. and Chang, H. Y.** (2009). Genome-wide views of chromatin structure. *Annu Rev Biochem* **78**, 245-71.
- Rayapureddi, J. P., Kattamuri, C., Steinmetz, B. D., Frankfort, B. J., Ostrin, E. J., Mardon, G. and Hegde, R. S.** (2003). Eyes absent represents a class of protein tyrosine phosphatases. *Nature* **426**, 295-8.
- Rida, P. C. and Chen, P.** (2009). Line up and listen: Planar cell polarity regulation in the mammalian inner ear. *Semin Cell Dev Biol* **20**, 978-85.
- Ryals, B. M. and Rubel, E. W.** (1988). Hair cell regeneration after acoustic trauma in adult *Coturnix* quail. *Science* **240**, 1774-6.
- Saburi, S., Hester, I., Fischer, E., Pontoglio, M., Eremina, V., Gessler, M., Quaggin, S. E., Harrison, R., Mount, R. and McNeill, H.** (2008). Loss of *Fat4* disrupts PCP signaling and oriented cell division and leads to cystic kidney disease. *Nat Genet* **40**, 1010-5.
- Sahly, I., Andermann, P. and Petit, C.** (1999). The zebrafish *eya1* gene and its expression pattern during embryogenesis. *Dev Genes Evol* **209**, 399-410.
- Sang, L., Collier, H. A. and Roberts, J. M.** (2008). Control of the reversibility of cellular quiescence by the transcriptional repressor *HES1*. *Science* **321**, 1095-100.

- Sarma, K. and Reinberg, D.** (2005). Histone variants meet their match. *Nat Rev Mol Cell Biol* **6**, 139-49.
- Schonberger, J., Wang, L., Shin, J. T., Kim, S. D., Depreux, F. F., Zhu, H., Zon, L., Pizard, A., Kim, J. B., Macrae, C. A. et al.** (2005). Mutation in the transcriptional coactivator EYA4 causes dilated cardiomyopathy and sensorineural hearing loss. *Nat Genet* **37**, 418-22.
- Shen, Q., Zhong, W., Jan, Y. N. and Temple, S.** (2002). Asymmetric Numb distribution is critical for asymmetric cell division of mouse cerebral cortical stem cells and neuroblasts. *Development* **129**, 4843-53.
- Siekmann, A. F., Standley, C., Fogarty, K. E., Wolfe, S. A. and Lawson, N. D.** (2009). Chemokine signaling guides regional patterning of the first embryonic artery. *Genes Dev* **23**, 2272-7.
- Sierro, F., Biben, C., Martinez-Munoz, L., Mellado, M., Ransohoff, R. M., Li, M., Woehl, B., Leung, H., Groom, J., Batten, M. et al.** (2007). Disrupted cardiac development but normal hematopoiesis in mice deficient in the second CXCL12/SDF-1 receptor, CXCR7. *Proc Natl Acad Sci U S A* **104**, 14759-64.
- Silver, S. J., Davies, E. L., Doyon, L. and Rebay, I.** (2003). Functional dissection of eyes absent reveals new modes of regulation within the retinal determination gene network. *Mol Cell Biol* **23**, 5989-99.
- Silver, S. J. and Rebay, I.** (2005). Signaling circuitries in development: insights from the retinal determination gene network. *Development* **132**, 3-13.
- Smith, C. A., Lau, K. M., Rahmani, Z., Dho, S. E., Brothers, G., She, Y. M., Berry, D. M., Bonneil, E., Thibault, P., Schweisguth, F. et al.** (2007). aPKC-mediated phosphorylation regulates asymmetric membrane localization of the cell fate determinant Numb. *EMBO J* **26**, 468-80.
- Sollner, C., Rauch, G. J., Siemens, J., Geisler, R., Schuster, S. C., Muller, U. and Nicolson, T.** (2004). Mutations in cadherin 23 affect tip links in zebrafish sensory hair cells. *Nature* **428**, 955-9.
- Staton, A. A., Knaut, H. and Giraldez, A. J.** (2011). miRNA regulation of Sdf1 chemokine signaling provides genetic robustness to germ cell migration. *Nat Genet* **43**, 204-11.
- Stoick-Cooper, C. L., Weidinger, G., Riehle, K. J., Hubbert, C., Major, M. B., Fausto, N. and Moon, R. T.** (2007). Distinct Wnt signaling pathways have opposing roles in appendage regeneration. *Development* **134**, 479-89.
- Strutt, D. I.** (2002). The asymmetric subcellular localisation of components of the planar polarity pathway. *Semin Cell Dev Biol* **13**, 225-31.
- Tagami, H., Ray-Gallet, D., Almouzni, G. and Nakatani, Y.** (2004). Histone H3.1 and H3.3 complexes mediate nucleosome assembly pathways dependent or independent of DNA synthesis. *Cell* **116**, 51-61.
- Thaller, M. C., Schippa, S. and Rossolini, G. M.** (1998). Conserved sequence motifs among bacterial, eukaryotic, and archaeal phosphatases that define a new phosphohydrolase superfamily. *Protein Sci* **7**, 1647-52.

- Theisen, H., Haerry, T. E., O'Connor, M. B. and Marsh, J. L.** (1996). Developmental territories created by mutual antagonism between Wingless and Decapentaplegic. *Development* **122**, 3939-48.
- Theveneau, E., Marchant, L., Kuriyama, S., Gull, M., Moepps, B., Parsons, M. and Mayor, R.** (2010). Collective chemotaxis requires contact-dependent cell polarity. *Dev Cell* **19**, 39-53.
- Thiery, J. P., Acloque, H., Huang, R. Y. and Nieto, M. A.** (2009). Epithelial-mesenchymal transitions in development and disease. *Cell* **139**, 871-90.
- Thisse, C. and Thisse, B.** (2008). High-resolution in situ hybridization to whole-mount zebrafish embryos. *Nat Protoc* **3**, 59-69.
- Tingaud-Sequeira, A., Andre, M., Forge, J., Barthe, C. and Babin, P. J.** (2004). Expression patterns of three estrogen receptor genes during zebrafish (*Danio rerio*) development: evidence for high expression in neuromasts. *Gene Expr Patterns* **4**, 561-8.
- Tootle, T. L., Silver, S. J., Davies, E. L., Newman, V., Latek, R. R., Mills, I. A., Selengut, J. D., Parlikar, B. E. and Rebay, I.** (2003). The transcription factor Eyes absent is a protein tyrosine phosphatase. *Nature* **426**, 299-302.
- Valentin, G., Haas, P. and Gilmour, D.** (2007). The chemokine SDF1a coordinates tissue migration through the spatially restricted activation of Cxcr7 and Cxcr4b. *Curr Biol* **17**, 1026-31.
- van Amerongen, R. and Nusse, R.** (2009). Towards an integrated view of Wnt signaling in development. *Development* **136**, 3205-14.
- Vicent, G. P., Nacht, A. S., Smith, C. L., Peterson, C. L., Dimitrov, S. and Beato, M.** (2004). DNA instructed displacement of histones H2A and H2B at an inducible promoter. *Mol Cell* **16**, 439-52.
- Villablanca, E. J., Renucci, A., Sapede, D., Lec, V., Soubiran, F., Sandoval, P. C., Dambly-Chaudiere, C., Ghysen, A. and Allende, M. L.** (2006). Control of cell migration in the zebrafish lateral line: implication of the gene "tumour-associated calcium signal transducer," *tacstd*. *Dev Dyn* **235**, 1578-88.
- Vincent, J. P. and Dubois, L.** (2002). Morphogen transport along epithelia, an integrated trafficking problem. *Dev Cell* **3**, 615-23.
- Vollrath, M. A., Kwan, K. Y. and Corey, D. P.** (2007). The micromachinery of mechanotransduction in hair cells. *Annu Rev Neurosci* **30**, 339-65.
- Voog, J., D'Alterio, C. and Jones, D. L.** (2008). Multipotent somatic stem cells contribute to the stem cell niche in the *Drosophila* testis. *Nature* **454**, 1132-6.
- Wang, L., Sewell, W. F., Kim, S. D., Shin, J. T., MacRae, C. A., Zon, L. I., Seidman, J. G. and Seidman, C. E.** (2008). Eya4 regulation of Na<sup>+</sup>/K<sup>+</sup>-ATPase is required for sensory system development in zebrafish. *Development* **135**, 3425-34.

- Wang, Y., Li, G., Stanco, A., Long, J. E., Crawford, D., Potter, G. B., Pleasure, S. J., Behrens, T. and Rubenstein, J. L. (2011). CXCR4 and CXCR7 have distinct functions in regulating interneuron migration. *Neuron* **69**, 61-76.
- Wartlick, O., Kicheva, A. and Gonzalez-Gaitan, M. (2009). Morphogen gradient formation. *Cold Spring Harb Perspect Biol* **1**, a001255.
- Whitfield, T. T. (2005). Lateral line: precocious phenotypes and planar polarity. *Curr Biol* **15**, R67-70.
- Whitfield, T. T., Granato, M., van Eeden, F. J., Schach, U., Brand, M., Furutani-Seiki, M., Haffter, P., Hammerschmidt, M., Heisenberg, C. P., Jiang, Y. J. et al. (1996). Mutations affecting development of the zebrafish inner ear and lateral line. *Development* **123**, 241-54.
- Williams, J. A. and Holder, N. (2000). Cell turnover in neuromasts of zebrafish larvae. *Hear Res* **143**, 171-81.
- Wilson, A. L., Shen, Y. C., Babb-Clendenon, S. G., Rostedt, J., Liu, B., Barald, K. F., Marrs, J. A. and Liu, Q. (2007). Cadherin-4 plays a role in the development of zebrafish cranial ganglia and lateral line system. *Dev Dyn* **236**, 893-902.
- Wodarz, A. and Nathke, I. (2007). Cell polarity in development and cancer. *Nat Cell Biol* **9**, 1016-24.
- Wolffe, A. P. and Matzke, M. A. (1999). Epigenetics: regulation through repression. *Science* **286**, 481-6.
- Wu, K., Li, A., Rao, M., Liu, M., Dailey, V., Yang, Y., Di Vizio, D., Wang, C., Lisanti, M. P., Sauter, G. et al. (2006). DACH1 is a cell fate determination factor that inhibits cyclin D1 and breast tumor growth. *Mol Cell Biol* **26**, 7116-29.
- Xiao, A., Li, H., Shechter, D., Ahn, S. H., Fabrizio, L. A., Erdjument-Bromage, H., Ishibe-Murakami, S., Wang, B., Tempst, P., Hofmann, K. et al. (2009). WSTF regulates the H2A.X DNA damage response via a novel tyrosine kinase activity. *Nature* **457**, 57-62.
- Xiong, W., Dabbouseh, N. M. and Rebay, I. (2009). Interactions with the abelson tyrosine kinase reveal compartmentalization of eyes absent function between nucleus and cytoplasm. *Dev Cell* **16**, 271-9.
- Xu, P. X., Adams, J., Peters, H., Brown, M. C., Heaney, S. and Maas, R. (1999). Eya1-deficient mice lack ears and kidneys and show abnormal apoptosis of organ primordia. *Nat Genet* **23**, 113-7.
- Xu, P. X., Cheng, J., Epstein, J. A. and Maas, R. L. (1997a). Mouse Eya genes are expressed during limb tendon development and encode a transcriptional activation function. *Proc Natl Acad Sci U S A* **94**, 11974-9.
- Xu, P. X., Woo, I., Her, H., Beier, D. R. and Maas, R. L. (1997b). Mouse Eya homologues of the Drosophila eyes absent gene require Pax6 for expression in lens and nasal placode. *Development* **124**, 219-31.
- Xu, P. X., Zheng, W., Laclef, C., Maire, P., Maas, R. L., Peters, H. and Xu, X. (2002). Eya1 is required for the morphogenesis of mammalian thymus, parathyroid and thyroid. *Development* **129**, 3033-44.

- Yates, L. L., Schnatwinkel, C., Murdoch, J. N., Bogani, D., Formstone, C. J., Townsend, S., Greenfield, A., Niswander, L. A. and Dean, C. H.** The PCP genes *Celsr1* and *Vangl2* are required for normal lung branching morphogenesis. *Hum Mol Genet* **19**, 2251-67.
- Yu, Y., Davicioni, E., Triche, T. J. and Merlino, G.** (2006). The homeoprotein *six1* transcriptionally activates multiple protumorigenic genes but requires *e\_zrin* to promote metastasis. *Cancer Res* **66**, 1982-9.
- Yu, Y., Khan, J., Khanna, C., Helman, L., Meltzer, P. S. and Merlino, G.** (2004). Expression profiling identifies the cytoskeletal organizer *e\_zrin* and the developmental homeoprotein *Six-1* as key metastatic regulators. *Nat Med* **10**, 175-81.
- Zallen, J. A.** (2007). Planar polarity and tissue morphogenesis. *Cell* **129**, 1051-63.
- Zimmerman, J. E., Bui, Q. T., Liu, H. and Bonini, N. M.** (2000). Molecular genetic analysis of *Drosophila* eyes absent mutants reveals an eye enhancer element. *Genetics* **154**, 237-46.
- Zimmerman, J. E., Bui, Q. T., Steingrimsson, E., Nagle, D. L., Fu, W., Genin, A., Spinner, N. B., Copeland, N. G., Jenkins, N. A., Bucan, M. et al.** (1997). Cloning and characterization of two vertebrate homologs of the *Drosophila* eyes absent gene. *Genome Res* **7**, 128-41.
- Zou, D., Silvius, D., Fritsch, B. and Xu, P. X.** (2004). *Eya1* and *Six1* are essential for early steps of sensory neurogenesis in mammalian cranial placodes. *Development* **131**, 5561-72.



## CURRICULUM VITAE



Indra Wibowo was born in Malang, East Java, Indonesia on 6<sup>th</sup> of July 1979. In the years of 1997-2001, he pursued Bachelor's study majoring in Biology at School of Technology and Life Sciences, Bandung Institute of Technology, Bandung, West Java, Indonesia. In 2003, he received Netherlands Fellowship Program-Academic Program (NFP-AP) to study Master in Biotechnology at Wageningen University, The Netherlands. During his Master's study, he did his internship on zebrafish brain development at Hubrecht Laboratory, Utrecht, under supervision of Dr. Dana Zivkovic. He then performed his thesis entitled: "Characterization of carp immune-related genes during parasite infection; and Expression and purification of recombinant carp IL-10" under supervision of Dr. Maria Forlenza and Dr. Geert Wiegertjes at the Cell Biology and Immunology (CBI) Group, Wageningen University. In 2005, he obtained Master's degree in Biotechnology, specializing in Cellular and Molecular Biology, from Wageningen University. From December 2005 until April 2006, he got opportunity to work at the CBI Group as a post-master student. In October 2006, he was awarded a doctorate fellowship by the Centre of Genomic Regulation (CRG), Barcelona, Spain. He was enrolled at Pompeu Fabra University, Barcelona, Spain and he started his doctorate program at the Sensory Cell Biology and Organogenesis Group, Cell and Developmental Biology Program, CRG, under supervision of Dr. Hernán López-Schier. Recently, he got a teaching position at School of Technology and Life Sciences, Bandung Institute of Technology, Bandung, Indonesia.